

RECRUITMENT AND FUNCTION OF ORP1L ON THE *COXIELLA BURNETII*
PARASITOPHOUS VACUOLE

Anna Victoria Justis

Submitted to the faculty of the University Graduate School
in partial fulfillment of the requirements
for the degree
Doctor of Philosophy
in the Department of Microbiology and Immunology,
Indiana University

February 2018

Accepted by the Graduate Faculty of Indiana University, in partial fulfillment of the requirements for the degree of Doctor of Philosophy.

Doctoral Committee

Stacey D. Gilk, Ph.D., Chair

Stanley M. Spinola, M.D.

David Nelson, Ph.D.

December 7, 2017

Gustavo A. Arrizabalaga, Ph.D.

Maureen A. Harrington, Ph.D.

Dedication

“To the voices in our heads that tell us we aren’t good enough:
do be quiet.”

-Carrie Hope Fletcher, *All That She Can See*

Acknowledgements

I would like to acknowledge the many people and programs that supported this work:

Stacey Gilk, my PI and mentor;

Minal Mulye, Dhirthriman Samanta, Tatiana Clement-Mordente, Brianne Zapata, and

Bayleigh Schuler, my fellow lab members;

Drs. Stanley Spinola, Dave Nelson, Maureen Harrington, and Gustavo Arrizagalaga,

members of my advisory and research committees;

Drs. Janis Blum and Mark Kaplan, who oversaw the Immunology and Infectious

Disease T32 program, for funding this work;

The Indiana Biology of Intracellular Pathogens (BIP) group, for discussion and critical

feedback;

Cindy Booth, Janis Stringer, Dan Smith, Andy Boyle, and Cathy Collins, MCIM staff;

2013 IBMG cohort and my fellow graduate students at IUSM and IUPUI;

The Indiana BioMedical Gateway Program and specifically, Tara Hobson-Prater,

Brandy Boyer-Wood, and Lauren Easterling;

Scientific Toasters at IUSM Toastmasters Club, Toastmasters District 11, all of the

members therein, and Dr. Randy Brutkiewicz, a mentor of mentors;

My parents, Caty and Glen, and my sister, Sierra; and

My wonderful husband, Eric

Recruitment and function of ORP1L on the *Coxiella burnetii* parasitophorous vacuole

Coxiella burnetii, the zoonotic agent of human Q fever and chronic endocarditis, is an obligate intracellular bacterial pathogen. The *Coxiella* intracellular niche, a large, lysosome-like parasitophorous vacuole (PV), is essential for bacterial survival and replication. There is growing evidence that host cell cholesterol trafficking plays a critical role in PV development and maintenance, prompting an examination of the role of cholesterol-binding host protein ORP1L (Oxysterol binding protein-Related Protein 1, Long) during infection. ORP1L is a multi-functional cholesterol-binding protein involved in late endosome/lysosome (LEL) trafficking, formation of membrane contact sites between LEL and the endoplasmic reticulum (ER), and cholesterol transfer from LEL to the ER. ORP1L localizes to the PV at novel membrane contact sites between the ER and the PV membrane. Ectopically expressed ORP1L in *Coxiella*-infected cells localizes to the PV membrane early during infection, before significant PV expansion and independent of other PV-localized proteins. Further, the N-terminal ORP1L Ankyrin repeats are both necessary and sufficient for PV localization, suggesting that protein-protein interactions, and not protein-lipid interactions, are primarily involved in PV association. *Coxiella* employs a Type IVB Secretion System (T4BSS) to translocate effector proteins into the host cytoplasm and manipulate various cellular functions. ORP1L is not found on the PV of a *Coxiella* mutant lacking a functional T4BSS, indicating a secreted bacterial protein is likely responsible for ORP1L recruitment. We identified a *Coxiella* mutant with a

transposon insertion in CBU_0352 that exhibits a 50% decrease in ORP1L recruitment, suggesting that *Coxiella* CBU_0352 interacts directly or indirectly with ORP1L. Finally, we found that ORP1L depletion using siRNA alters PV dynamics, resulting in smaller yet more fusogenic *Coxiella* PVs. Together, these data suggest that ORP1L is specifically recruited to the PV, where it plays a novel role in *Coxiella* PV development and interactions between the PV and the host cell.

Stacey D. Gilk, Ph.D., Chair

Table of Contents

List of Tables	x
List of Figures	xi
List of Abbreviations	xiii
Chapter I. Background and Rational	1
Q fever and <i>Coxiella burnetii</i>	1
Cholesterol in eukaryotic cells	11
Cholesterol is a factor in <i>C. burnetii</i> infection	15
Aims of this research.....	20
Chapter II. Methods	21
Bacteria and mammalian cells	21
Generation of plasmids.....	21
Mammalian cell transfection and immunofluorescence assay (IFA).....	25
Live cell microscopy	26
Recruitment and PV measurements.....	27
siRNA knockdown in HeLa cells	27
Fluorescent Infection Foci Forming Unit (FFU) assay	29
Lentivirus preparation and infection	29
<i>C. burnetii</i> transformation, selection, and anoxic culture	30
Data analysis	30

Chapter III. ORP1L is specifically recruited to the PV by <i>C. burnetii</i>	33
ORP1L co-localizes with PV marker, CD63	33
ORP1L ankyrin repeats are necessary and sufficient to localize GFP to the PV membrane.....	33
Active <i>C. burnetii</i> Type IVB Secretion System is required for ORP1L recruitment	37
Active <i>C. burnetii</i> Type IVB Secretion System is required for ORP1L recruitment	36
ORP1L is recruited early during infection, prior to PV expansion	38
ORP1L is recruited independently of other endosomal PV marker	40
Tn235 <i>C. burnetii</i> exhibits a decrease in ORP1L recruitment	42
Heterologously expressed CBU_0352 localizes to the host ER	46
Chapter IV. ORP1L participates in membrane contact sites between the PV and ER and modulates PV dynamics during <i>C. burnetii</i> infection.....	49
ORP1L exhibits a striated localization pattern on the PV which is abrogated by mutating the FFAT motif.....	49
ORP1L localizes to PV-ER membrane contact site	49
Disruption of ORP1L -containing protein complexes results in larger PVs.....	52
Reduced ORP1L expression results in reduced PV size but no change in bacterial growth.....	54
Chapter V. Discussion	62
ORP1L PV localization	62

ORP1L-containing PV-ER membrane contact sites.....	71
ORP1L effect on PV dynamics.....	67
Chapter VI. Future Directions	71
Characterizing CBU_0352	71
Identifying additional ORP1L-interacting proteins	76
Investigating ORP1L function.....	77
A tool for unbiased investigation of <i>C. burnetii</i> secreted proteins.....	80
References	84
Curriculum Vitae	

List of Tables

Table 1. Primers used in this study.....31

List of Figures

Figure 1. <i>Coxiella burnetii</i> lifecycle in epithelial cells	9
Figure 2. Cholesterol-dependent conformational changes in ORP1L	14
Figure 3. GFP-tagged ORP1L localizes to the <i>C. burnetii</i> PV membrane.	19
Figure 4. ORP1L co-localizes with CD63 on the PV membrane	34
Figure 5. Ankyrin repeat domains are necessary and sufficient to target ORP1L to the PV.....	36
Figure 6. ORP1L PV localization is T4BSS-dependent	37
Figure 7. ORP1L is recruited to the PV prior to significant expansion.....	39
Figure 8. PV size in untransfected and ORP1L-GFP expressing cells	41
Figure 9. ORP1L is recruited to the PV independently of Rab7	42
Figure 10. Mutant #235 is deficient in ORP1L recruitment	44
Figure 11. <i>cbu0352</i> mutant clones are deficient in ORP1L recruitment	45
Figure 12. Heterologously expressed CBU_0352 does not localize to the <i>C. burnetii</i> PV.....	47
Figure 13. Heterologously expressed CBU_0352 localizes to the host ER	48
Figure 14. ORP1L exhibits FFAT motif-dependent striated pattern on the PV.....	50
Figure 15. ORP1L on the PV co-localizes with the ER	51
Figure 16. Electron microscopy reveals membrane contact sites between the PV and ER	54
Figure 17. Over-expression of mutant ORP1L results in larger PVs	55
Figure 18. Depletion of VapB results in larger PVs.	56

Figure 19. Depletion of ORP1L results in smaller PVs.....	58
Figure 20. Depletion of ORP1L with single siRNA duplex results in smaller PVs.....	59
Figure 21. Depletion of ORP1L does not alter Rab7 or RILP PV-localization.	60
Figure 22. Possible mechanisms of CBU_0352 function in ORP1L recruitment.....	65
Figure 23. Model for ORP1L in membrane contact sites between the <i>C. burnetii</i> parasitophorous vacuole (PV) and host cell endoplasmic reticulum.	72
Figure 24. ORP1L knockdown in MH-S cells by lentiviral shRNA.....	79

List of Abbreviations

293T	human embryonic kidney epithelial cells
AA	amino acids
ABCA3	ATP-binding cassette transporter sub-family A member 3
ACCM-2	acidified citrate cysteine medium-2
Ank	ankyrin repeat domain
Δ Ank	ankyrin repeat domain deletion
AnkG	ankyrin repeat family protein G
Anl	<u>azido</u> <u>nor</u> <u>leucine</u>
ATCC	American type culture collection
ATP	adenosine triphosphate
BlaM	β -lactamase
BP	base pair
cAMP	cyclic adenosine monophosphate
Cas9	CRISPR associated protein 9
CAT	chloramphenicol
CC	coiled-coil
CCV	<i>Coxiella</i> - containing vacuole
CD63	cluster of differentiation 63; also Lamp3
CERT	ceramide transfer protein
CHO	Chinese hamster ovary cells
COPII	vesicle coat protein 2

CRISPR	clustered regularly interspaced short palindromic repeats
CvpB	<i>Coxiella</i> vacuolar protein B
CvpD	<i>Coxiella</i> vacuolar protein D
CyaA	adenylate cyclase toxin
CzcD	cobalt-zinc-cadmium regulating gene D
DHCR24	24-dehydrocholesterol reductase
DotA	defect in organelle trafficking gene A
DotB	defect in organelle trafficking gene B
Dot/Icm	defect in organelle trafficking/intracellular multiplication
dpi	days post infection
ElpA	ER-localizing protein A
ER	endoplasmic reticulum
ET	electron tomography
<i>et al.</i>	<i>et alia</i> ; and others
EV	empty vector
FBS	fetal bovine serum
FDA	Federal Drug Administration
FFAT	two phenylalanines (<u>FF</u>) in an <u>a</u> cidic <u>t</u> ract
FFU	foci forming unit
FITC-dex	fluorescein isothiocyanate-dextran
FRAP	fluorescence recovery after photobleaching
FRET	fluorescence resonance energy transfer

GFP	green fluorescent protein
GM130	cis-Golgi matrix protein, 130
GTP	guanosine triphosphate
HA	human influenza hemagglutinin
HeLa	human adenocarcinoma cervical epithelial cells
HOPS	homotypic fusion and protein sorting
IcmD	intracellular multiplication gene D
IFA	immunofluorescence assay
Kan	kanamycin
KDEL	amino acid sequence: lysine, aspartic acid, glutamic acid, leucine; ER retention signal
KPBT	<i>Klebsiella pneumoniae</i> oxaloacetate decarboxylase
KO	knock out
Lamp1	lysosomal-associated membrane protein 1
Lamp2	lysosomal-associated membrane protein 2
Lamp3	lysosomal-associated membrane protein 3; also CD63
LC3	microtubule-associated protein 1A/1B-light chain 3
LCV	large cell variant
LDL	low density lipoprotein
LE	late endosome
LEL	late endosome/lysosome
LY	Lucifer yellow

LysA	diaminopimelic acid decarboxylase
mCherry	monomeric red fluorophore
MCS	membrane contact site
MEF	mouse embryonic fibroblasts
Met	methionine
MetRS	methionyl-tRNA synthetase
MH-S	mouse alveolar macrophage-derived cell line
mTurquoise	monomeric cyan fluorophore
MOI	multiplicity of infection
MVB	multivesicular body
mVenus	monomeric green fluorophore
NBD	7-nitrobenz-2-Oxa-1,3-diazon-4-yl
NIH	National Institutes of Health
NLL	L13N, Y260L, H301L; mutant form of MetRS enzyme
NMII	Nine Mile phase II
NPC1	Niemann-Pick disease type C1 protein
NT	non-targeting
nt	nucleotide
ORD	oxysterol-binding protein related domain
Δ ORD	oxysterol-binding protein related domain deletion
ORP1L	oxysterol-binding protein-related protein (ORP) 1, long
OSBP	oxysterol-binding protein

p150 ^{Glued}	protein subunit of dynactin
p62	sequestosome 1
PBS	phosphate buffered saline
PCR	polymerase chain reaction
PFA	<u>para</u> <u>formal</u> <u>dehyde</u>
PH	plekstrin homology
PmrAB	pneumococcal multidrug resistance proteins A and B
PVDF	<u>poly</u> <u>vinylidene</u> <u>f</u> luoride
PV	parasitophorous vacuole
Rab	ras in the brain
Rab1b	Rab protein 1b
Rab7	Rab protein 7
Rab9	Rab protein 9
RILP	Rab-interacting lysosomal protein
RFP	red fluorescent protein
RNA	<u>ribo</u> <u>nucleic</u> <u>a</u> cid
RPMI	Roswell Park Memorial Institute medium
Sec	secretory translocon
SCR	scrambled
SCV	small cell variant
SDS-PAGE	sodium dodecyl sulfate polyacrylamide gel electrophoresis
sgRNA	small guide RNA

shRNA	small hairpin RNA
siRNA	small interfering RNA
SNARE	<u>s</u> oluble <u>N</u> -ethylmaleimide-sensitive factor <u>a</u> ttachment protein <u>r</u> eceptors
<i>sp.</i>	species
STARD3	StAR-related lipid transfer domain containing 3
T4BSS	type IVB secretion system
TBS	tris-buffered saline
TCA	trichloroacetic acid
TEM	transmission electron microscopy
THP-1	human peripheral blood monocyte cell line
tRNA	transfer RNA
USA	United States of America
UV	ultraviolet
VAMP	vesicle associated membrane protein
Vamp3	vesicle associated membrane protein 3
Vamp7	vesicle associated membrane protein 7
Vamp8	vesicle associated membrane protein 8
VAP	<u>V</u> AMP- <u>a</u> ssociated ER <u>p</u> rotein
vATPase	vacuolar ATPase H ⁺ transporter

Chapter I. Background and Rational

Q fever and *Coxiella burnetii*

Historic perspective

In 1935, an outbreak of unknown febrile disease was observed among slaughterhouse workers in Brisbane, Queensland, Australia. Edward Derrick endeavored to identify the etiological source of the illness named “Q” fever for “query” fever of unknown cause. When blood was transferred from the infected workers to guinea pigs in the laboratory, the guinea pigs also developed febrile disease [1]. At nearly the same time, an unidentified infectious agent was discovered during field studies in Montana, USA. Ticks collected in Nine Mile valley caused febrile illness in the guinea pigs on which they fed. Ultimately, a laboratory acquired infection with the Nine Mile agent resulted in researchers comparing the two isolates and immunological cross-protection studies confirmed that these illnesses were caused by the same organism [2]. The bacteria was named *Coxiella burnetii* after researchers Cox and Burnet who each contributed to its characterization.

Once the bacteria was identified, the world continued to see outbreaks of Q fever (reviewed in [3]). For example, eight separate outbreaks occurred among Allied soldiers in southern Europe during World War II, and domestic outbreaks occurred in Amarillo, Texas and Chicago, Illinois during the mid-1940s [4-6]. These events were connected to livestock and revealed the aerosol route of transmission as well as the potential public health impact of *C. burnetii* infection [7]. Additional laboratory acquired

infections at the National Institutes of Health revealed that the bacteria has a low infectious dose [8, 9]. During the Cold War, the American military identified *C. burnetii* as a possible agent of biological warfare. Experiments carried out at Dugway Proving Ground in Utah established the feasibility of such use and a small number of human experiments carried out in the 1950s clarified the dynamics of *C. burnetii* infection [10-12]. Analysis of these early studies together with data from inhaled infection models in guinea pigs has determined the median inhaled infectious dose to be between 1 and 15 organisms [13-15]. Due to these concerns, *C. burnetii* remains classified as a category B potentially aerosolized biological weapon under the Centers for Disease Control Select Agent program [16].

Animal infection

Q fever is a zoonotic disease that is endemic worldwide and affects humans as well as a broad range of animals. *C. burnetii* is likely enzootic in domestic ruminants as well as wild animals [17, 18] and has been isolated from mammals, birds [19], reptiles [20], and ticks [2]. While many studies have isolated *C. burnetii* from ticks and laboratory experiments have shown that several species of tick can serve as a *C. burnetii* vector, transmitting the bacteria by blood meal or transovarially, the actual risk of disease transmission in the field is not clear (reviewed in [21]).

Infected animals shed the small cell variant (SCV) form of *C. burnetii* into the environment via bodily secretions, including urine, feces, milk, and birth products. *C. burnetii* is commonly found in raw milk, for example, and consumption of contaminated unpasteurized milk can cause human infection [22]. One survey of milk samples from 134

commercial processing plants in 41 states found *C. burnetii* DNA in 95.5% of samples [23]. Another study of milk from 316 bulk storage tanks, each containing milk pooled from a herd of dairy cattle, found the 94.3% of samples tested positive for *C. burnetii* by PCR [24]. Furthermore, bacteria from infected animals can be disseminated into the environment, where it can remain viable on fomites for years [25]. Contaminated soils can become aerosolized and lead to human infection by inhalation. There is a high prevalence of antibodies against *C. burnetii* among livestock in the USA: 41.6% of goats, 16.5% of sheep, and 3.4% of cattle are seropositive for antibodies against *C. burnetii* [17], leading to a somewhat high risk of human exposure.

It follows that exposure to domestic ruminants results in the greatest number of *C. burnetii* human infections [26, 27]. This is supported by the finding from individual case studies and outbreak investigations, that occupational exposures in research facilities, farm environments, and slaughterhouses are commonly reported (reviewed in [17]). One study tracked human Q fever cases in Germany and observed the seasonality of community outbreaks shift from primarily occurring in winter-spring to primarily occurring in spring-summer. This shift followed changes in the temporal patterns of sheep husbandry in the region [28]. This exposure route is also supported by the sources of recent Q fever outbreaks in Europe. 29 human cases were identified in a small town in the French Alps during the spring seasons of 1995 and 1996. The outbreak was traced to contaminated sheep waste from a nearby slaughterhouse [29]. The largest human Q fever epidemic ever recorded occurred in the Netherlands from 2007-2010, during which over 4000 human cases were identified. This outbreak spread

from a dairy goat farm that experienced *C. burnetii*-related spontaneous abortion rates of up to 80% among its herd during the onset of the human outbreak [30, 31].

Human infection

C. burnetii infection in humans is most often asymptomatic and self-limiting. For example, during one Q fever outbreak in Switzerland during the early 1980s, 415 infections were diagnosed by serology. Of these cases 54% were asymptomatic and interestingly, only 12.5% of infected children showed symptoms [32]. In the 40% of patients who develop acute symptomatic disease, this manifests as fever and flu-like symptoms. Rarely, Q fever may present as acute neurological disease or as a hyper-inflammatory syndrome associated with hepatitis [33, 34]. Additionally, weakness and tiredness persisting for years and termed Q Fever Fatigue Syndrome has been observed in approximately 20% of acute Q fever patients [35, 36]. Regardless of whether the primary infection is symptomatic or asymptomatic, a small number of infections lead to chronic Q fever [32, 37]. Chronic Q fever can manifest months to years after initial infection and most often presents clinically as endocarditis [38]. Houpijian *et al.* determined that *C. burnetii* is responsible for approximately half of blood culture negative cases of infectious endocarditis [39]. Left untreated, Q fever endocarditis can be fatal [40]. Regardless of the specific manifestation, an 18-month course of treatment with doxycycline and chloroquine is the recommended treatment for human *C. burnetii* infection and can prevent relapse in greater than 95% of Q fever endocarditis patients [41, 42].

Treating Q fever in pregnant women poses particular challenges [43]. Active *C. burnetii* infection during pregnancy can result in poor outcomes including fetal growth retardation, premature delivery, spontaneous abortion, or stillbirth [44]. One study of patients diagnosed with Q fever during pregnancy observed complications in 80 % of mothers who were not treated for the infection. Furthermore, the worst outcomes were observed among mothers who were infected during the first trimester [45]. Although no controlled human studies have been conducted, treatment of pregnant patients with chloroquine for long periods is contraindicated due to evidence of fetal harm seen in animal studies. Since 1996, treatment with cotrimoxazole for at least 5 weeks has been used to treat pregnant Q fever patients, reducing the risk of fetal and maternal complications [43]. Because cotrimoxazole is bacteriostatic, however, bactericidal treatment must be administered after delivery in order to clear the infection [46].

The clinical presentation of Q fever is variable and often non-specific, very likely resulting in underreporting and an underestimation of the incidence among humans. Between 1948 and 1986, a total of 1,396 human cases of Q fever were included in national disease surveillance reports for the USA [17]. In Germany, an annual incidence of 0.1-3.1 per million for human Q fever was observed between 1979-1999 [28]. Due to number of asymptomatic infections, actual disease incidence is likely much higher than that found in these studies.

Intracellular niche

C. burnetii is an obligate intracellular bacteria, only replicating within a niche intracellular compartment termed the *Coxiella*-containing vacuole (CCV) or the parasitophorous vacuole (PV). The bacteria relies on passive mechanisms of attachment and entry into host cells [47]. Lipid raft localized host integrin $\alpha_v\beta_3$ likely serves as the binding receptor for *C. burnetii*, and host phagocytosis is responsible for bacterial entry [48, 49]. Immediately following phagocytosis by the host cell, the bacterium is found within a tight fitting endosome [50]. This nascent PV sequentially acquires Rab5 and then Rab7, markers of early and late endosomes respectively. [51, 52]. Further, Campoy *et al.* have reported that several endocytic SNARE proteins, which mediate the final stages of docking and fusion events between vesicle membranes, contribute to PV development, indicating that the PV matures through the canonical endocytic pathway [53].

The mature PV is a large, modified phagolysosome that is distinct from other intracellular host or pathogen compartments [54]. The PV membrane is highly fusogenic, interacting with multiple host vesicle types, including endocytic, phagosomal, lysosomal, autophagic, as well as early, late, and recycling endosomal vesicles. These fusion events contribute to the unique combination of protein markers and functional characteristics of the mature PV and allow for rapid expansion of the PV, which ultimately can occupy the majority of the cytoplasmic space within a cell [50]. Interactions between the PV and host endocytic pathway have been shown by trafficking of the experimental fluid-phase markers fluorescein isothiocyanate-dextran

(FITC-dex) and Lucifer yellow (LY) to the PV lumen [55]. Vamp8, a SNARE protein that participates in homotypic fusion between late endosomes localizes to the PV early during infection at 1-12 hpi [53]. The PV is also decorated with Rab7, a late endosomal marker, throughout infection [56]. Furthermore, the endosomal compartment expands during *C. burnetii* infection, indicating that the bacteria is manipulating this pathway [57]. The PV also interacts with the autophagy pathway, as shown by LC3 localization to the PV membrane [56]. Additionally, induction of autophagy by amino acid starvation supports *C. burnetii* growth and PV expansion [58]. Rab1b, a marker of the anterograde transport pathway between the ER and the Golgi apparatus, is recruited to the PV membrane later than 6 hpi. Additionally, knockdown of Rab1b by siRNA results in significantly smaller PVs and reduced *C. burnetii* growth [59]. Function and organization of the Golgi apparatus are required for normal formation and expansion of the PV. This was demonstrated by studies on Sar1, a small GTPase involved in formation of COPII-coated transport vesicles that bud from the ER. Ectopic expression of a mutant form of Sar1 results in disassembly of the Golgi apparatus and significant decrease in the number of expanded, spacious PVs [59]. The Golgi membrane itself, defined by the protein and lipid markers GM130 and sphingomyelin derived from C₆-NBD-ceramide are excluded from the *C. burnetii* PV [55, 60]. Finally, the nuclear protein, p62, is also excluded from the PV membrane, indicating that neither nuclear nor Golgi membranes directly contribute to that of the PV [60].

The mature PV is a degradative organelle with many characteristics of true lysosomes. The SNARE protein Vamp7, which participates in fusion between late

endosomes and lysosomes, localizes to the PV and is required for normal expansion of PV membrane [53]. The lysosomal proteins vATPase, Lamp1, and Lamp2 also localize to the PV membrane [55, 60]. PVs also contain active lysosomal enzymes including acid phosphatase and Cathepsin D [55, 61]. Howe *et al.* showed that treatment of infected cells with chloramphenicol results in collapse of this spacious vacuole, showing that bacterial protein synthesis is required for PV maintenance and that *C. burnetii* actively sustains PV size and function [62].

Intracellular lifecycle

The *C. burnetii* lifecycle is biphasic and involves the transition between two developmental morphotypes, the small cell variant (SCV) and the large cell variant (LCV), which differ in gene expression, structure, and growth rate (Figure 1). The SCV is the small, electron dense, non-replicating form, which is almost completely metabolically inactive and resistant to many environmental insults. The SCV can survive exposure to drying, heat, pressure, osmotic stress, sonication, UV light, and many disinfectants [63, 64]. This dormant, resilient developmental stage is long-lived and can survive in extracellular environments, including contaminated soils and other fomites, for years [25, 65, 66]. Upon passive phagocytosis by a host cell, bacterial metabolism is induced by the acidic environment of the intracellular niche [67]. The SCV transitions to the LCV form during a two day-long lag phase beginning immediately after entry. LCVs then divide in log phase for approximately four days before reaching stationary phase and beginning the transition to the SCV form [50]. The LCV is the only form that replicates within the host and is metabolically very active. While both developmental forms are

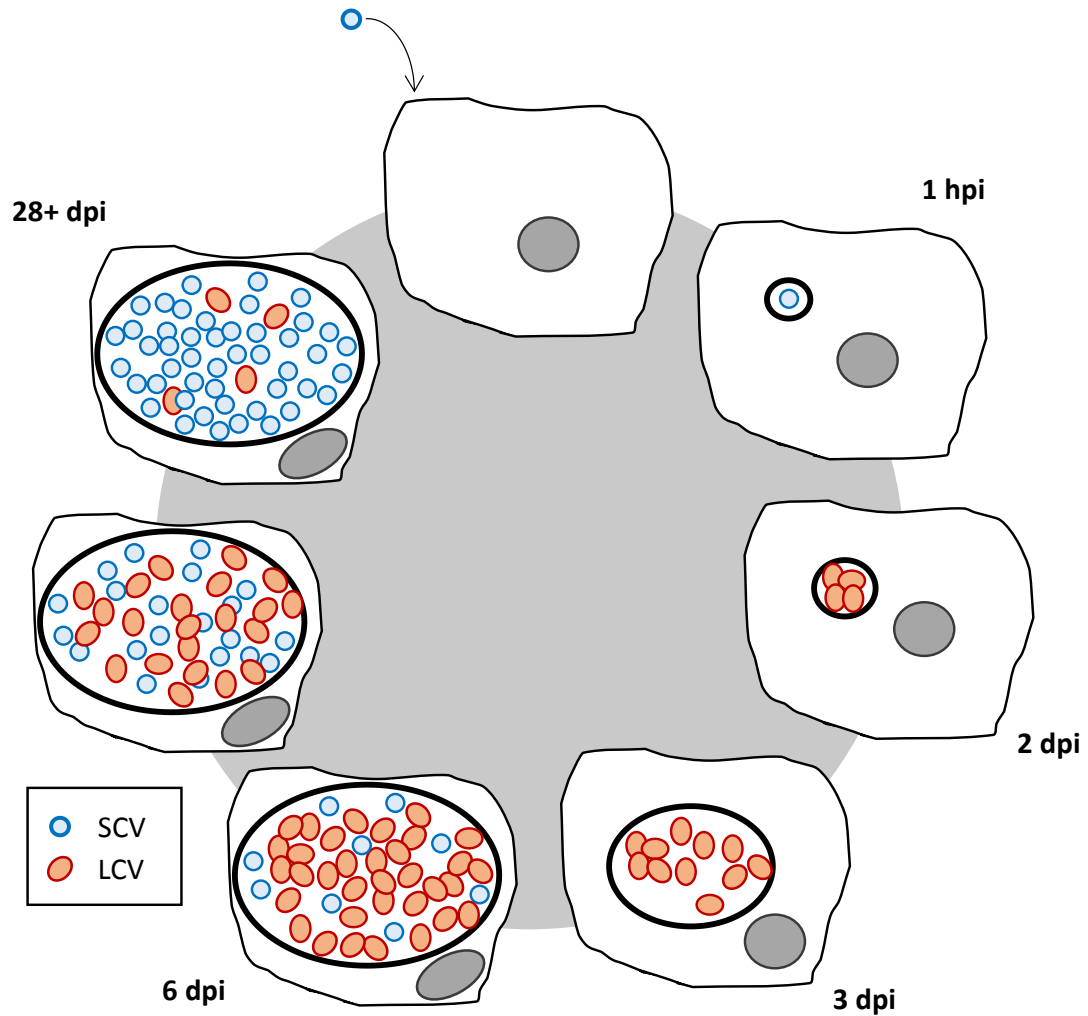


Figure 1. *Coxiella burnetii* lifecycle in epithelial cells

C. burnetii lifecycle in epithelial cells. SCVs are passively phagocytosed and transition to LCVs during the first 2 days of infection. Beginning approximately 2 dpi, the PV expands rapidly and LCVs replicate. LCVs begin transitioning into SCVs approximately 6 dpi. *C. burnetii* can remain within the living host cell for over a month and does not employ any known mechanisms to exit. hpi = hours post infection; dpi = days post infection; SCV = small cell variant (blue); LCV = large cell variant (red).

capable of infecting host cells, it is likely that the SCV is the infectious form encountered during naturally occurring infection as this is the more stable extracellular state [68].

Type IVB Secretion System

The major *C. burnetii* virulence factor and method of manipulating host cells is the type IVB secretion system (T4BSS). The T4BSS comprises a needle-like protein complex that translocates bacterial effector proteins across the inner and outer bacterial membrane as well as the PV membrane and into the host cell cytoplasm in order to manipulate various host cellular functions. This system is conserved between *Coxiella* and *Legionella sp.*, including the human pathogen, *Legionella pneumophila* [69, 70]. A recent report suggests that the *C. burnetii* T4BSS may also be capable of translocating DNA, presenting another possible method of host cell manipulation by the bacteria [71]. Mutations in the T4BSS protein components, DotA, DotB, and IcmD, have been shown to prevent translocation of effectors [72-74]. Characterization of these mutants show that the T4BSS is essential for growth and long-term survival of *C. burnetii* in host cells [75, 76].

More than 130 effector proteins are predicted to be translocated by the T4BSS. While the function of many of these proteins remains unknown, individually characterized effectors have been shown to target a variety of host functions including signal transduction [77], gene transcription [78], apoptosis [79], autophagy [58], and vesicular trafficking [74, 80] to support PV biogenesis and bacterial replication. Mutation of these secreted proteins individually has revealed intracellular growth defects, indicating that many serve important non-redundant functions during *C. burnetii* infection. Analysis of *C. burnetii* genomes has revealed the presence of many

eukaryotic-like features, including F-box motifs and at least 13 proteins that contain ankyrin repeat domains [76, 81]. Most of these eukaryotic domain containing proteins are proven to be translocated by the T4BSS [79, 82]. It is hypothesized that these eukaryotic-like proteins were acquired by interdomain horizontal gene transfer [83, 84].

Effector translocation relies on either an intrinsic signal sequence or shuttle proteins. Most effectors contain a C-terminus E-block motif which functions as a secretory signal [85, 86]. A subset of effectors are also dependent upon the chaperone proteins, IcmW and IcmS, which facilitate interactions between effectors and the T4BSS complex [69]. To determine the timing of effector translocation, Newton *et al.* created reporter constructs encoding constitutively expressed effector proteins fused to a β -lactamase enzyme lacking a signal sequence (BlaM). Using a host cytoplasmic fluorescent reporter substrate that changes emission color when cleaved by the translocated BlaM enzyme allows fusion protein translocation to be detected by a color change from green to blue [74]. Translocation of effector proteins into the host cell cytoplasm occurs within 8-12 hours post infection in epithelial (HeLa) cells and within 1-4 hours post infection in bone marrow-derived macrophages [51]. This approach does not reveal when specific effectors are translocated but it does, however, provide the first evidence that T4BSS-dependent translocation can occur early during infection.

Cholesterol in eukaryotic cells

Development of the PV requires the rapid, coordinated acquisition and manipulation of host cell membranes. Cholesterol is an important lipid component of

eukaryotic cell membranes and greatly influences membrane structure and function. Structurally, cholesterol affects membrane fluidity and permeability, with higher cholesterol levels resulting in increased membrane rigidity [87]. Due to these properties, the presence of cholesterol allows for increased ordering and discrete functional regions within membranes. Cholesterol-rich micro-domains known as lipid rafts, for example, serve as specialized signaling platforms involved in signal transduction [88]. Further, intracellular cholesterol is a critical regulator of Golgi trafficking [89], endocytic trafficking [90], and intra-organellar membrane contact sites [91].

Cellular cholesterol is heterogeneously distributed between the various membranes of the cell (reviewed in [92]). Between 60 and 90% of total cellular cholesterol resides in the plasma membrane, where it comprises 20-25% of the lipid molecules within that membrane. Moderate amounts of cholesterol are also found in endocytic and trans-Golgi compartments, while less than 1% of total cellular cholesterol is found in the endoplasmic reticulum (ER) membrane [93]. When cholesterol accumulates in the ER membrane, the excess can be trafficked to other cell membranes or esterified and packaged into lipid storage organelles, lipid droplets [94].

Endogenous cholesterol is synthesized *de novo* in the ER and trafficked to the plasma membrane before distribution throughout the cell. Exogenous cholesterol is acquired by receptor-mediated endocytosis of low density lipoproteins (LDL) or chylomicron remnants [95]. LDL particles are internalized by clathrin-mediated endocytosis and transported through the endocytic pathway to lysosomes, where cholesterol esters are hydrolyzed to free cholesterol for cellular use. Regardless of the

source, cholesterol can be transported throughout the cell by both vesicular and non-vesicular (e.g., cholesterol transport proteins and membrane contact sites) trafficking pathways.

In addition to its role in membrane fluidity, cholesterol regulates membrane trafficking and signaling through a large family of sterol sensor and transfer proteins. Cholesterol distribution is controlled in part by sterol binding and transfer proteins, such as those in the human oxysterol binding protein (OSBP)-related protein family. There are 12 mammalian OSBP-related protein family members, sharing two common domains: a highly conserved sterol-binding domain near the C-terminus and most also have a pleckstrin homology domain in the N-terminal half of the protein, which binds phosphatidylinositol lipids in membranes [96-98].

ORP1L

One member of this family, oxysterol-binding protein (OSBP)-related protein 1 long (ORP1L), localizes to late endosomes and lysosomes (LEL). This is confirmed by co-localization with the small GTPases, Rab7 and Rab9, as well as Lamp1 [99, 100]. ORP1L has dual functions: 1) regulating cholesterol-dependent endosomal trafficking along microtubules and 2) formation of membrane contact sites (MCS) between late endosomes/lysosomes and the ER. ORP1L undergoes cholesterol-dependent conformational changes that control whether endosomes interact with microtubules or with the ER (Figure 2; reviewed in [101]). When bound to cholesterol, ORP1L adopts a compact conformation (Figure 2A) with the N-terminal ankyrin repeats binding the Rab7/RILP (Rab-interacting lysosomal protein) complex and the C-terminal ORD (OSBP-

related domain) binding cholesterol [99, 102]. When ORP1L is in this conformation, RILP is free to bind the homotypic fusion and protein sorting (HOPS)-tethering complex, which in turn binds the dynactin subunit p150^{Glued} and dynein [103, 104]. Dynactin, the dynein activator complex, directly interacts with the motor protein dynein, increasing dynein motor processivity and facilitating the link between LEs and microtubules [105]. This interaction with dynein facilitates minus end-directed transport of endosomes along microtubules [90, 106]. In the absence of cholesterol binding by ORD, ORP1L

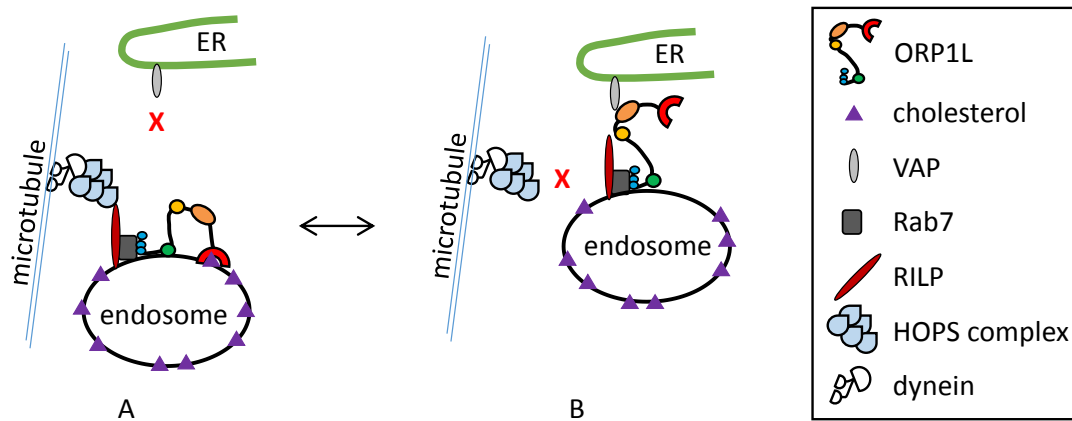


Figure 2. Cholesterol-dependent conformational changes in ORP1L

ORP1L exists in two conformations on the endosomal membrane, interacting with Rab7/RILP in both conformations. (A) Cholesterol-bound ORP1L takes on a condensed conformation, allowing RILP to interact with the HOPS and dynein motor complexes. Together, these interactions result in minus-end directed movement of the endosome along microtubules toward the perinuclear space. (B) When ORP1L is not bound to cholesterol it adopts an extended conformation, disrupting the interaction between RILP and the HOPS complex. Instead, ORP1L forms membrane contact sites by binding VAP on the ER.

adopts an extended conformation (Figure 2B), allowing the ORP1L FFAT (two phenylalanines (FF) in an acidic tract) motif to interact with the resident ER protein VAP (VAMP-associated ER protein) [107]. As a result of binding to both the ER and LEL, ORP1L forms MCS between these two organelles and disrupts the protein complex mediating the association between Rab7/RILP and microtubules [102]. Related to its role in late endosome trafficking, ORP1L impacts transport of LDL cholesterol to the ER [108], multivesicular body (MVB) formation, and membrane protein degradation [109]. These roles in lipid trafficking may additionally influence transcriptional regulation of cholesterol efflux genes [110].

Recent work from the Ridgway laboratory provides evidence that ORP1L is directly involved in transfer of cholesterol from LEL to the ER in cultured human cells. ORP1L null cells contain cholesterol enriched, perinuclear LELs, indicating that cholesterol taken up by the cell was retained within LELs [111]. This is consistent with the role of ORP1L in regulating endosome positioning reported by the Neefjes group [103, 112] (Figure 2A). Cells lacking ORP1L also contained decreased esterified cholesterol relative to total cholesterol at the same time that cholesterol synthesis was elevated and LDL uptake was unchanged, indicating that less cholesterol is trafficked to the ER in these cells compared to control cells [111].

Cholesterol homeostasis is a critical factor in *C. burnetii* infection

Multiple reports have implicated cholesterol as an important factor during *C. burnetii* infection. Howe and Heinzen showed that fillipin labels the PV membrane with

an intensity similar to that of the plasma membrane and the lipid raft protein flotillin-1 localizes to the PV membrane [113]. Together, these findings indicated the PV membrane was rich in sterols, possibly including cholesterol. Further, multiple inhibitor studies indicated that cholesterol was important during *C. burnetii* infection. Replication is inhibited in Chinese hamster ovary (CHO) cells treated with inhibitors of cholesterol metabolism [114]. Additionally, a screen of FDA-approved small molecule inhibitors revealed that disrupting cholesterol homeostasis broadly attenuates *C. burnetii* growth in human macrophage-like THP-1 cells [115]. Specifically, a subset of drugs was identified that alter intracellular cholesterol distribution in such a way that filipin labeling is increased on the plasma membrane and within endo-lysosomal vesicles. 57 of 62 such compounds fully inhibited *C. burnetii* intracellular replication. The same publication reported that knockdown of NPC1 by siRNA significantly attenuates bacterial growth [115]. NPC1 is a protein required for transferring cholesterol from the lumen of endolysosomes into the endolysosomal membrane so that it can be subsequently transferred to the ER [116]. The importance of NPC1 illustrates the possibility that cholesterol egress from the endolysosomal PV is critical to *C. burnetii* growth.

In order to explore the role of cholesterol during *C. burnetii* infection, Gilk *et al.* developed a cholesterol-free cell culture system using mouse embryonic fibroblasts (MEFs) in which DHCR24, the enzyme responsible for the final enzymatic step in cholesterol synthesis, was deleted, preventing the synthesis of endogenous cholesterol. This gene deletion results in cells that accumulate desmosterol in cell membranes in place of cholesterol. This model serves as a powerful tool to explore the role of

cholesterol during *C. burnetii* infection when host cells are grown in the absence or presence of exogenous cholesterol [48]. Initial experiments showed no significant difference in *C. burnetii* replication in cells lacking both endogenous and exogenous cholesterol compared to cells grown in media containing a basal level of exogenous cholesterol [48]. Follow up experiments investigated the effect of adding additional exogenous cholesterol above basal levels to the cholesterol-negative MEFs. This allowed investigators to measure the bacterial response to increasing cholesterol levels. Mulye *et al.* showed that increased cholesterol concentrations in host cells is detrimental to the *C. burnetii*. Bacterial growth is inhibited in a dose-dependent manner when host cells are cultured with increasing concentrations of exogenous cholesterol beyond basal levels. Indeed, excess cholesterol leads to lysis of *C. burnetii* within the PV by a pH-dependent mechanism [117]. Multiple host-targeted cholesterol-altering drugs were shown to significantly reduce bacterial viability and result in PVs containing lysed bacteria. These phenotypes could be rescued by co-treatment with bafilomycin, a drug which inhibits vacuolar ATPase (vATPase) thereby preventing lysosomal acidification. Furthermore, lytic PVs in infected cells with high cholesterol exhibited reduced fusogenicity with fluid-phase endocytic vesicles. Mulye *et al.* measured this by quantifying the intensity of fluorescently labeled dextran that trafficked to PVs under various conditions, reporting that PVs with lysed bacteria acquired less dextran than PVs in cells with basal cholesterol levels [117]. Together with data showing that alteration of host cholesterol trafficking can impair bacterial growth, this suggests that *C. burnetii*

survival is inhibited and PV dynamics are altered by increased concentration and/or altered intracellular localization of cholesterol.

C. burnetii targets cholesterol pathways

In addition to being sensitive to the concentration and localization of cholesterol within the host cell, *C. burnetii* infection results in changes in host cell cholesterol homeostasis. Total intracellular cholesterol levels increase as much as 73% in Vero cells infected with *C. burnetii* [113]. This was initially hinted at by changes in gene expression observed in host cells upon infection which showed that genes involved in cholesterol efflux and storage are upregulated [118, 119]. Lipid droplets have been observed in association with the PV in infected primary human alveolar macrophages [120], and lipid droplet formation is induced in mouse alveolar macrophage cells upon infection [121]. The evidence suggests the hypothesis that *C. burnetii* may manipulate host cell cholesterol levels and trafficking to promote its survival. This evidence suggests that cholesterol is harmful to *C. burnetii*, and we hypothesize that the bacteria may be manipulating host cells in order to promote pathogenesis.

ORP1L localizes to the C. burnetii PV membrane

In order to avoid harmful exposure to cholesterol, we hypothesize that *C. burnetii* may manipulate host mechanisms controlling cholesterol levels in the PV membrane. Given the cholesterol-dependent role of ORP1L in late endosome and lysosome trafficking, we hypothesized that ORP1L could be one such host target. As a first investigatory step, we examined ORP1L localization during *C. burnetii* host cell infection. ORP1L localization was observed in uninfected and infected HeLa cells expressing ORP1L fused to green fluorescent protein (GFP). By live cell microscopy, ORP1L-GFP localized to small vesicular structures in

uninfected cells (Figure 3A), consistent with published observations that ORP1L is found on

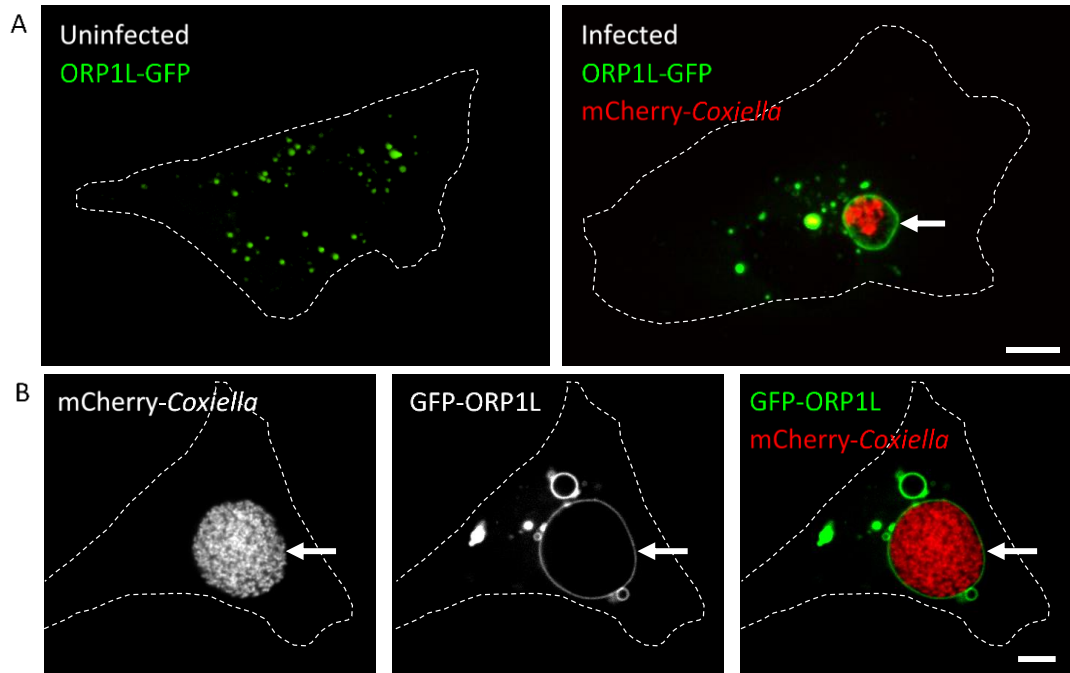


Figure 3. GFP-tagged ORP1L localizes to the *C. burnetii* PV membrane.

Live cell confocal microscopy images of uninfected or infected HeLa cells expressing ORP1L-GFP (A). In uninfected HeLa cells, ORP1L-GFP is found on vesicular structures (A, left). ORP1L-GFP also localizes to the PV membrane (A, arrow) in HeLa cells infected for three days with *C. burnetii* expressing red fluorescent protein mCherry. GFP-ORP1L also localizes to the *C. burnetii* PV (B, arrow). Cell boundaries are shown with dotted white lines. Scale bars = 10 μ m.

endosomes [110]. In *C. burnetii*-infected cells, ORP1L-GFP also localized to the *C. burnetii* PV [122] (Figure 3A). N-terminal GFP-ORP1L exhibited the same localization pattern (Figure 3B), showing that the location of the GFP tag does not affect the localization of ORP1L.

Aims of this research

While high levels of cholesterol in the PV membrane has been shown to kill *C. burnetii*, the bacteria does successfully survive and replicate within host cells, which require cholesterol, during natural infection. We hypothesize that *C. burnetii* manipulates cholesterol homeostasis to survive within the host, and ORP1L may be one host factor targeted by *C. burnetii* in order to reduce cholesterol levels in the PV.

Aim 1: Determine whether ORP1L localization to the PV occurs passively or is actively driven by *C. burnetii*. If ORP1L is targeted by *C. burnetii* to manipulate host cholesterol, we hypothesize that ORP1L will be recruited to the PV by a bacteria-specific mechanism. In order to determine if this is the case, we will characterize the timing of ORP1L localization to the PV as well as the bacterial and host factors that affect ORP1L PV localization.

Aim 2: Determine the role ORP1L may play while localized to the PV. Multiple functions of ORP1L have been identified during normal endo-lysosomal function and we will investigate whether ORP1L functions in the same way during *C. burnetii* infection. We hypothesize that ORP1L may participate in cholesterol trafficking at membrane contact sites and/or control trafficking and fusion of the *C. burnetii* PV with endo-lysosomal vesicles.

Chapter II. Methods

Bacteria and mammalian cells

Coxiella burnetti Nine Mile Phase II (NMII; clone 4, RSA439) and mCherry-expressing *C. burnetti* NMII [123] were purified from Vero cells (African green monkey kidney epithelial cells, ATCC CCL-81; American Type Culture Collection, ATCC, Manassas, VA) and stored as previously described [124]. For experiments examining T4BSS-dependent recruitment of ORP1L, NMII and the *icmD* mutant [73] were grown for 4 days in ACCM-2, washed twice with PBS (phosphate buffered saline), and stored as previously described [125]. The multiplicity of infection (MOI) was optimized for each bacteria stock for <1 internalized bacterium per cell. Vero and human cervical epithelial cells (HeLa; ATCC CCL-2) were maintained in RPMI 1640 medium (Corning, New York, NY) containing 10% fetal bovine serum (FBS) (Atlanta Biologicals, Norcross, GA) at 37°C and 5% CO₂. Human embryonic kidney epithelial cells (293T, ATCC CRL-326) were maintained in DMEM medium (Corning) containing 10% FBS.

Generation of plasmids

ORP1L-GFP constructs

Full length, wild type ORP1L-GFP was a generous gift of J. Neefjes (Netherlands Cancer Institute). This plasmid contains ORP1L amplified from human cDNA. For construction of ORP1L domain GFP constructs, ORP1L domains [100] were amplified using full length ORP1L-GFP as a template and cloned into the BsrG1 site of

pcDNA6.2/N-EmeraldGFP using In-Fusion (Takara Bio USA, Mountain View, California). The pcDNA6.2/N-ORP1L-EmeraldGFP construct that we created is referred to as “ORP1L-GFP” in this work. The following primer combinations were used: Full length ORP1L (amino acids (AA) 1-950) = ORP1L-1-F and ORP1L-950-R; ORD (AA 510-950) = ORP1L-510-F and ORP1L-950-R; PH (AA 211-345) = ORP1L-211-F and ORP1L-345-R; Ank-PH (AA 1-408) = ORP1L-1-F and ORP1L-408-R; Ank (AA 1-237) = OFP1L-1-F and ORP1L-237-R; Δ Ank (AA 211-950) = ORP1L-211-F and ORP1L-1-R. FFAT mutant (D478A) was generated using site directed mutagenesis with primers ORP1L-D478A-F and ORP1L-D478A-R according to the manufacturer’s directions (Takara Bio USA). Primer sequences are in Table 1.

ORP1L FRET constructs

Turquoise-Venus-FRET-10 plasmid was a gift from Michael Davidson (Addgene plasmid #58158). To make the empty FRET vector plasmid (pcDNA6.2-mTurquoise-mVenus) Venus-Turquoise was amplified from Turquoise-Venus-FRET-10 plasmid and cloned into the BamHI and AgeI sites of pcDNA6.2-N-mCherry-DEST by In-Fusion, replacing the mCherry and *att* insertion sites. Full-length or Δ ORD ORP1L was amplified from ORP1L-GFP and cloned into the AgeI site of the pcDNA6.2-mTurquoise-mVenus by In-Fusion. The following primer pairs were used: full-length (AA 1-950) = ORP1L-1-FRET-F and ORP1L-950-FRET-R; and Δ ORD (AA 1-514) = SG060 and SG061. Primer sequences are in Table 1.

BioEASE constructs

ORP1L was amplified from ORP1L-GFP and cloned into BsrGI-digested pcDNA6.2-N-BioEASE-DEST by In-Fusion. The following primer combinations were used: Full-length ORP1L (AA 1-950) = SG107 and SG110; Ank (AA 1-237) = SG107 and SG 109; Δ Ank (AA 211-950) = SG108 and SG110. Primer sequences are in Table 1. These primers amplify the same ORP1L sequences as the corresponding GFP constructs, but contain sequences that are unique to the pcDNA6.2-N-BioEASE-DEST plasmid vector.

mCherry-CBU_0352 mammalian expression construct

Genomic DNA was isolated from *C. burnetii* anoxic culture grown for 4 days in ACCM- 2 media using the DNeasy UltraClean Microbial Kit (12224; Qiagen, Carlsbad, CA). The *cbu0352* coding region was amplified with primers SG350 and SG351 (sequences in Table 1) from *C. burnetii* NMII genomic DNA and cloned into BsrGI-digested pcDNA6.2-N-mCherry-DEST using In-Fusion.

CyaA constructs

cbu0352 was amplified with primers SG224 and SG225 (sequences in Table 1) from *C. burnetii* NMII genomic DNA and cloned into the Sall site of pJB-Kan-CyaA or pJB-CAT-CyaA using In-Fusion cloning.

cbu0352 suicide plasmid

Following a previously published cloning strategy [126], a two-step process was used to construct the suicide plasmid. The genomic regions (approximately 2000 bp) immediately up and downstream of the *cbu0352* locus were amplified from *C. burnetii* NMII genomic DNA and cloned into BamHI- and Sall-digested pJC-CAT vector by 3-way

In-Fusion, introducing a PstI restriction site between the two fragments. Next, the LysCA cassette was amplified from the pJC-CAT-LoxP-LysCA-LoxP plasmid and cloned into the PstI site in the intermediate plasmid. The following primer pairs were used: *cbu0352* 5' flanking region (2047 base pairs (BP)) = SG259 and SG260; *cbu0352* 3' flanking region (2000 BP) = SG261 and SG262; and LysCA cassette = SG257 and SG256. Primer sequences are in Table 1.

FLAG-tagged CBU_0352 constructs

To make the N-terminal fusion, *cbu0352* was amplified with primers SG240 and SG241 from *C. burnetii* NMII genomic DNA and cloned into the Sall site of pJB-Kan-3xFLAG. For the C-terminal fusion, *cbu0352* was amplified with primers SG242 and SG243 (sequences in Table 1) and cloned into the PstI site of the same plasmid.

sgRNA constructs for CRISPR

The lentiCRISPRv2 plasmid was a gift from Feng Zhang (Addgene plasmid # 52961). ORP1L small guiding RNAs (sgRNAs) were designed using the CRISPR Design tool (Zhang Lab, MIT, 2015) and cloned into lentiCRISPRv2 with a protocol modified from the Zhang Lab [127]. Phosphorylated DNA oligonucleotide pairs were annealed and cloned into BsmBI-digested lentiCRISPRv2 using T4 Ligase (ThermoFisher Scientific, Waltham, MA). The following oligonucleotide pairs were used: ORP1LsgRNA1 = (SG289 and SG290); ORP1LsgRNA2 = (SG291 and SG292); ORP1LsgRNA3 = (SG293 and SG294). Primer sequences are in Table 1.

2xHA-MetRS^{NLL} construct

pAM1, containing the mutant *E. coli* gene, MetRS^{NLL}, was a gift from David Tirrell (Addgene plasmid # 51401, [128]). MetRS^{NLL} contains three mutant residues in the methionine (Met)-binding pocket of the MetRS enzyme (L13N, Y260L, and H301L), resulting in an enzyme that activates azidonorleucine (AnI) in place of methionine [129]. MetRS^{NLL} was amplified from pAM1 with primers SG038 and SG039 and cloned into the pCR-Blunt II-TOPO plasmid using the Zero Blunt TOPO PCR Cloning Kit (450245, Invitrogen) to create the intermediate pCR-Blunt II-TOPO-MetRS^{NLL}. MetRS^{NLL} was isolated from this intermediate plasmid by Sall digestion and ligated into the Sall site of pJB-CAT-2xHA with T4 Ligase to create an N-terminally HA-tagged MetRS^{NLL} driven by p1169, a constitutively active *C. burnetii* promoter.

Mammalian cell transfection and immunofluorescence assay (IFA)

HeLa cells (2×10^4 cells per well of a 24 well plate) were plated on acid-washed glass coverslips and simultaneously transfected with 0.4 μg of plasmid DNA with Fugene6 (Promega, Madison, WI) according to the manufacturers reverse transfection protocol. Plasmid stocks for transfection were prepared using the Endotoxin-free Maxiprep Kit (MilliporeSigma, Saint Louis, MO). Approximately 24 hours post-transfection, cells were infected with *C. burnetii* in 0.25 mL RPMI with 10% FBS for two hours at 37°C, 5% CO₂, washed extensively with PBS, and incubated in RPMI+FBS. At the indicated times post-infection, the cells were washed 3x in PBS and fixed with 4% paraformaldehyde (PFA) in PBS for 15 minutes. Cells were permeabilized and blocked

by treatment with 0.1% saponin/1% bovine serum albumin (BSA)/PBS for 15 minutes, and then incubated with mouse anti-CD63 (556019; BD Biosciences, San Jose, CA) or rabbit anti-Lamp1 (ab24170; Abcam, Cambridge, MA), and guinea pig anti-*C. burnetii* serum [130] for one hour in saponin/BSA/PBS. Following incubation with AlexaFluor secondary antibodies (Invitrogen, Carlsbad, CA) in saponin/BSA/PBS, coverslips were mounted on glass slides using ProLong Gold with DAPI (Invitrogen), allowed to dry overnight, and visualized using a Leica inverted DMI6000B microscope (63X oil objective). Images were captured using a DFC365FX camera with Leica Application Suite X software (version1.5.0) and formatted for publication using ImageJ software (NIH, Bethesda, MD).

Live cell microscopy

For localization of ORP1L domain GFP constructs, HeLa cells were transfected and infected with mCherry-expressing *C. burnetii* as described above. At 3 days post infection, the cells were collected, plated in ibidi μ -Dishes (ibidi, Verona, Wisconsin), and visualized live on the Leica microscope described above.

For ER localization studies, HeLa cells were transfected with mCherry-CBU_0352 or the mCherry empty vector (EV), as above. After 48 hours, cells were transduced with the ER marker KDEL-GFP CellLights BacMam, expressing GFP fused to the ER signal sequence of calreticulin and the ER retention signal amino acid sequence, KDEL, (ThermoFisher Scientific, C10590, MOI of 10) and incubated overnight. Cells were trypsonized, re-plated on ibidi μ -dish, and allowed to adhere for several hours before

being visualized on Nikon Eclipse Tí inverted light microscope (Nikon Instruments Inc., Melville, NY) with a 100X objective. Images were captured with ORCA-Flash 4.0 LT PLUS Digital CMOS Camera (Hamamatsu Corporation, Bridgewater, NJ) and NIS Elements BR Analysis software (Nikon Instrument Inc.).

Recruitment and PV measurements

Fixed cells were visualized with the Leica microscopy described above, and CD63-positive or Lamp1-positive PVs were visually scored as GFP-positive or negative to determine ORP1L-GFP recruitment. PVs with co-localization between the PV marker (CD63 or Lamp1) and protein of interest were scored as positive. Images were captured using a DFC365FX camera with Leica Application Suite X software (version 1.5.0). For recruitment of ORP1L to wild type and *lcmD* mutant PVs, 15-20 PVs were scored for each of four independent experiments. For PV size measurements, each PV was imaged and the cross-sectional area at the widest part of the PV was measured with ImageJ software.

siRNA knockdown in HeLa cells

ORP1L and non-targeting ON-TARGETplus SMARTpool siRNA duplexes were obtained from GE Dharmacon (Lafayette, CO). HeLa cells (1.2×10^5 cells) were transfected with 50 nM siRNA in 6 well plates using DharmaFECT 1 according to the manufacturer's reverse transfection protocol (GE Dharmacon). Two days later, the cells were infected with *C. burnetii* for one hour as described above, trypsinized, and

transfected a second time with 50 nM siRNA in 24 well plates (2.5×10^4 cells per well). At the given time points, wells were processed for either immunoblotting, FFU growth assay, or IFA. Single target ORP1L siRNA (UGCCAGUGCCGGAUUCUGAdTdT, [103]) was obtained from MilliporeSigma. Cells were transfected with 50 nM siRNA. For immunoblotting, cells were harvested in 2% sodium dodecyl sulfate (SDS) in tris-buffered saline (TBS). Total protein (15 μ g) was separated by SDS-PAGE, transferred to polyvinylidene difluoride (PVDF) membrane (EMD Millipore, Kankakee, IL), blocked in Odyssey Blocking Buffer (P/N 927-40000, LI-COR, Lincoln, NE) diluted 1:1 with PBS, and probed with rabbit anti-ORP1L (Abcam 131165) or rabbit anti-VapB (Abcam ab101113) diluted 1:1000 in 1% BSA/PBS, and mouse anti-GAPDH (ThermoFisher MA5-15738), diluted 1:4000 in BSA/PBS, followed by incubation with LI-COR infrared secondary antibodies (ThermoFisher) diluted 1:10,000 in Odyssey Blocking Buffer/PBS. Blots were imaged using an Odyssey Tc Imager (LI-COR) and bands quantitated using Image Studio Software (LI-COR). ORP1L or VAP knockdown efficiency was calculated by first normalizing to GAPDH, and then to the non-targeting control.

For Rab7 and RILP localization experiments, 2.5×10^4 HeLa cells were transfected with 50nM ORP1L or non-targeting ON-TARGETplus SMARTpool siRNA duplexes in 24-well plates. 24 hours later, cells were transfected with EGFP-Rab7A or RILP-GFP plasmids using standard Fugene6 transfection protocol and incubated overnight. The next day, double-transfected cells were infected with mCherry-expressing *C. burnetii*. 3 days post infection, cells were fixed and stained for IFA. EGFP-Rab7A was a gift from Qing Zhong (Addgene plasmid # 28047 [131]).

Fluorescent Infection Foci Forming Unit (FFU) assay

To quantify bacterial growth in HeLa cells, FFU assays were performed as previously described [50]. Briefly, bacteria were released from infected HeLa cells by incubating for 5 minutes in sterile water and pipetting up and down, followed by serial dilutions in 2% RPMI and addition to Vero cell monolayers in 24-well plates. After 5 days, the cells were fixed with methanol and visualized with Hoechst 33342 Solution (ThermoFisher), and rabbit anti-*C. burnetii* antibody followed by goat anti-rabbit Alexa Flour 488 secondary antibody. Fluorescent foci were visualized using an EVOS FL Auto Imaging System (ThermoFisher) and counted using ImageJ. Each experiment was done in duplicate.

Lentivirus preparation and infection

To generate lentivirus particles, HEK293T cells were plated in a 6-well plate at 1×10^6 cells per well and simultaneously transfected using Fugene6 with packaging and shRNA plasmids: 300ng pCMV-VSV-G, 250ng pRSV-Rev, 500ng pMDLg/pRRE, 1000ng shRNA targeting plasmid. At 24, 48, and 72 hours post transfection, the supernatant was collected, pooled, filtered through a .22 μ M syringe filter, and concentrated approximately 10X using Lenti-X Concentrator (Takara Bio USA) according to the manufacturer's instructions. Concentrated lentivirus was aliquoted and stored at -80°C. Lentivirus concentration in these preparations was quantified using the Lent-X qRT-PCR Titration Kit (Takara Bio USA).

C. burnetii transformation, selection, and anoxic culture

For each transformation, 1 T75 flask containing 20mL of *C. burnetii* anoxic culture was grown for 4 days and pelleted at 19,000 xg for 15 minutes. Bacteria was washed once in 30 mL cold 10% glycerol, pelleted as above, and suspended in 100 μ L cold 10% glycerol. 50 μ L of bacteria was mixed with 10 μ g of plasmid DNA, transferred to an ice cold 0.1 cm electroporation cuvette and electroporated at 1.8 kV, 500 Ω , 25 μ F.

Immediately after electroporation, 950 μ L serum-free RPMI was added and mixed by pipetting. 100 μ L of transformation mix was added to 6mL media in a T25 flask and incubated 24-48 hours at 5% CO₂, 2.5% O₂ before adding appropriate antibiotics for selection (Chloramphenicol at 3 μ L/mL; Kanamycin at 275 μ g/mL). When the culture became turbid (6-12 days, depending on the transfection efficiency), it was passaged to new T25 flasks with 6mL media at several inocula (50 μ L, 100 μ L, or 200 μ L passed). The most dilute initial culture that became turbid within 5-7 days was plated to isolate single clones by limiting dilution in a 96-well plate. 6 days later, wells with single clones were identified and allowed to grow 4 additional days before expanding by transferring the entire culture to 24-well plate wells containing 500 μ L media.

Data analysis

Image processing and PV size measurements were done with ImageJ software (W.S. Rasband, National Institutes of Health, Bethesda, MD). Statistical analyses were performed using appropriate tests in Prism (GraphPad Software, Inc., La Jolla, CA).

Table 1. Primers used in this study	
Primer Name	Sequence
ORP1L-1-F	ATGGACGAGCTGTACAAGATGAACACAGAAGCGGAGCAAC
ORP1L-1-FRET-F	TCAGATCCCCACCGTTATGAACACAGAAGCGGAGCAAC
ORP1L-950-FRET-R	TGGTGGCGACCGGTGGATAAATGTCAATAAATGTCAGGCAAATTG
ORP1L-211-F	ATGGACGAGCTGTACAAGAAACCTCTTGACCTTGCCAGGGTG
ORP1L-510-F	ATGGACGAGCTGTACAAGAGAAAACACAGAATGTCCGAAGAAAAAGAC
ORP1L-237-R	AATATCACTCTGTACATTATCGTTTCAATGCTTTGTAGATGACC
ORP1L-408-R	AATATCACTCTGTACATTAAGAAGCTTCTGAGACAACCTCAAC
ORP1L-950-R	AATATCACTCTGTACATTAATAAATGTCAGGCAAATTGAAG
ORP1L-D478A-F	GCGAGGACGAGTTCTATGCTGCGCTGTCAGATTCCGA
ORP1L-D478A-R	TCGGAATCTGACAGCGCAGCATAGAACTCGTCCTCGC
SG038	AGATTACGCTGTGACATGACTCAAGTCGCGAAGAAAATTCTGG
SG039	GCATGCCTCAGTCGACCCAGTGCTTCAACCTGCC
SG060	TCAGATCCCCACCGTTATGAACACAGAAGCGGAGCAAC
SG061	CATGGTGGCGACCGGTGGCATTCTGTGTTTTCTACTGCCC
SG107	ATCAACAAGTTTGTACATGAACACAGAAGCGGAGCAAC
SG108	ATCAACACTTTGTACAAGAAACCTCTTGACCTTGCCAGG
SG109	TCAACCACTTTGTACAATATCGTTTCAATGCTTTGTAGATGAC
SG110	TCAACCACTTTGTACAATAAATGTCAGGCAAATTGAAG
SG220	TCATAAACACAGCTACGGGTTTGG
SG221	CTTTCACACCTTCAAACGGACC
SG224	TTCCGGCTATGTGACATGCTTATAACAAGGTGTACATTCTTC
SG225	GCATGCCTCAGTCGATTAAAGCTTATAACAAGGTGTACATTCTTC
SG240	CATGCCTCAGTCGACTTAAAGCTTATAACAAGGTGTACATTC
SG241	CGATGACAAGGTCGACATGCATACTCACGAACATC
SG242	TGTAGTCCATCTGCAGAAGCTTATAACAAGGTGTACATTC
SG243	CATGAAGGAGGCTGCAGATGCATACTCACGAACATCATC
SG257	TCCCAGGCATTTATACGCCAAC
SG258	TCCGTTGAGAGTATGCCGCTACC
SG259	GTGGCTCTGCTTGAAACACTAGTGC
SG260	AATTGCAAACACTGGGGCCTATGG
SG261	ACCAGCTAATGGAGACAGTCATACTGG
SG262	TCACCCTTAAACTCAGCGCTTGC
SG350	ATGGATGAGCTGTACATGCATACTCACGAACATCATCATCA
SG351	TCAACCACTTTGTACCTTTGTTATTAAAGCTTATAACAAGGTGTACATTCTTCA
SG289	CACCGTGTGTGCATAACATCATCGT
SG290	AAACACGATGATGTTATGCACACAC
SG291	CACCGCTGAGATGAGCCTAAACCCA

Table 1, continued	
SG292	AAACTGGGTTTAGGCTCATCTCAGC
SG293	CACCGGCATGGAATGCACTGATTGG
SG294	AAACCCAATCAGTGCATTCCATGCCGGTC

Chapter III. ORP1L is specifically recruited to the PV by *C. burnetii*

ORP1L co-localizes with PV marker CD63

ORP1L was previously localized to the PV membrane by live cell imaging. To confirm this finding, HeLa cells transfected with ORP1L-GFP and infected with wild type *C. burnetii* were analyzed by IFA and stained for CD63. CD63, also known as lysosomal-associated membrane protein 3 (Lamp3), is a lysosome and PV marker used to delineate the *C. burnetii* PV membrane [132]. ORP1L clearly co-localizes with CD63 (Figure 4), confirming that ORP1L indeed localizes to the PV membrane during *C. burnetii* infection.

ORP1L ankyrin repeats are necessary and sufficient to localize GFP to the PV membrane

ORP1L contains multiple domains responsible for both protein-protein and protein-lipid interactions (Figure 5A). Three N-terminal ankyrin repeats interact with the small GTPase Rab7 [133]. ORP1L association with the ER is mediated through an FFAT motif that binds the ER protein VAP [102]. The pleckstrin homology (PH) domain binds with low affinity and high specificity to the signaling lipids PI(3,4)P₂ and PI(3,4,5)P₃ [100], while the C-terminal ORD binds cholesterol and several oxysterol species [134, 135]. To identify the ORP1L domain(s) responsible for PV localization, we generated GFP fusions of the ORP1L domains and assessed their localization using live cell imaging of *C. burnetii*-infected cells (Figure 5B, C). Like wild type ORP1L, ORP1L with a mutated FFAT motif localized to the PV. Removal of the cholesterol-binding domain (Δ ORD) did not alter the PV localization and the ORD domain by itself was cytoplasmic, indicating

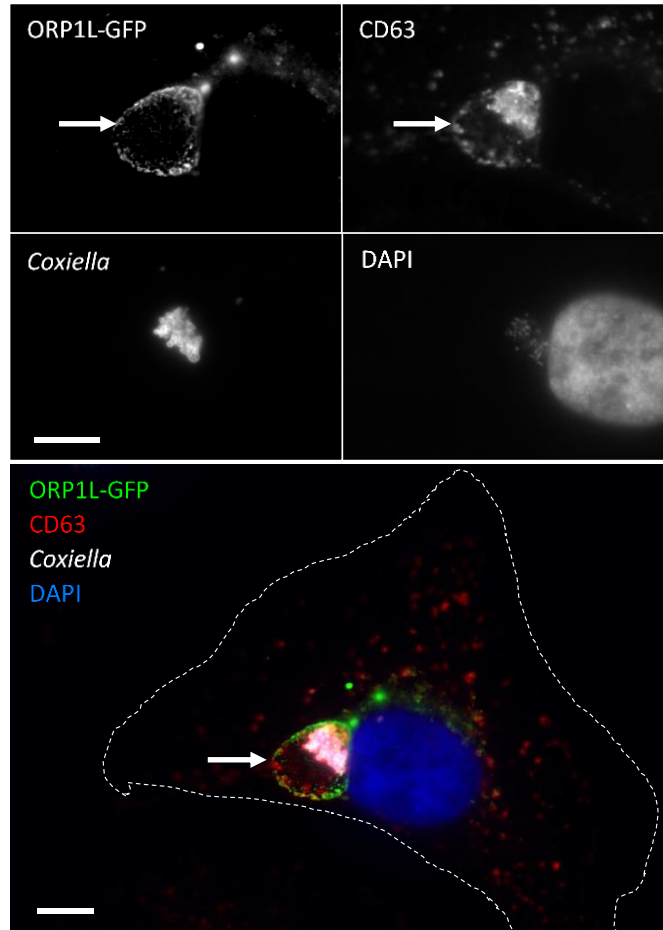
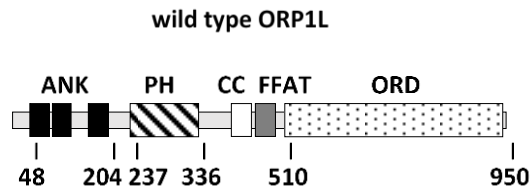


Figure 4. ORP1L co-localizes with CD63 on the PV membrane

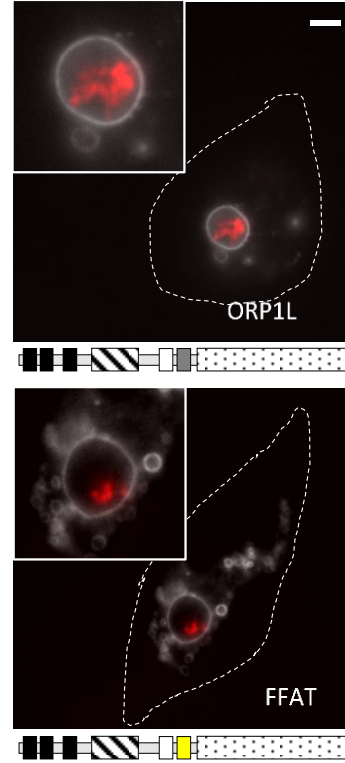
Fixed immunofluorescence microscopy images of uninfected or infected HeLa cells expressing ORP1L-GFP. ORP1L-GFP localizes to the PV membrane in HeLa cells infected for three days with wild type *C. burnetii*. Cell boundary is shown with dotted white line. CD63 is a marker for the PV membrane. Scale bars = 10 μm .

cholesterol is not significantly involved in ORP1L PV localization. In addition to cholesterol, the signaling lipids PI(3,4)P₂ and PI(3,4,5)P₃ also appear to be insufficient for PV localization, as GFP fusions of the phosphoinositide-binding PH domain was also

A



B



C

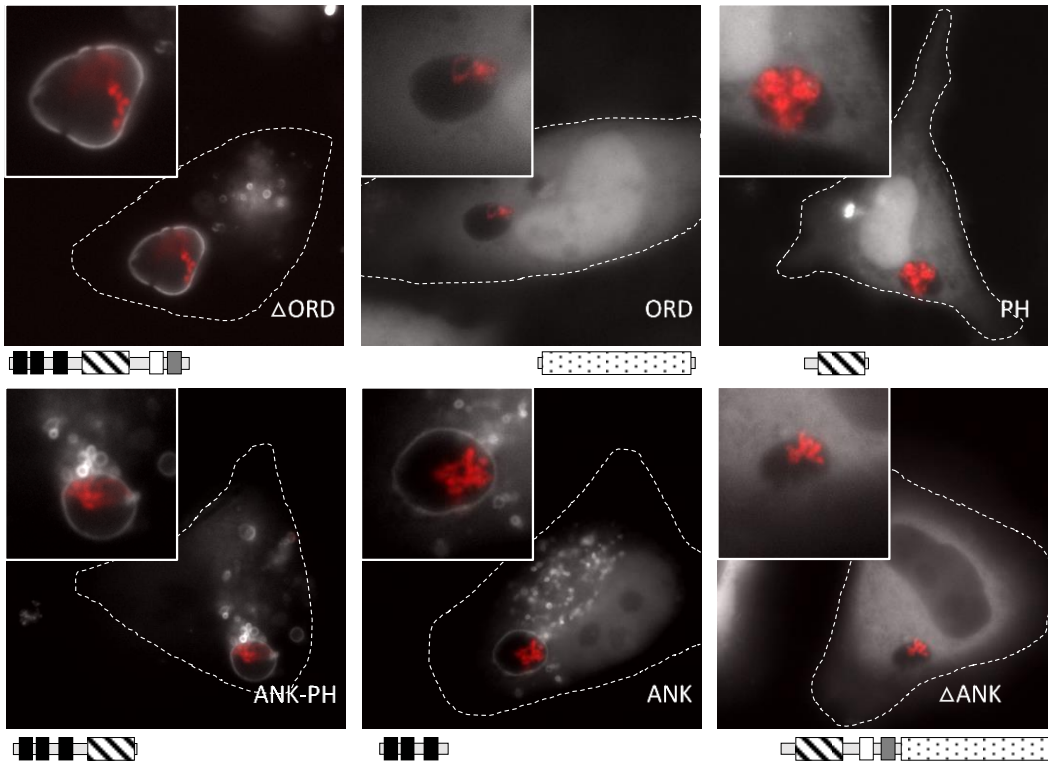
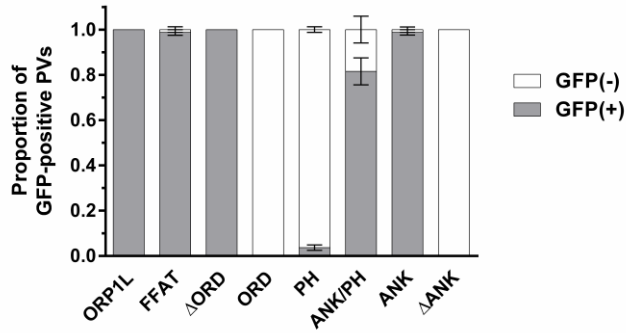


Figure 5. Ankyrin repeat domains are necessary and sufficient to target ORP1L to the PV

(A) Stick diagram of ORP1L protein domains. ANK = ankyrin repeats (black), PH = plekstrin homology domain (stripe), CC = coiled-coil domain (white), FFAT = two phenylalanines in an acidic tract (gray), ORD = OSBP-related ligand binding domain (dots). Numbers represent amino acid position. (B) HeLa cells were transfected with C-terminal GFP constructs and infected with mCherry-expressing *C. burnetii*. Domain constructs are represented below each image. At 3 days post infection, live cells were imaged by wide field fluorescence microscopy. FFAT mutant (D478A) (magenta), Ank-PH, and Ank localize to the PV membrane, while ORD, Δ Ank, and PH remain cytoplasmic without PV membrane localization. Green = ORP1L-GFP, Red = mCherry-*C. burnetii*. Scale bar = 10 μ m. (C) Quantification of PV localization of ORP1L domain constructs. Shown are the results from two independent experiments, with at least 30 PVs per condition per experiment. Error bars represent SEM.

cytoplasmic with no PV association. In contrast, PV localization was observed for both the ORP1L ankyrin repeat domain along with the PH domain (Ank-PH) and the ORP1L ankyrin repeat domain alone (Ank). To determine if the ankyrin repeats are required for PV association, we generated an ORP1L ankyrin truncation mutant (Δ Ank). Δ Ank-GFP did not localize to the PV and was cytoplasmic, demonstrating that the N-terminal ankyrin repeats are necessary and sufficient for ORP1L association with the PV. Further, these data show that protein-protein interactions, and not protein-lipid interactions, are primarily responsible for ORP1L PV localization.

Active *C. burnetii* Type IVB Secretion System is required for ORP1L recruitment

The *C. burnetii* T4BSS transports bacterial effector proteins across the PV membrane and into the host cell cytoplasm where they manipulate host cell functions

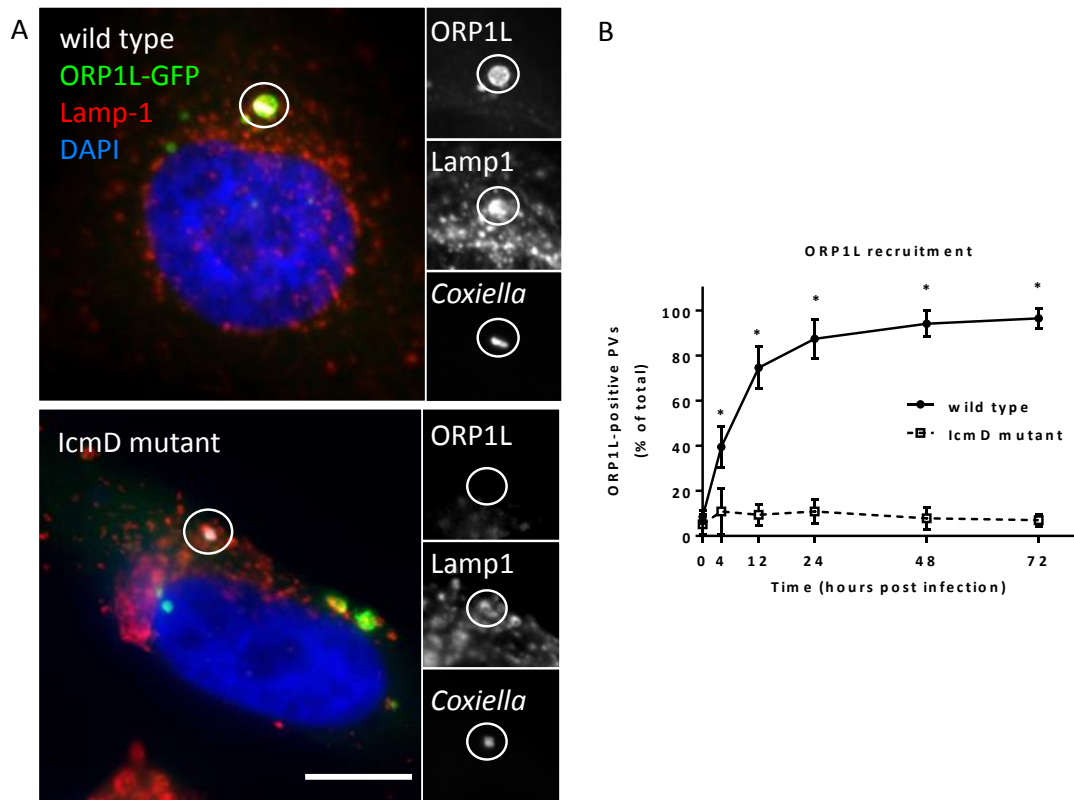


Figure 6. ORP1L PV localization is T4BSS-dependent

Light microscopy images of HeLa cells transfected with ORP1L-GFP and then infected with *C. burnetii* for 2 days (A). ORP1L-GFP is recruited to the PV of wild type (top) but not lcmD mutant (bottom) bacteria. Green = ORP1L-GFP, Red = Lamp1, Gray = *C. burnetii*, Blue = DAPI. The PV (circled) is shown magnified with individual fluorescent channels. Scale bar = 10 μ m. (B) The number of ORP1L-positive PVs was quantified over a 72 hour time course of infection in HeLa cells infected with wild type (solid) or lcmD mutant (dashed) *C. burnetii*. Cells were transfected with ORP1L-GFP, infected, stained for *C. burnetii* and Lamp1, and visually scored for the presence or absence of ORP1L on the PV. Each data point represents the average of 3 or 4 experiments, with at least 20 PVs counted per experiment. Error bars represent standard error of the mean (SEM). Means for each condition within a timepoint were compared by the Holm-Sidak method of multiple t-tests. * = $p < 0.01$.

such as vesicular trafficking and apoptosis (reviewed in [136]). T4BSS effector proteins recruit several host cell proteins to the PV including clathrin [137] and LC3 [138]. To determine if the T4BSS or secreted effectors are involved in ORP1L PV localization, we examined ORP1L-GFP-expressing cells infected with either wild type *C. burnetii* or a *C. burnetii* mutant lacking *lcmD*, an essential component of the T4BSS [73]. Cells were fixed and stained for *C. burnetii* and Lamp1, a lysosomal protein that also serves as a marker for the *C. burnetii* PV. Unlike PVs harboring wild type bacteria, ORP1L-GFP did not localize to PVs containing the *lcmD* mutant (Figure 6A). When quantified, over 85% of wild type PVs were ORP1L-positive by 24 hours post infection, with nearly 95% being positive by 48 hours (Figure 6B). In contrast, less than 10% of the *lcmD*-mutant PVs were positive at any point during a 72 hour infection, demonstrating that the T4BSS is required for ORP1L localization to the *C. burnetii* PV.

ORP1L is recruited early during infection, prior to PV expansion

T4BSS-dependent localization of ORP1L to the PV could occur either through fusion with endosomes, or through direct recruitment by a PV-associated protein. ORP1L does not contain transmembrane domains, and membrane association requires binding to membrane proteins and lipids. We therefore hypothesized that ORP1L interacts with the PV by protein-protein or protein-lipid interactions, and is not delivered through membrane fusion events during PV expansion. To test this, we assessed the timing of PV expansion relative to ORP1L PV localization. To determine when PV expansion occurs in HeLa cells, we measured PVs harboring either wild type or

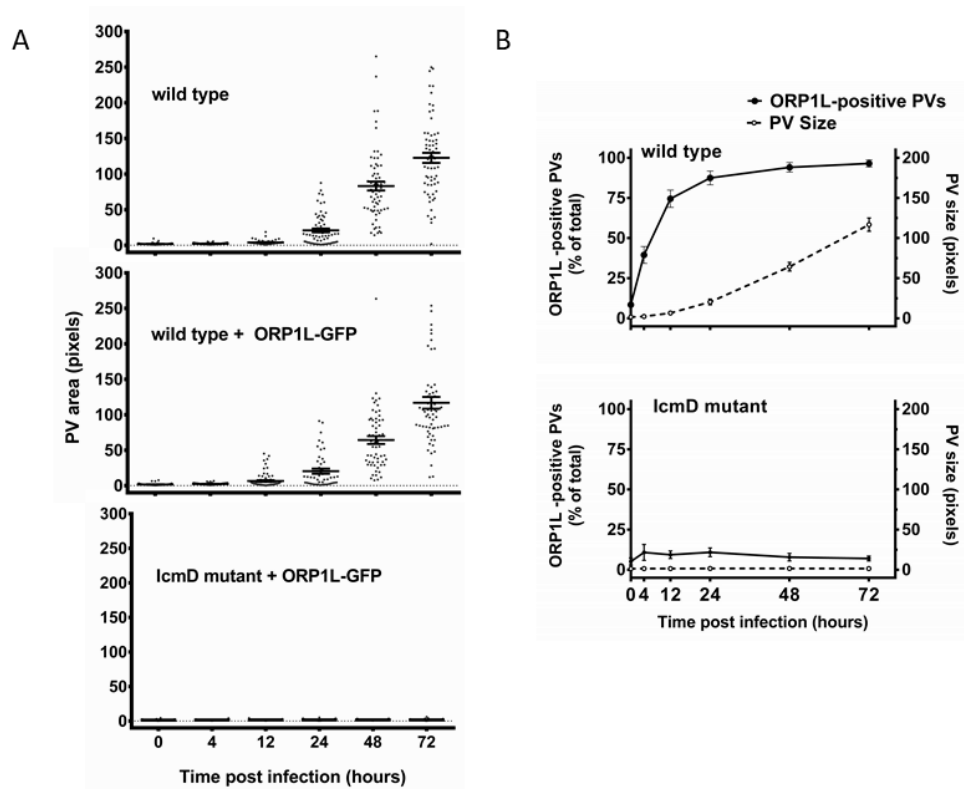


Figure 7. ORP1L is recruited to the PV prior to significant expansion
 Measurements of PV size shows that PVs harboring wild type bacteria expand between 24 and 48 hours, while lcmD mutant PVs do not expand (A). HeLa cells, untransfected or expressing ORP1L-GFP, were infected with either wild type *C. burnetii* or the lcmD mutant. At the indicated times, the cells were fixed, stained for *C. burnetii* and CD63, and the PVs measured using ImageJ. PVs harboring wild type bacteria expanded between 24 and 48 hours, while lcmD PVs did not expand. Shown are individual PV measurements from three separate experiments, with at least 20 PVs per timepoint per experiment. Bars represent mean \pm SEM. (B) Comparison of ORP1L localization compared to PV expansion; ORP1L localizes to the PV 12 hours prior to significant expansion of wild type PVs (top). Error bars represent SEM.

lcmD mutant bacteria during a 72 hour infection time course (Figure 7A). PVs harboring lcmD mutant bacteria never expanded although a very small amount of replication was observed. This is consistent with the role of the T4BSS in PV fusion and expansion [73, 80]. For wild type bacteria, a small amount of expansion was observed by 24 hours, with the vast majority of PVs expanding between 24 and 48 hours. At 48 hours post infection, there was a small but statistically significant difference in PV size between untransfected and ORP1L-GFP transfected cells (Figure 8). However, the timing of expansion was identical, suggesting that ectopic expression of ORP1L-GFP does not affect the overall timing of expansion. When PV size was compared to ORP1L PV localization in wild type PVs, ORP1L was present on the PV prior to significant expansion and therefore before significant fusion of additional vesicles with the PV (Figure 7B). Furthermore, ORP1L recruitment was independent of PV size, as wild type ORP1L-positive PVs were nearly identical in size to lcmD mutant ORP1L-negative PVs at early time points (Figure 7A). Based on these data, we hypothesize ORP1L is directly recruited by a PV membrane-localized protein prior to PV expansion.

ORP1L is recruited independently of another endosomal PV marker

ORP1L binds Rab7 [100], a late-endosomal protein that also localizes to the PV and plays a role, though the mechanism remains unknown, in PV biogenesis [56, 139]. We hypothesized that the lack of ORP1L on lcmD mutant PVs could be due to the absence of a binding partner, Rab7. We observed, however, that Rab7 localizes to both wildtype and lcmD mutant PVs, whereas ORP1L only localizes to wild type PVs (Figure

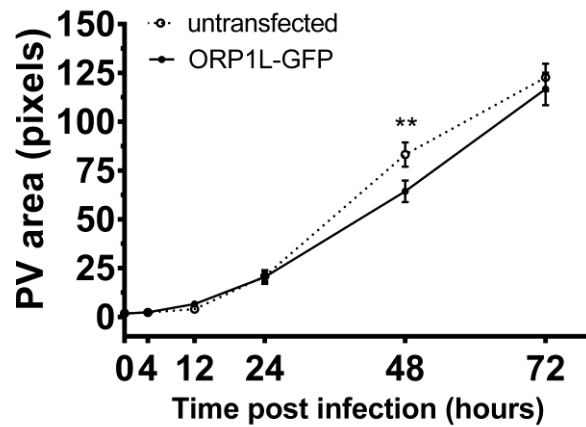


Figure 8. PV size in untransfected and ORP1L-GFP expressing cells

At 48 hours post infection, wild type PVs in cells ectopically expressing ORP1L-GFP are smaller than untransfected cells. Error bars represent SEM. Means were compared by ordinary one-way ANOVA with Sidak's multiple comparisons tests. ** = $p < 0.01$.

6B). Moreover, the kinetics of Rab7 localization was nearly identical in the first 24 hours, at which time nearly 90% of both wild type and lcmD mutant PVs were Rab7 positive (Figure 9). Interestingly, PVs harboring the lcmD mutant began to lose Rab7 localization after 24 hours, suggesting the T4BSS is necessary to retain or acquire additional Rab7 at later time points. This data indicates, at least during early PV development, ORP1L is recruited independently from Rab7.

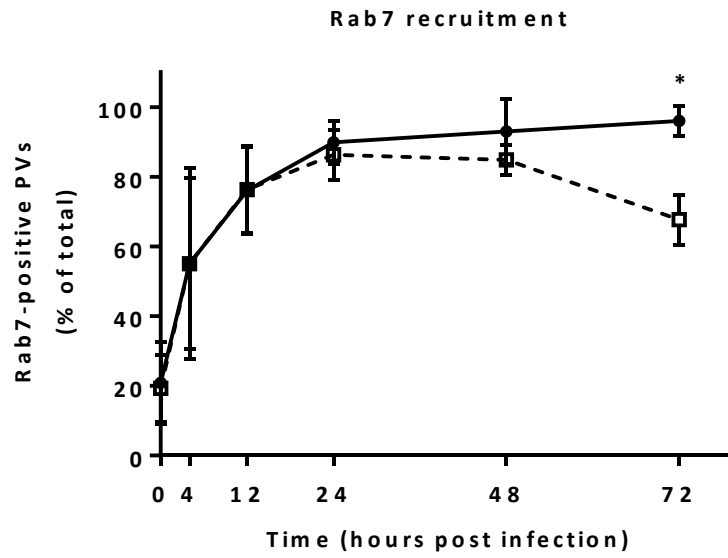


Figure 9. ORP1L is recruited to the PV independently of Rab7

The number of Rab7-positive PVs was quantified over a 72 hour time course of infection in HeLa cells infected with wild type (solid) or lcmD mutant (dashed) *C. burnetii*. Cells were transfected with Rab7-GFP, infected, stained by immunofluorescence for *C. burnetii* and Lamp1, and visually scored for the presence or absence of Rab7 on the PV. (Same procedure as for ORP1L in Each data point represents the mean from 3 or 4 independent experiments, with 20 PVs counted per experiment. Error bars represent standard deviation. Data from each condition within a timepoint was compared by the Holm-Sidak method of multiple t-tests. * = p-value <0.05.

Tn235 *C. burnetii* exhibits a decrease in ORP1L recruitment

In order to investigate which *C. burnetii* effector protein or proteins are involved in recruiting ORP1L to the PV, we utilized mutants with transposon insertions in genes encoding known or predicted T4BSS effector proteins [140]. These mutants also

express GFP. *IcmD* mutant bacteria, which we have previously shown does not recruit ORP1L to the PV (Figure 6B), were a negative control. HeLa cells transfected with ORP1L-mCherry were infected with wild type or mutant *C. burnetii*, allowed to grow for 3 days and processed for IFA. PVs were scored as mCherry positive or negative and as expected, greater than 95% of wild type PVs were ORP1L-positive and fewer than 5% of *IcmD* mutant PVs were ORP1L-mCherry positive (Figure 10A). Interestingly, disruption of the *IcmS* gene did not disrupt ORP1L recruitment. *IcmS* encodes for half of the *IcmSW* chaperone which is required for secretion of a subset of T4BSS effector [69, 141]. This mutant is predicted to be deficient in the secretion of several effector proteins, yet it does not significantly affect ORP1L recruitment, supporting the hypothesis that ORP1L recruitment is the result of the action of a specific effector and not general T4BSS function. One effector mutant was significantly deficient in ORP1L recruitment to the PV. Only 50% of mutant 235 PVs were ORP1L-positive at 3 days post infection (Figure 10), indicating that the transposon in mutant 235 disrupted a gene involved in ORP1L recruitment.

Once we identified a mutant that was deficient in ORP1L recruitment to the PV, we next sought to confirm the location of the transposon within the bacterial genome and determine whether we had a clonal population. To this end, we designed a primer set centered about the genomic locus where the transposon was reported to have inserted in this strain, nt 457 of the *cbu0352* gene [140] (Figure 11A). Genomic DNA was isolated from mutant 235 or wild type *C. burnetii* and the *cbu0352* locus was amplified by PCR, revealing that both the wild type and mutant *cbu0352* locus was present in the

mutant 235 stock. This could indicate that either a gene duplication event has occurred, resulting in multiple copies of the *cbu0352* being present, or that the strain is a mixed population of wild type and mutant bacteria. We next isolated single clones of mutant 235 by limiting dilution in ACCM-2 media. After expanding these clonal populations and screening the *cbu0352* locus by PCR as above, we observed that each clonal population

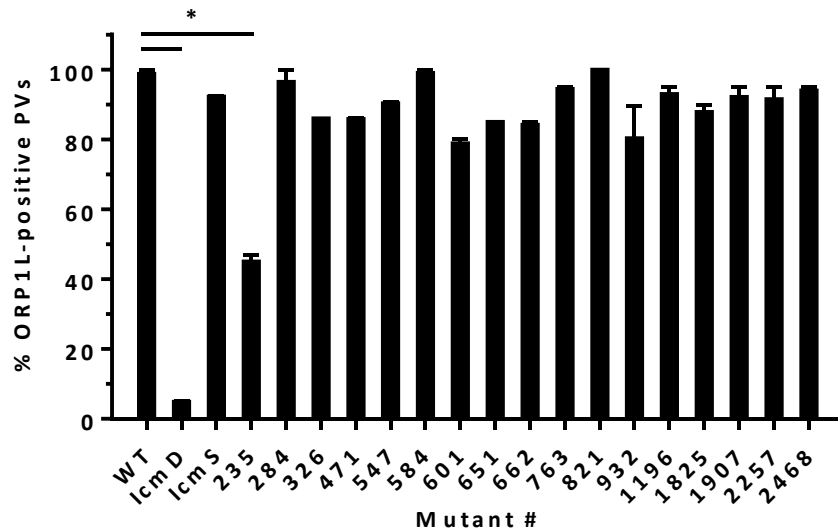


Figure 10. Mutant #235 is deficient in ORP1L recruitment

Proportion of ORP1L-positive PVs in HeLa cells 72 hpi with wild type (WT) or mutant *C. burnetii*. Cells were transfected with ORP1L-mCherry, infected, stained by immunofluorescence for *C. burnetii* and CD63, and visually scored for the presence or absence of ORP1L on the PV. Data are represented as the mean from two independent experiments with bars representing range. Each group was compared to WT by repeated measures one-way ANOVA with Greenhouse-Geisser correction and Dunnett's multiple comparisons. * = $p < 0.05$.

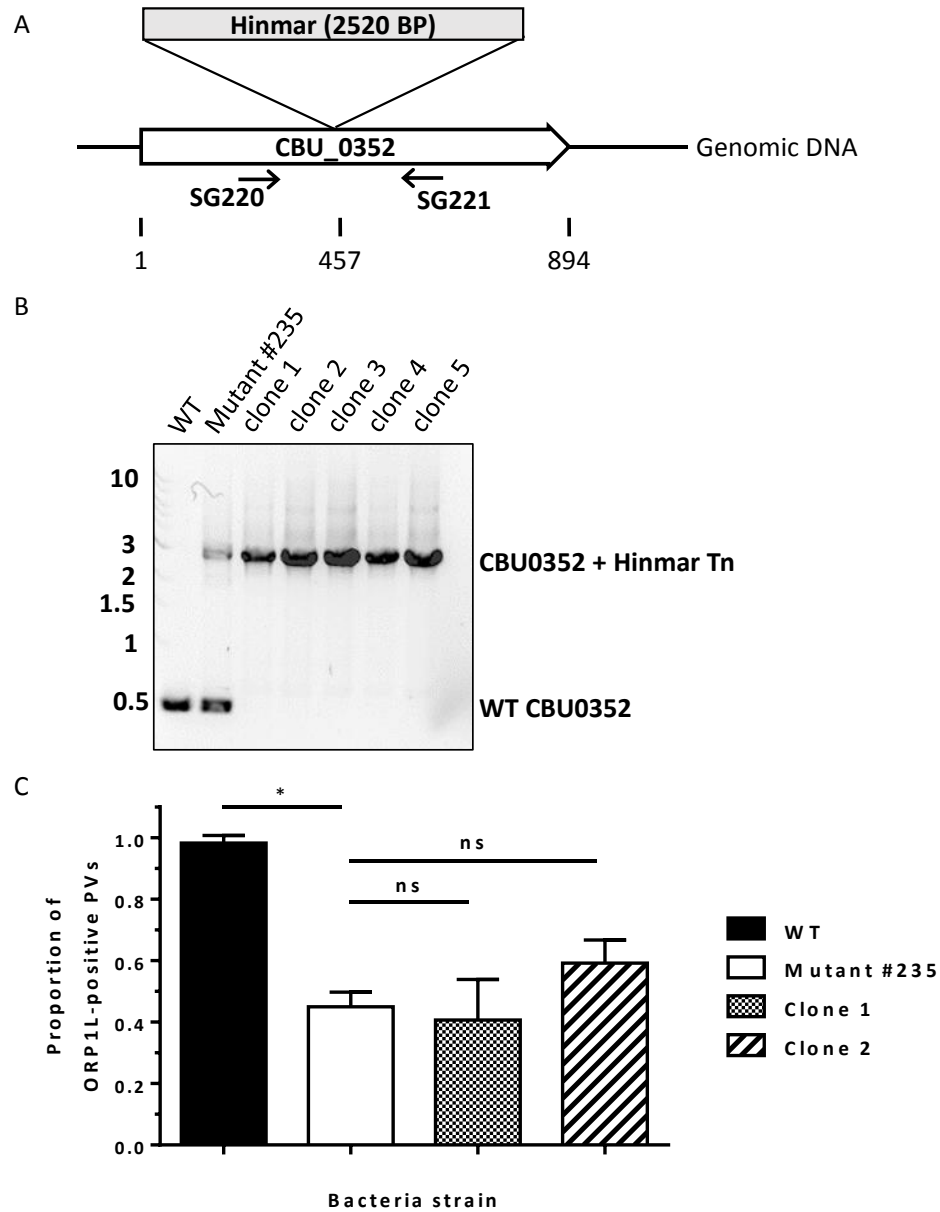


Figure 11. *cbu0352* mutant clones are deficient in ORP1L recruitment

(A) Diagram of the *cbu0352* genomic locus, showing the Hinmar transposon insertion site at nt 457 and the primers used to screen for the insertion (SG220 and SG221). (B) The *cbu0352* locus was amplified from wild type, Tn235 population, or clonal Tn235 *C. burnetii* genomic DNA and products were separated by electrophoresis on an agarose gel. All clonal population contain only the mutant *cbu0352* locus. (C) Proportion of ORP1L-positive PVs in cells infected with wild type (WT), Mutant #235, Tn352 clone 1, and Tn352 clone 2 *C. burnetii*. Data are represented as means from two independent experiments with bars representing range. Each group was compared to Mutant #235 by repeated measures one-way ANOVA with Dunnett's multiple

only carried mutant *cbu0352* loci (Figure 11B). This result indicates that the mutant 235 stock was a mixed population. All subsequent experiments were performed with the clonal population.

We next interrogated the ORP1L recruitment phenotype of the Tn235 mutant clones. At 3 days post infection, mutant clones have approximately the same proportion of ORP1L-positive PVs compared to the mixed population (Figure 11C). Together, these data indicate that CBU_0352 is involved in ORP1L recruitment to the *C. burnetii* PV, though this interaction may occur by either a direct or indirect mechanism.

Heterologously expressed CBU_0352 localizes to the host ER

CBU_0352 has not been functionally characterized in previous works, but is reported to contain an E-block motif, the T4BSS secretion signal, based on computational analysis [141], making it a putative effector protein. CBU_0352 is annotated as a cobalt-zinc-cadmium resistance protein, CzcD, having homology to transmembrane cation transporters that are present in a broad range of bacterial species.

In order to determine the possible subcellular localization of this *C. burnetii* protein within the host cell, we ectopically expressed CBU_0352 fused to mCherry in HeLa cells. Because CBU_0352 is involved in recruiting ORP1L to the PV membrane, we hypothesized that CBU_0352 would be present on the PV as well. To test this, we infected HeLa cells expressing mCherry-CBU_0352 with wild type NMII *C. burnetii*. At

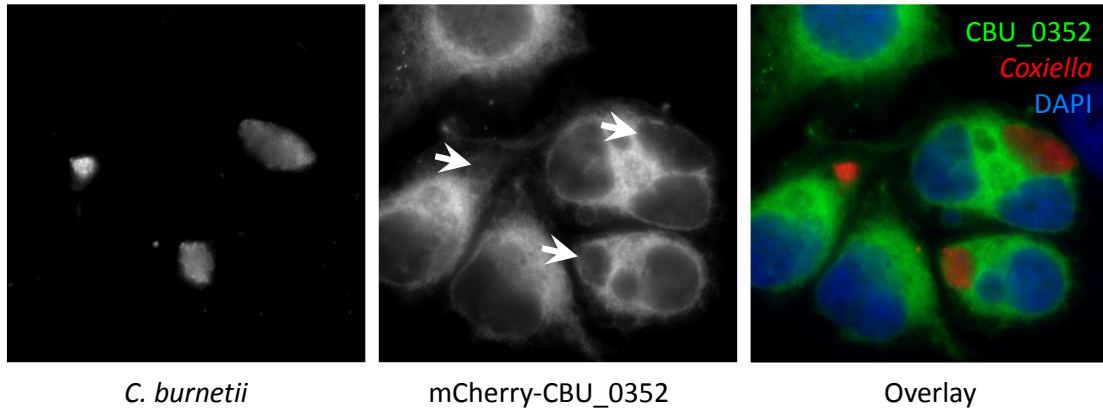


Figure 12. Heterologously expressed CBU_0352 does not localize to the *C. burnetii* PV

HeLa cells were transfected with mCherry-CBU_0352, infected with wild type *C. burnetii*, fixed, and stained by immunofluorescence for *C. burnetii*, and observed. CBU_0352 does not localize to the lumen or membrane of the PV. It does, however, appear to localized to a network throughout the host cytoplasm. Arrows indicate PV.

four days post infection, we observed no CBU_0352 on the PV membrane (Figure 12). We did, however, observe that heterologous CBU_0352 is present throughout the cell and exhibits a striated pattern. ORP1L on the PV co-localizes with the ER, so we tested whether CBU_0352 may also co-localize with an ER-localized GFP in these cells. We observed significant co-localization between ER-GFP and mCherry-CBU_0352 (Figure 13). This data suggests that, if secreted, CBU_0352 could localize to the host ER, though further investigation is needed to determine if bacterially expressed CBU_0352 also localizes to the ER.

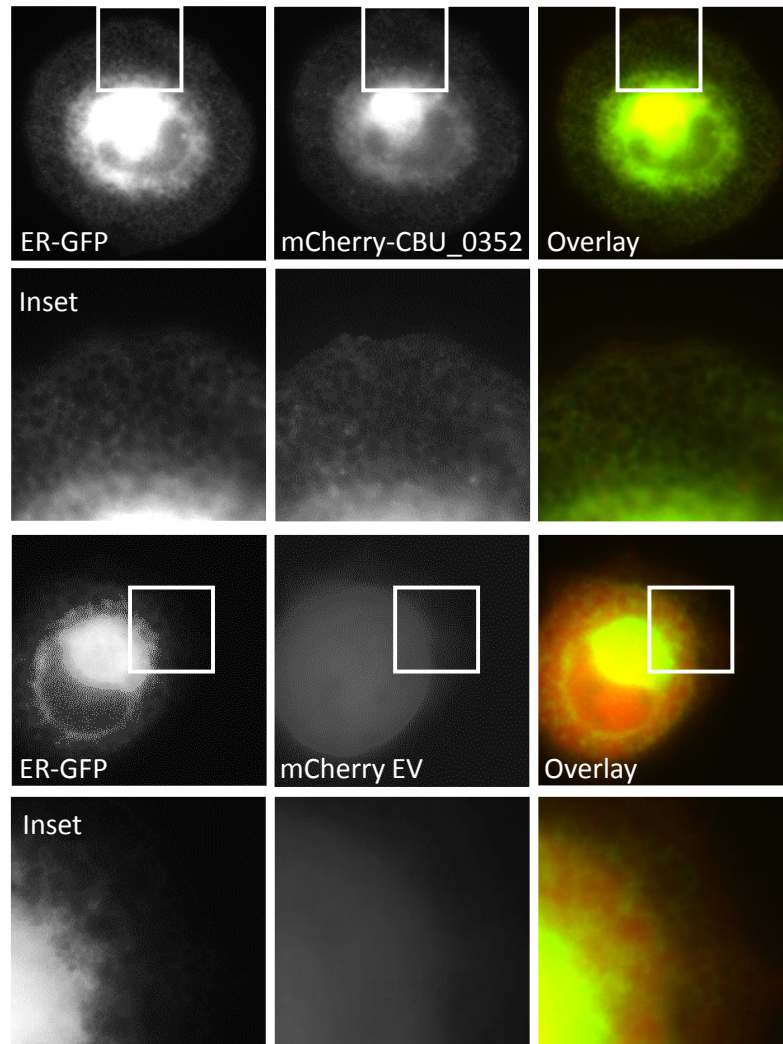


Figure 13. Heterologously expressed CBU_0352 localizes to the host ER

Live cell fluorescence microscopy images of *C. burnetii*-infected HeLa cells expressing ER-localized green fluorescent protein and mCherry-CBU_0352 or mCherry empty vector (EV). CBU_0352 co-localizes with the host ER. Red = mCherry-CBU_0352, Green = ER-GFP. Boxed area magnified in inset.

Chapter IV. ORP1L participates in membrane contact sites between the PV and ER and modulates PV dynamics during *C. burnetii* infection

ORP1L exhibits a striated localization pattern on the PV which is abrogated by mutating the FFAT motif

Using confocal microscopy to more precisely define ORP1L localization on the PV membrane, a striking ER-like reticulate pattern was observed. This was seen most clearly when looking at the surface of the PV membrane (Figure 14A). We hypothesized that the PV ORP1L reticulate pattern was due to ORP1L interacting with the ER via the FFAT motif. To test this, we mutated the FFAT motif such that it could no longer bind to VAP and examined the ORP1L pattern on the *C. burnetii* PV. While the ORP1L FFAT mutant still localized to the PV, the reticulate pattern was lost (Figure 14B), suggesting PV-associated ORP1L also binds to VAP on the ER.

ORP1L localizes to PV-ER membrane contact sites

To further confirm this observation, we tested for co-localization between PV-associated ORP1L and the ER marker KDEL-RFP (red fluorescent protein) [see Materials and Methods]. We observed significant overlap between PV-associated ORP1L-GFP and KDEL-RFP (Figure 15), demonstrating that ORP1L can simultaneously interact with both the PV and the ER. Together with the domain studies, these data suggest that PV-associated ORP1L binds to a PV membrane protein via the ankyrin repeats, while the FFAT motif binds to VAP on the ER cytosolic surface. The finding that ORP1L

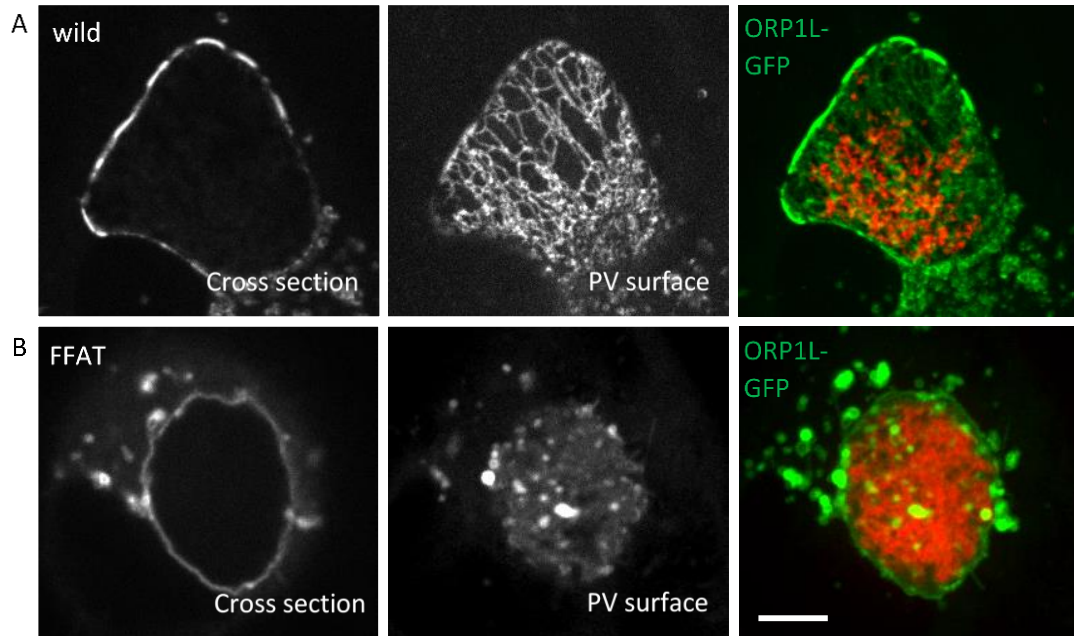


Figure 14. ORP1L exhibits FFAT motif-dependent striated pattern on the PV

Live cell confocal microscopy images of ORP1L-GFP on the *C. burnetii* PV. HeLa cells were transfected with wild type ORP1L-GFP (A) or FFAT mutant, ORP1L (D478A)-GFP (B). Three days after infection with mCherry-expressing *C. burnetii*, the PVs were identified by phase microscopy and fluorescence imaged by live cell spinning disk confocal microscopy. When the surface of the PV is examined, wild type ORP1L exhibits a striated pattern. This pattern is disrupted by the FFAT D478A mutation, which prevents binding to the ER protein VAP. Red = *C. burnetii*, Green = ORP1L-GFP. Scale bare = 10 μ m.

simultaneously associates with both the PV and the ER suggests the presence of membrane contact sites (MCS) between these two membranes. MCS are sites where membranes closely interact with an intermembrane distance of approximately 10-30 nm, or the length of a single protein. Given that this is the first indication of MCS

between the *C. burnetii* PV and ER, our lab used transmission electron microscopy (TEM) and electron tomography (ET) to more closely define the interactions between these two membranes. By TEM, the ER was found in close apposition to the PV membrane at several sites in HeLa cells (Figure 16A). Close interactions were also observed between

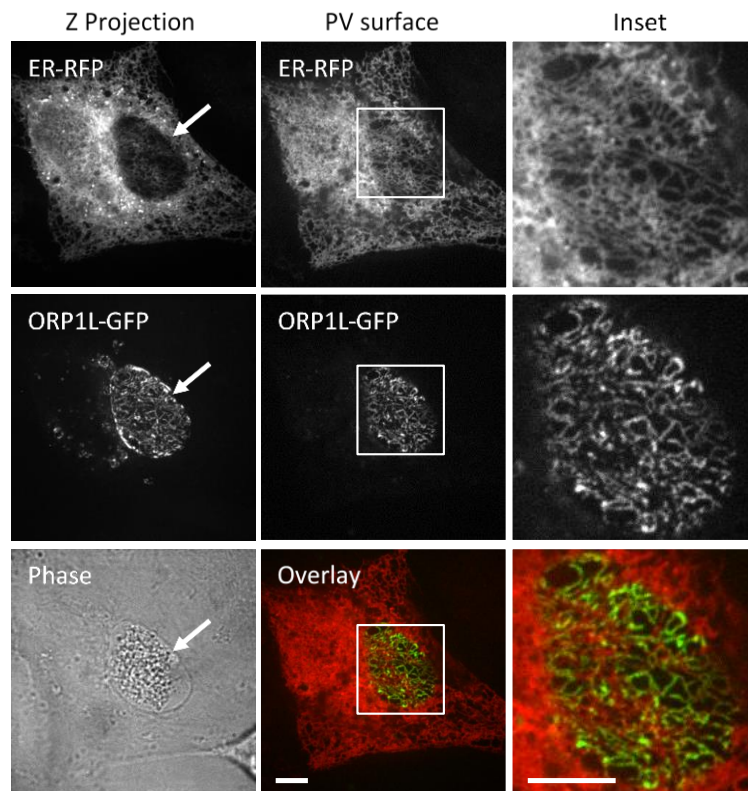


Figure 15. ORP1L on the PV co-localizes with the ER

Live cell fluorescence microscopy images of *C. burnetii*-infected HeLa cells expressing ER-localized red fluorescent protein (KDEL-RFP) and ORP1L-GFP. The maximum Z projection shows the flattened confocal stack through the entire cell, while the PV surface is a confocal slice of the top surface of the PV (arrows indicate PV membrane). Magnification of the boxed PV (Inset) shows that ORP1L-GFP on the PV co-localizes with the host ER. Red = ER, Green = ORP1L-GFP. Scale bars = 10 μ m.

the PV and ER in Vero epithelial cells and THP-1 human macrophage-like cells (Figure 16 B, C), indicating this interaction is not cell type specific. Using ET to generate a higher resolution 3-D structure, the laboratory identified numerous PV-ER MCS with less than 20nm distance between the two membranes as well as sites where the PV and ER appear to be in direct contact [122]. These data demonstrate the presence of novel membrane contact sites, on the scale of a protein complex, between the *C. burnetii* PV and the host endoplasmic reticulum.

Disruption of ORP1L -containing protein complexes results in larger PVs

As ORP1L is specifically recruited by *C. burnetii* to PV, we next explored the function of ORP1L on the vacuole. Our results suggest that ORP1L binds to both an unknown PV-localized protein (via N-terminal ankyrin repeats) and the ER protein VAP (through the FFAT domain), forming a multi-protein complex bridging the PV and ER membranes. We next asked if disrupting the ORP1L protein complex affects PV formation.

To disrupt PV-ER MCS we first employed a dominant negative approach. HeLa cells expressing ORP1L-GFP, the FFAT mutant ORP1L (D478A)-GFP, Δ Ank-GFP, or GFP alone were infected with *C. burnetii* and PVs measured at 48 hours post infection (Figure 17). Compared to cells expressing cytoplasmic GFP, ORP1L-GFP overexpression did not result in statistically significant changes in PV size. The D478A mutation disrupts the FFAT motif in ORP1L. This mutant localizes to the *C. burnetii* PV, but cannot bind to VAP on the ER. The Δ Ank mutant is not prevented from interacting with ER, but does not

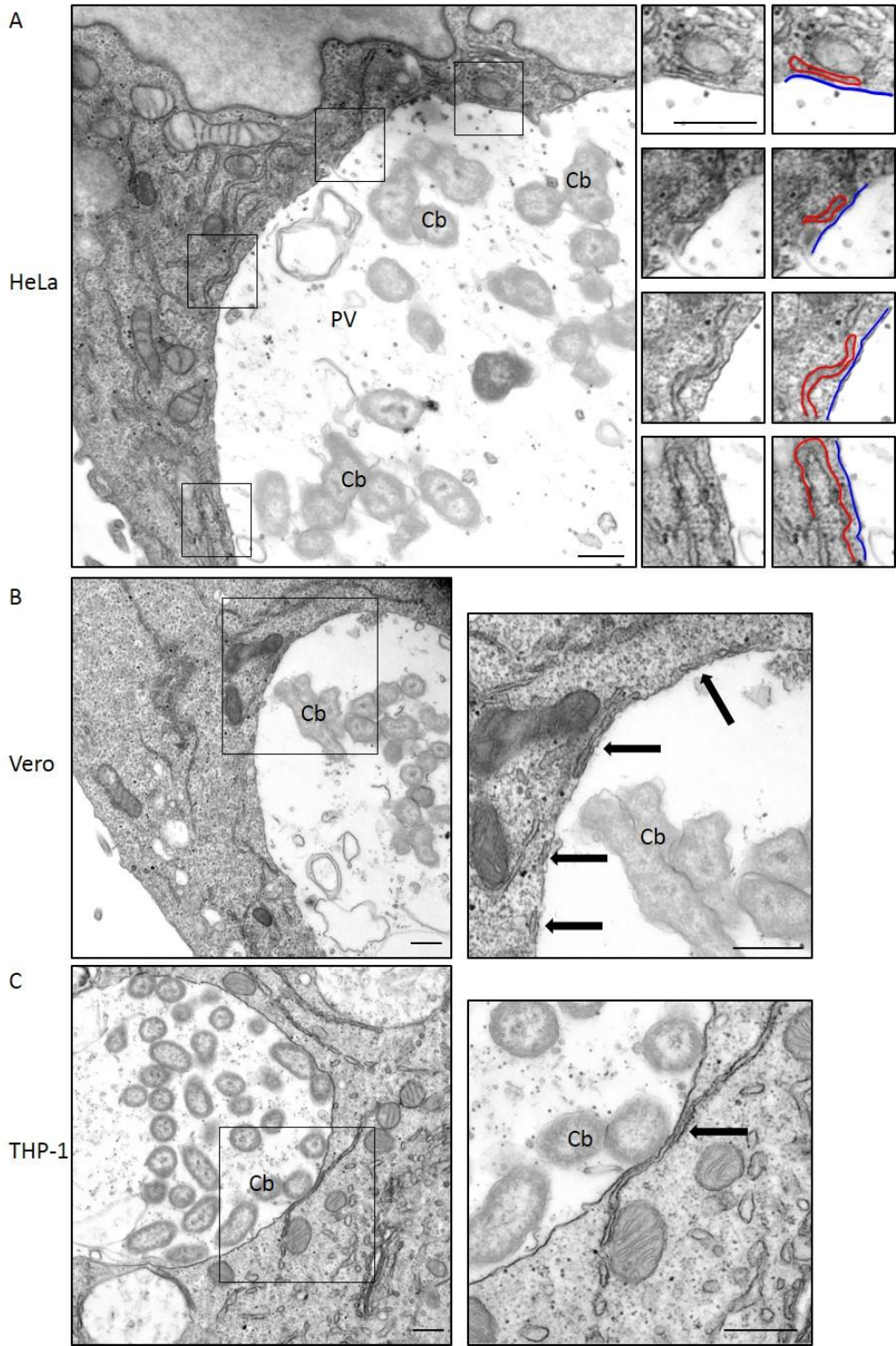


Figure 16. Electron microscopy reveals membrane contact sites between the PV and ER

Transmission electron micrographs of HeLa (A), Vero (B), and THP-1 (C) cells infected with *C. burnetii* for 1 day (THP-1) or 2 days (HeLa, Vero). (A) The boxed areas are further magnified, showing areas where the PV membrane (outlined in blue) and ER membrane (red) are in close proximity. (B, C) Magnified areas are boxed and arrows show PV-ER MCS. Cb = *C. burnetii*; PV = parasitophorous vacuole. Scale bars = 200 nm.

localize to the PV (Figure 17A). Ectopic expression of either D478A or Δ Ank ORP1L- GFP results in larger PVs than expressing wild type ORP1L-GFP or GFP alone (Figure 17B). This suggests disrupting PV-ER MCS has a positive effect on PV size.

Our next approach to disrupt the ORP1L-containing MCS was to reduce expression of the ER-localized ORP1L binding partner, VAP, using a pool of four siRNAs. At day 4 post infection, the PVs in VAP depleted cells were significantly larger than PVs in control cells throughout infection (Figure 18). This indicates that disrupting PV-ER membrane contact sites allows the PV to expand more quickly early during infection while PV expansion is somewhat delayed in control cells. Together with previous data, this indicates that disrupting the PV-ER membrane contact sites results in increased PV size, indicating that contact with the ER may contribute to limiting PV expansion.

Reduced ORP1L expression results in reduced PV size but no change in bacterial growth

To further understand the role of ORP1L during *C. burnetii* colonization of host cells, we used an ON-TARGETplus siRNA pool to deplete ORP1L. ORP1L protein levels

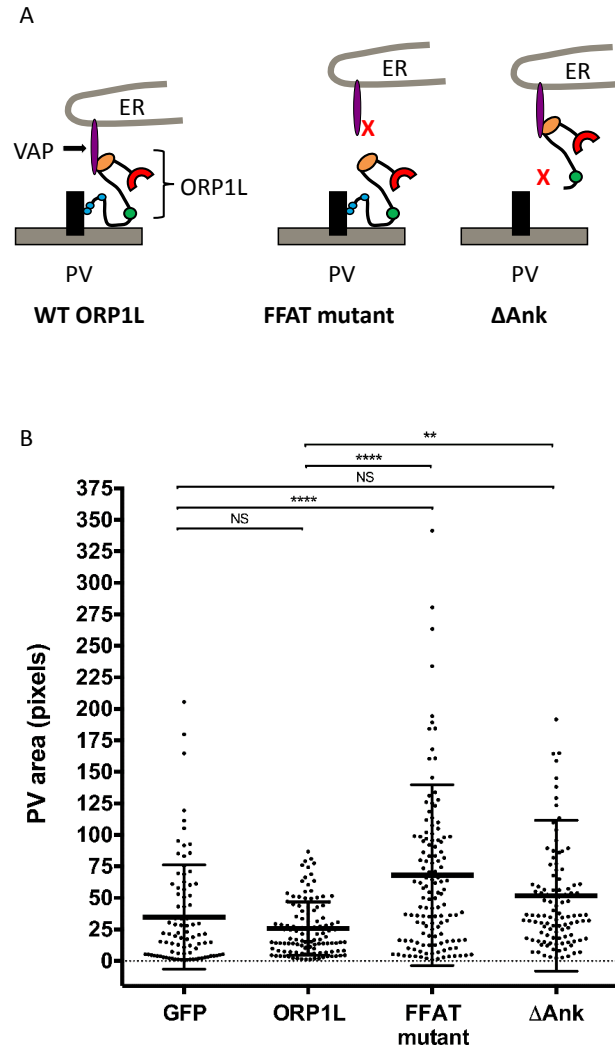


Figure 17. Over-expression of mutant ORP1L results in larger PVs
 PV measurements in cells overexpressing ORP1L mutants that disrupt the ORP1L multiprotein complex at PV-ER membrane contact sites. HeLa cells were transfected with GFP or GFP fusions of wild type ORP1L, mutated FFAT ORP1L, or Δ Ank ORP1L, and infected 24 hours later with *C. burnetii* (A). At 48 hours post infection, the cells were fixed with paraformaldehyde and PV membrane stained with anti-CD63. The PV size was determined using ImageJ and analyze by one-way ANOVA (B). Shown are individual PV measurements from four separate experiments, with at least 20 PVs per experiment. Error bars indicate standard deviation from the mean. * = $p < 0.5$; ** = $p < 0.05$; *** = $p < 0.005$; **** = $p < 0.0005$.

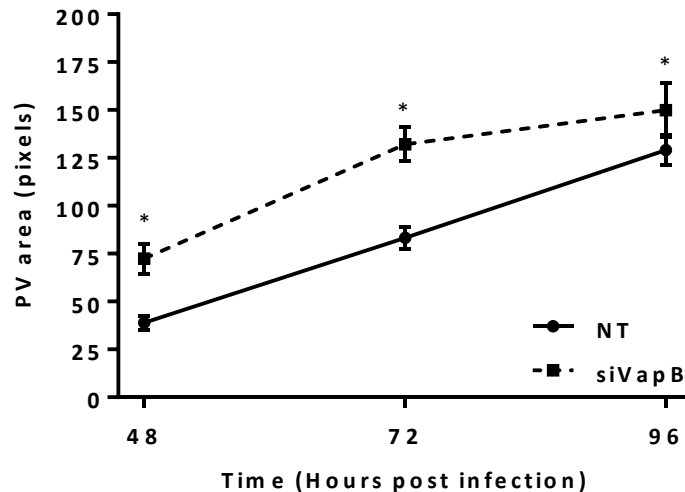


Figure 18. Depletion of VapB results in larger PVs.

HeLa cells were treated with siRNA and then infected 2 days later (0 hpi). Infected cells were re-transfected with siRNA at 0 hpi and samples. PV measurements in cells treated with non-targeting (NT; solid line) or VapB-targeted siRNA (siVapB; dashed line). At 48, 72 or 96 hpi coverslips were fixed with paraformaldehyde and processed for immunofluorescence with anti-CD63 and anti-*C. burnetii*. PV area was determined using ImageJ and means compared by ordinary one-way ANOVA with Sidak’s multiple comparisons test. Data are represented as means from three independent experiments with at least 30 PVs per condition in each experiment. * = $p < 0.0001$. Error bars represent standard deviation.

were decreased by 90% at the time of infection, with levels remaining less than 30% of non-targeting control siRNA for the duration of a 6 day infection time course (Figure 19A). At two and three days post infection, the PV size in ORP1L-depleted cells was similar to control cells (Figure 19B). However, while control PVs continued to expand approximately four-fold between days three and six, PVs in ORP1L-depleted cells had

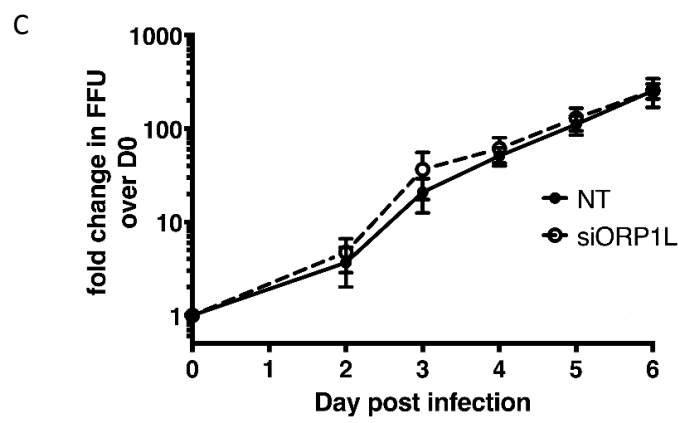
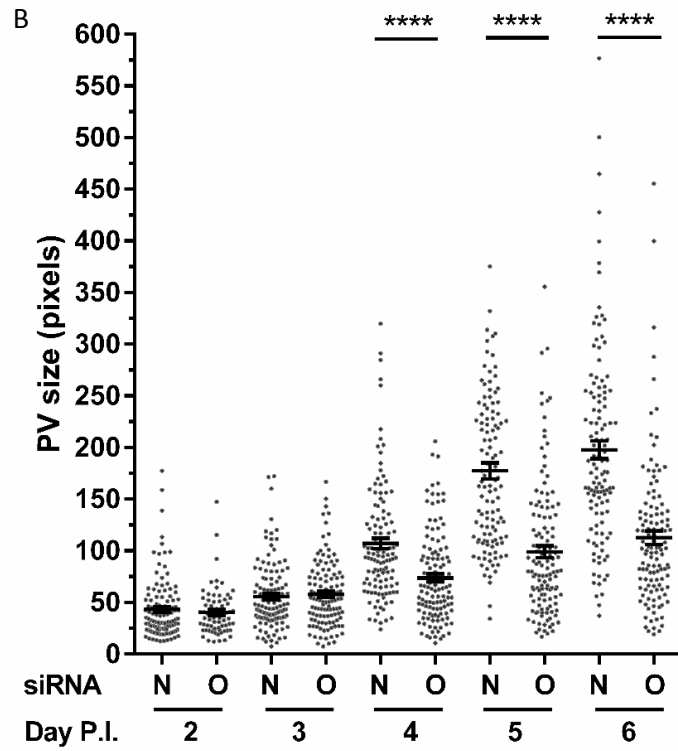
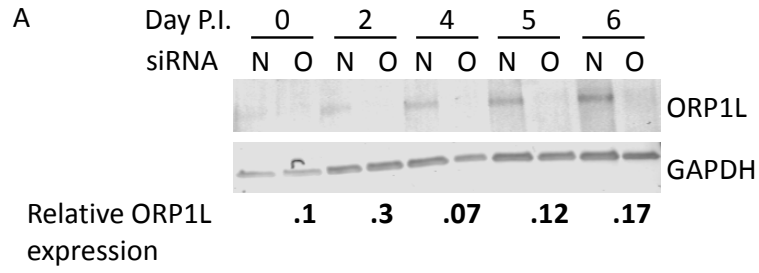


Figure 19. Depletion of ORP1L results in smaller PVs.

HeLa cells were treated with siRNA and then infected 2 days later (day 0 post infection (p.i.)). Infected cells were re-transfected with siRNA at 0 days p.i., and samples processed for immunoblotting, immunofluorescence, or growth assays. (A) ORP1L protein expression in cells treated with either non-targeting (N) or ORP1L siRNA (O) over a six day *C. burnetii* infection. Cell lysates were immunoblotted and ORP1L protein levels quantitated by normalizing to the loading control GAPDH. ORP1L protein levels remained less than 30% of the non-targeting control for the duration of the experiment. Shown is a representative blot from 6 experiments. (B) PV measurements in cells with either wild type or depleted ORP1L. At various times post infection, coverslips were fixed with paraformaldehyde and the PV membrane stained with anti-CD63 and anti-*C. burnetii*. The PV size was determined using ImageJ and standard error of the mean determined by ordinary one-way ANOVA with Sidak's multiple comparisons test. The scatter plot shows individual PV measurements from three independent experiments, with at least 30 PVs per condition in each experiment. Bars indicate average \pm SEM. **** = $p < 0.0001$. (C) *C. burnetii* growth in ORP1L-depleted cells is similar to control cells. The number of viable bacteria was determined by fluorescent foci unit (FFU) assay at the days indicated, and normalized to day 0 to determine fold change in bacterial growth. The results are expressed as the mean of three experiments done in duplicate. Error bars represent SEM.

significantly less expansion, and were half the size of non-targeting PVs at day 6.

Similarly sized PVs were observed at day 6 post infection in cells treated with a single siRNA duplex (Figure 20). Interestingly, nearly the same number of viable bacteria were recovered from both control and ORP1L-depleted cells (Figure 19C). Rab7 and RILP, however, both localized to the PVs of control and ORP1L-depleted cells, indicating the smaller PVs in ORP1L-depleted cells are not due to the absence of Rab7 or RILP from the PV and confirming that Rab7 and RILP are not sufficient to recruit ORP1L to the PV

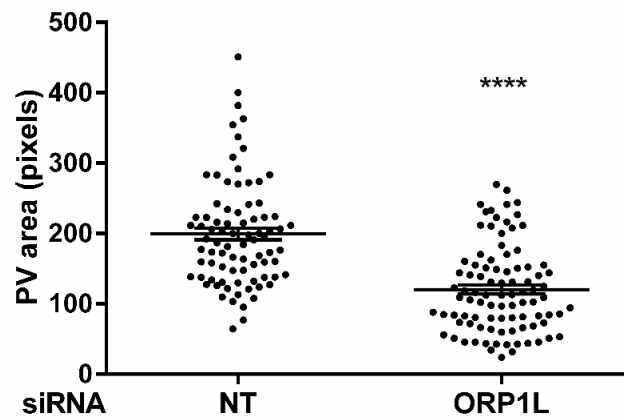


Figure 20. Depletion of ORP1L with single siRNA duplex results in smaller PVs.

HeLa cells were treated with a single siRNA duplex at 50nM. At 6 days post infection, coverslips were fixed with paraformaldehyde and the PV membrane stained with anti-CD63 and anti-*C. burnetii*. The PV size was determined using ImageJ and means compared by unpaired Welch's t-test. The scatter plot shows individual PV measurements from two experiments, with at least 40 PVs per condition in each experiment. Bars indicate average \pm SEM. **** = $p < .0001$

(Figure 21). These data suggest ORP1L plays a role in PV expansion. Further, a large, spacious PV is not required for robust bacterial growth.

The smaller PVs that are observed upon ORP1L-depletion appear to contradict the observations of larger PVs upon disruption of the ORP1L-containing PV-ER membrane contact site complexes. This apparent inconsistency may be explained by ORP1L having multiple functions: it can participate in MCS as well as regulating trafficking and fusion of LEL vesicles. While depleting VAP or overexpressing ORP1L

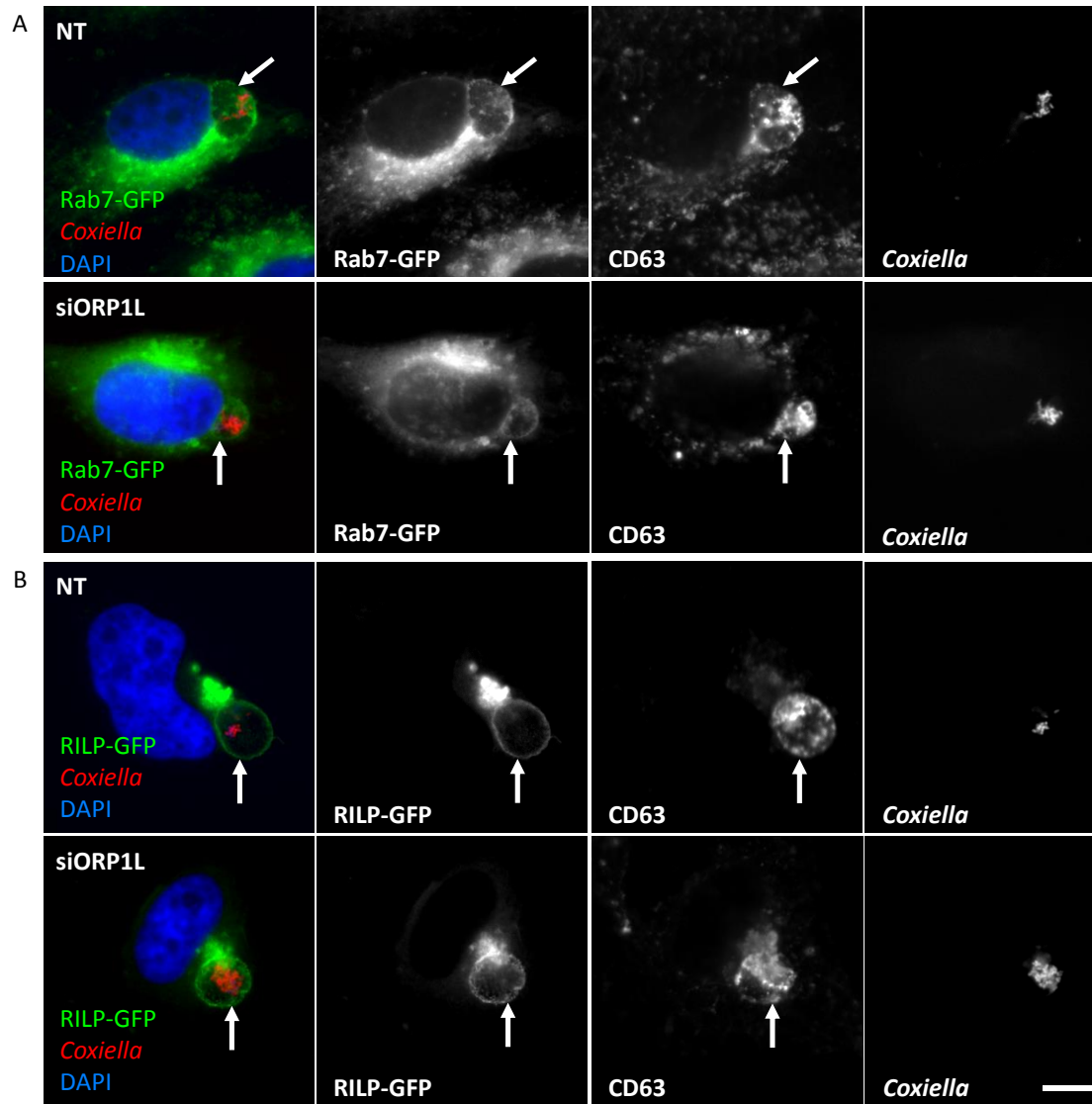


Figure 21. Depletion of ORP1L does not alter Rab7 or RILP PV-localization.

HeLa cells were treated with siRNA, transfected with plasmid DNA the next day, and then infected 1 day later. At 2 days post infection, cells were fixed and stained for CD63 and *Coxiella*. Both Rab7-GFP (A) and RILP-GFP (B) localize to the *Coxiella* PV in cells treated with siRNA targeting ORP1L or non-targeting (NT) negative control. Scale bar = 10 μ m. Depletion of ORP1L does not alter Rab7 or RILP PV-localization.

mutants, wild type ORP1L retained its LEL trafficking regulation function. By depleting wild type ORP1L, we observe the effect of losing both functions of ORP1L.

Chapter V. Discussion

ORP1L PV localization

We have defined the temporal dynamics of ORP1L localization to the PV and identified several factors involved in recruitment of this endo-lysosomal protein during *C. burnetii* infection. Our data show that ORP1L localization to the *C. burnetii* PV requires both the N-terminal ankyrin repeats and a functional *C. burnetii* Type 4B secretion system (T4BSS). The requirement for the ankyrin repeats indicates that protein-protein interactions are primarily responsible for ORP1L association with the PV. In uninfected cells, ORP1L ankyrin repeats are known to physically interact with the GTPase Rab7, where ORP1L binds and modulates the function of Rab7 on LELs [100]. ORP1L preferentially interacts with the GTP-bound active form of Rab7. Fluorescence recovery after photobleaching (FRAP) experiments showed that ORP1L overexpression results in prolonged residence of eGFP-Rab7 on LEL membranes and slowing the rate of replacement of bleached eGFP-Rab7 with unbleached protein [100]. This result suggests that ORP1L stabilizes GTP-bound Rab7. Despite both Rab7 and ORP1L localizing to the *C. burnetii* PV, our data indicates that Rab7 is not sufficient for ORP1L localization to the PV (Figure 9). The ankyrin repeats are also required for ORP1L localization during adenovirus infection, where the adenovirus protein RID α binds to the ORP1L sterol-binding domain in the formation of endosome-ER MCS in order to modulate the immune response to infection [108, 142]. Several *C. burnetii* T4BSS effector proteins localize to the PV membrane [137], and are potential binding partners

for ORP1L. In an analogous system, the *Chlamydia trachomatis* protein IncD recruits the ceramide-transfer protein CERT to the bacterial inclusion, which in turn binds VAP on the ER to form inclusion-ER MCS [143, 144]. Thus, intracellular pathogens may have a common strategy to recruit host cell proteins in the formation of MCS with the ER.

Besides directly binding a T4BSS effector, a T4BSS effector protein might modulate the small GTPase Rab7, the ORP1L binding partner on late endosomes and lysosomes in uninfected cells [133]. Rab7 cycles between an active, GTP-bound form and an inactive, GDP-bound form. ORP1L can bind both forms and stabilizes GTP-bound Rab7, although it is not known if the Rab7 activation state affects ORP1L function [100]. A constitutively active mutant of Rab7 is found on the PV, and Rab7 is required for PV maturation and expansion through an unknown mechanism[56]. It is possible that a T4BSS effector protein regulates Rab7 activation, leading to the recruitment of ORP1L. We also cannot rule out the possibility that the lack of ORP1L on lcmD mutant PVs is indirectly due to a lack of PV maturation. However, because lcmD mutant bacteria remain viable for several days within the host cell and PVs harboring the lcmD mutant do support limited bacterial replication [73], maturation to an acidic phagolysosome is most likely not the sole requirement for PV ORP1L localization. This is further supported by ORP1L localization to the majority of wild type *C. burnetii* PVs at 12 hours post infection, shortly after T4BSS secretion is believed to begin at approximately 8 hours post infection. Further studies are needed to identify ORP1L PV binding partner(s) and understand how ORP1L is recruited to the PV membrane.

In this work, we screened 18 *C. burnetii* transposon mutants for deficiency in ORP1L localization to the PV. A mutation in the *C. burnetii* gene *cbu0352* leads to a reduced number of ORP1L-positive PVs, indicating that this protein is involved in ORP1L recruitment. The *cbu0352* mutant was included in the screen for ORP1L-interacting genes because it contains a computationally predicted E-block secretion signal sequence [141], making it a putative T4BSS effector protein. CBU_0352 is annotated as *CzcD.1* and is homologous with transmembrane cadmium-zinc-cobalt (Czc) transporters in other bacteria. These homologs have been shown to function as heavy metal ion transporters in a variety of species as well as playing a role in the transcriptional response to metal ion exposure. There are several potential mechanisms by which CBU_0352 could affect ORP1L localization (Figure 22): A) CBU_0352 may be secreted and directly interact with ORP1L, B) CBU_0352 may be secreted and indirectly affect ORP1L localization, C) CBU_0352 may not be secreted, and affect ORP1L localization by regulating the T4BSS, D) CBU_0352 supports the general health of the bacteria, nonspecifically allowing for manipulation of ORP1L localization.

If CBU_0352 is, in fact, a secreted T4BSS protein, it could traffic to the PV or ER membranes, recruiting ORP1L and/or participating in PV-ER membrane contact sites (Figure 22A). We have shown that heterologously expressed CBU_0352 localizes the ER, suggesting that it could interact with ORP1L at the PV-ER membrane we have observed. *C. burnetii* has previously been shown express ER-localized T4BSS effector proteins. Specifically, ER-localizing protein A (ElpA), targets to the ER during infection and disrupts the ER structure and secretory pathway function when heterologously expressed in

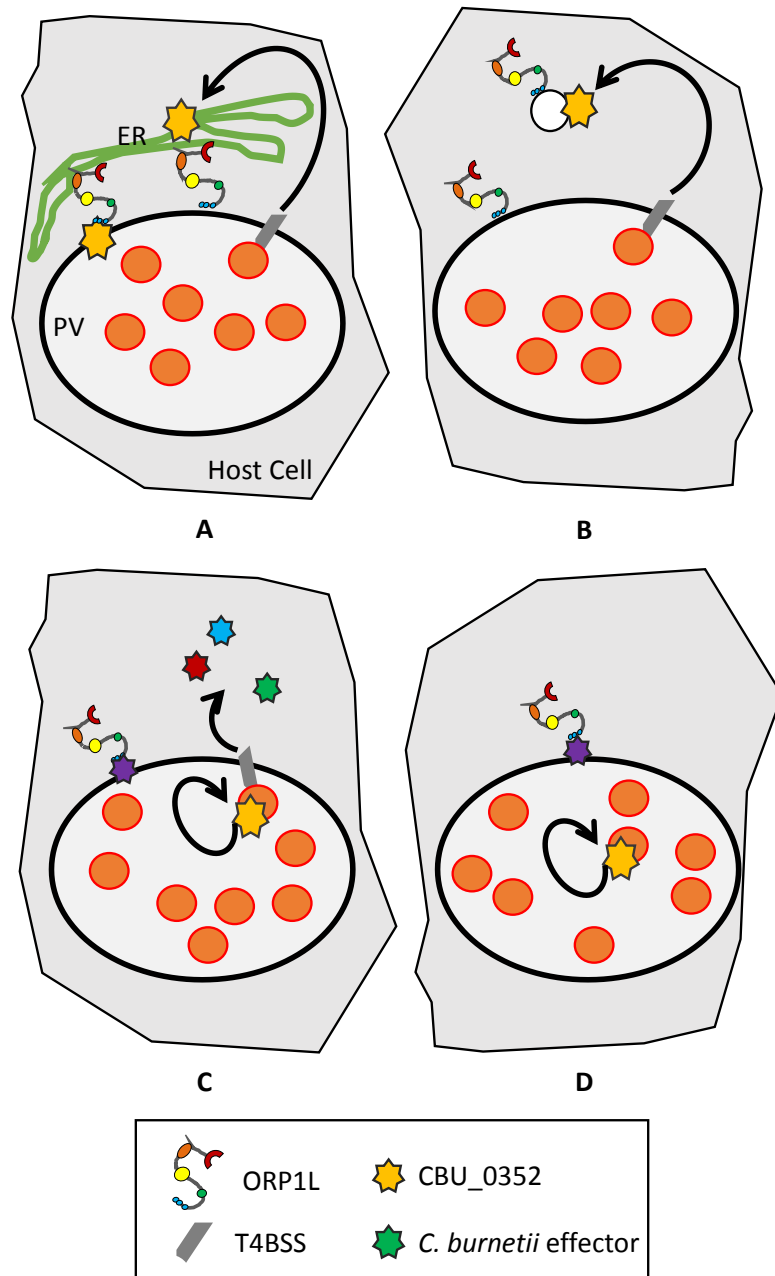


Figure 22. Possible mechanisms of CBU_0352 function in ORP1L recruitment

A) CBU_0352 may be secreted into the host cell, localize to the ER or PV membranes, and directly interact with ORP1L. B) CBU_0352 may be secreted into the host cell and indirectly affect ORP1L recruitment or localization. C) CBU_0352 may be necessary for proper T4BSS function, indirectly influencing ORP1L recruitment by another T4BSS effector. D) CBU_0352 may be needed for optimum *C. burnetii* health, indirectly influencing ORP1L recruitment.

eukaryotic cells [145]. CBU_0352 or additional effector proteins may manipulate ER functions to support *C. burnetii*. It is possible, however, that because CBU_0352 is a transmembrane protein that this localization is due to CBU_0352 lacking a eukaryotic ER export signal sequence, resulting in the protein getting “stuck” in the host ER and making this result uninformative. If CBU_0352 does not directly interact with ORP1L, it may do so indirectly, perhaps by directing fusion of vesicles containing ORP1L with the PV (Figure 22B).

Based on the function of homologous proteins, it is possible that CBU_0352 is not secreted by *C. burnetii*. In *Pseudomonas sp.*, *czcD* and other transporters are transcriptionally controlled by the two-component signal transduction system, *czcRS*. *czcD* activity also feeds back into this transcriptional system, down regulating its activity [146]. In *Ralstonia sp.*, *czcD* functions as a regulator of the Czc system and deletion of the gene results in constitutive transcription of *czc* genes in the absence of stimulation [147]. There are established examples of two-component signal transduction systems both controlling expression of heavy metal resistance genes such as *CzcD*, as well as being regulated themselves by metal ions [148]. The *C. burnetii* T4BSS is regulated by PmrAB two-component system [149], and is conceivable that CBU_0352 could influence the expression of T4BSS components or effector proteins through PmrAB or some other regulatory pathway (Figure 22C). Additionally, CBU_0352 could participate in maintaining metal ion homeostasis, so disrupting this gene leads to generally unhealthy bacteria that cannot drive ORP1L recruitment to the PV (Figure 22D). Much more work

is needed to determine the function of CBU_0352 and its role during *C. burnetii* infection.

ORP1L effect on PV dynamics

ORP1L depletion led to smaller PVs, yet did not have an effect on bacterial growth, suggesting that a large, spacious PV is not strictly required for *C. burnetii* growth. The experiments reported here were conducted in a permissive cell type in A similar observation was made recently in Lamp1/Lamp2 double knockout fibroblasts [150]. Further, a mutant in the *C. burnetii* T4BSS effector protein CvpB forms multiple PVs per cell, but does not have a growth defect *in vitro* [151, 152]. Collectively, *C. burnetii* appears to modulate a complex interplay of different, and possibly redundant, pathways to build the optimal vacuole to support bacterial replication. This is supported by the finding that a CvpB mutant has an attenuated virulence phenotype in the *in vivo* insect model *Galleria mellonella* [152]. The reason behind smaller PVs in the absence of ORP1L is not clear. Interactions between host vesicular trafficking and the PV membrane are not well understood, but it has been assumed that a significant portion of the PV membrane comes from fusion with host vesicles. It is possible that the ER might serve to stabilize the PV membrane in order to allow for expansion or that ER contact may prevent maximum expansion of the PV, with the absence or decrease in PV-ER MCS leading to altered PV membrane dynamics by altering fusion with host trafficking pathways.

The function of ORP1L and PV-ER MCS is not yet clear, and further investigation of the molecular machinery involved in endosome-PV fusion is needed. ORP1L belongs to a family of sterol-transfer proteins and binds phosphatidylinositol phosphates, oxysterols, and cholesterol. ORP1L may transfer cholesterol or other sterols between two membranes, similar to the proposed function of CERT at the *C. trachomatis* inclusion [143, 144]. ORP1L is hypothesized to transfer cholesterol from lysosomes to the ER independent of the lysosomal cholesterol transporter NPC1, during adenovirus infection, with the cholesterol then esterified and incorporated into lipid droplets [90, 153]. The cholesterol transfer function of ORP1L is further supported by a recent report that knocking out ORP1L results in changes in cholesterol homeostasis. These include a reduction in the relative proportion of cellular cholesterol that is esterified compared to wild type cells as well as the visualization of cholesterol accumulating within endosomal vesicles [111]. PV-ER MCS may also participate in the exchange of calcium or other small molecules, or be a mechanism to manipulate ER stress and apoptosis.

Disruption of these PV-ER MCS, either by mutant ORP1L overexpression or VAP depletion, results in larger PVs while ORP1L depletion results in smaller PVs, indicating ORP1L may play more than one role in PV membrane dynamics. In addition to participating in PV-ER MCS, ORP1L may play a direct role in fusion between the PV and host cell endosomes. It follows that smaller PVs resulting from ORP1L depletion may be the result of decreased fusion. In uninfected cells, ORP1L regulates tethering and subsequent fusion of endosomes with one another by mediating interactions between RILP and the HOPS complex [90]. Both Rab7 and RILP localize to the *C. burnetii* PV in the

absence of ORP1L, suggesting these proteins are not directly responsible for the size defect.

ORP1L depletion or PV-ER MCS disruption may have differential effects on subsets of endocytic host vesicles. For example, two subpopulations of late endosomes (LE) have been described in human cells defined by the localization of different cholesterol-binding and transporter proteins. These two populations represent sequential stages of cargo transport: StARD3 and ABCA3 define an “early” LE that recycles back to the plasma membrane, while ORP1L and NPC1 define a “late” LE that traffics to the ER [154]. We do not know whether StARD3/ABCA3-positive LEs interact or fuse with the PV, but these two transport systems could play somewhat redundant roles in supporting *C. burnetii* growth. Alternately, these two endosomal populations could interact with the PV by disparate mechanisms, leading to differential effects following disruption of PV-ER MCS. While the possible contributions of each of these factors to *C. burnetii* biology is not fully elucidated, there are several lines of evidence that these LE proteins do contribute bacterial survival. Although no role for StARD3 during *C. burnetii* infection has been reported, knockdown of either NPC1 or ABCA3 significantly restricts *C. burnetii* growth [115, 139]. Interactions between the PV and these two populations of vesicles or other types of vesicles known to interact with the PV could contribute to the various effects on PV dynamics that we have observed. Given the dual roles of ORP1L in endosomal fusion and endosome-ER membrane contact sites, further work is needed to understand the contribution of each role to the structure, size, and function of the PV as a replicative niche for *C. burnetii*.

In summary, this study demonstrates that ORP1L specifically localizes to the PV membrane in a bacterially-driven, T4BSS-dependent manner. The putative *C. burnetii* secreted protein, CBU_0352, influences ORP1L localization via an unknown mechanism. Additionally, we have shown that novel membrane contact sites (MCS) are present between the PV and host ER membranes. The sterol-binding protein ORP1L is one component of these MCS, and appears to play a role in PV membrane dynamics. Future experiments clarifying the function of CBU_0352, identifying the specific role of ORP1L on the PV, and elucidating the function of PV-ER interactions will give new insight into *C. burnetii* pathogenesis and host cell manipulation.

Chapter VI. Future Directions

ORP1L-containing PV-ER membrane contact sites

The endoplasmic reticulum plays essential roles in mammalian cells, including lipid and protein synthesis, calcium storage, and the cellular stress response. Membrane contact sites (MCS) between the ER and other cellular organelles serve as a location for exchange of small molecules and lipids. The formation of MCS relies on multi-protein complexes that tether the two membranes together within a distance of 15 nm [155]. Prior studies have implicated ORP1L, a member of the sterol transfer protein family, in the formation of LEL-ER MCS [102, 156]. Additionally, ORP1L localizes to the PV harboring the intracellular bacterial pathogen *Coxiella burnetii*. ORP1L can simultaneously bind to the *C. burnetii* PV and the ER, suggesting ORP1L is also a component of PV-ER MCS. This is the first description of MCS between the *C. burnetii* PV and an intracellular organelle [122], and is supported by a recent study showing that the ER marker calnexin is closely associated with the PV during *C. burnetii* infection [157].

Based on these data, we propose a model where PV-associated ORP1L binds to VAP on the ER, forming MCS between the PV and ER (Figure 23). This model is further supported by our observation of PV-ER MCS by electron microscopy. While our data suggest ORP1L and VAP are components of these MCS, other proteins or protein complexes may be involved and ORP1L may not be a component of every PV-ER MCS. Indeed, many lipid transfer proteins with FFAT motifs have been found at MCS between

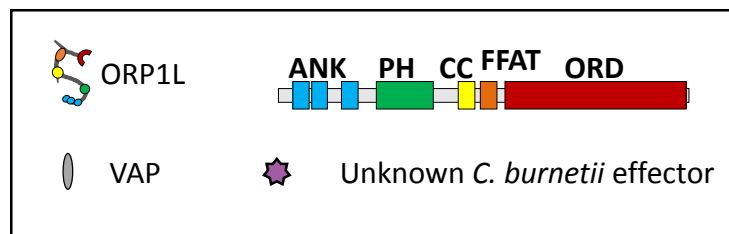
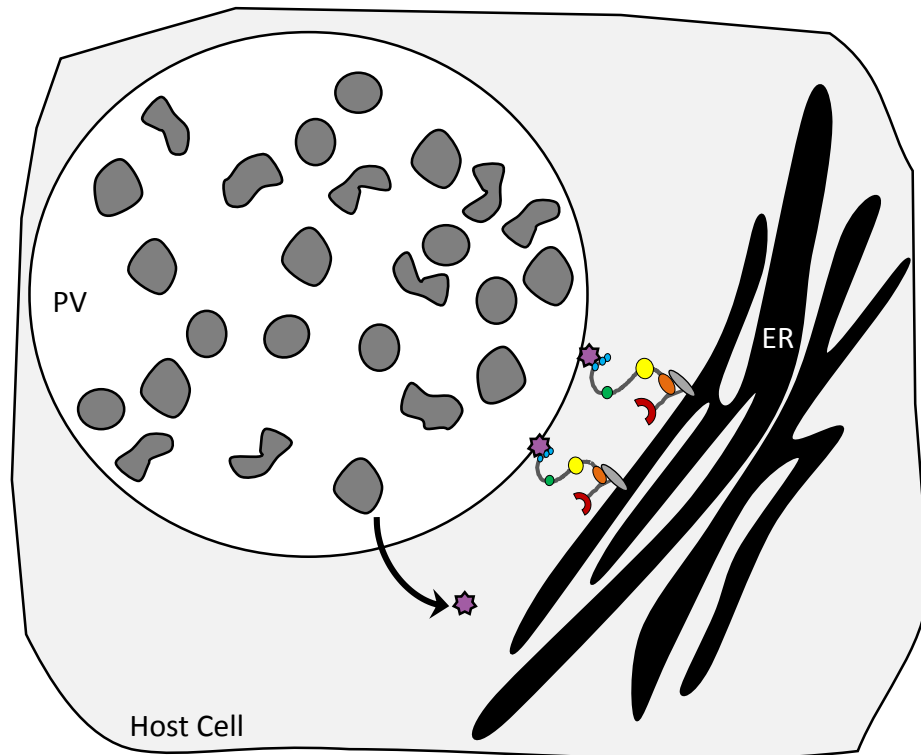


Figure 23. Model for ORP1L in membrane contact sites between the *C. burnetii* parasitophorous vacuole (PV) and host cell endoplasmic reticulum.

ORP1L is recruited directly or indirectly to the *C. burnetii* PV by the T4BSS, where it participates in membrane contact sites between the PV and host ER. ORP1L appears to interact with ER localized VAP.

the ER and the plasma membrane, Golgi, and mitochondria (reviewed in [158]). The *C. burnetii* genome encodes three proteins with putative FFAT motifs: CBU_0274, which encodes Excinuclease ABC subunit A, and two hypothetical proteins of unknown function, CBU_0328 and CBU_1370 (Dr. Paul A. Beare, unpublished). It is unlikely that the Excinuclease ABC subunit is secreted by the bacteria, however, the two hypothetical proteins could represent a mechanism by which *C. burnetii* could manipulate membrane contact sites between the ER and the PV or other membranes.

Characterizing CBU_0352

Is CBU_0352 a secreted protein?

In order to understand the role of CBU_0352 in ORP1L recruitment and its larger role during *C. burnetii* infection, it will be imperative to empirically determine if CBU_0352 is secreted into the host cell. By determining whether CBU_0352 is secreted, we may find out whether this protein is directly manipulating host cell biology or functioning in a bacterial cell-intrinsic manner. Commonly, affinity or fluorescent tag fusion proteins are used to visualize the localization of a protein of interest. *C. burnetii* effector proteins, however, are often expressed in such low abundance as to be undetectable using this method. I have attempted to visualize 3xFLAG-tagged CBU_0352 by IFA in HeLa cells infected with *C. burnetii* expressing this protein, but this method was not successful (did not result in signal above background). Consequently, the product of enzymatic reactions, such as for the β -lactamase fusion proteins described in Chapter I, are used as indirect indicators of translocation into the host cell. I plan to use the *B. pertussis* adenylate cyclase toxin, CyaA, as a qualitative reporter of

translocation [159], which is the standard in the *C. burnetii* field. When CyaA is present in the host cytoplasm, it is activated by calmodulin and converts adenosine triphosphate (ATP) into cyclic adenosine monophosphate (cAMP). cAMP levels can be measured colorimetrically as a surrogate for translocation of the fusion protein.

In order to determine if CBU_0352 is a translocated protein, I propose to use plasmids expressing CyaA alone, CBU_0352 fused to CyaA, and a known effector protein, CvpD, fused to CyaA [160]. Each plasmid will be expressed in wild type or DotA mutant NMII *C. burnetii*. The DotA mutant, which cannot translocate T4BSS effector proteins, and wild type bacteria expressing CyaA alone, which will not be translocated, will be used as negative controls. CyaA-CvpD expressed in wild type bacteria will serve as a positive control for translocation. If a significant increase in cAMP levels is observed in wild type *C. burnetii* expressing CyaA-CBU_0352 compared to mutant *C. burnetii* expressing the same fusion protein, this will indicate that CBU_0352 is indeed secreted during infection.

Does the CBU_0352 mutation broadly affect T4BSS function?

If we determine that CBU_0352 is not a secreted protein, one possible explanation of how a mutation in this gene could influence T4BSS-dependent ORP1L recruitment to the *C. burnetii* PV is that CBU_0352 plays a broader role in regulating or influencing T4BSS function. To test this, I propose to examine the function of the T4BSS in a CBU_0352 mutant background. The same CyaA-containing constructs described above will be expressed in the CBU_0352 transposon mutant background (Tn235 clone) and translocation will be assessed as described. If CBU_0352 mutant bacteria is unable

to translocate known effector fusion proteins (such as CyaA-CvpD), this will demonstrate that the T4BSS system is inhibited. This result would suggest that one or more of the effector proteins whose translocation is CBU_0352-dependent may be influencing ORP1L PV recruitment.

What is the effect of *cbu0352* deletion?

In order to explore the function of CBU_0352, I propose to delete the *cbu0352* locus from wild type NMII *C. burnetii* using the “loop-in, loop-out” method developed by Beare *et al.* [161]. A clean *cbu0352* deletion will be a useful tool to parse functions of CBU_0352. The mutant currently being used contains a transposon insertion at nt 457 and this placement leaves the possibility open that the N-terminal portion of the CBU_0352 protein is expressed. Expression of this truncated protein could result in a confounding phenotype resulting from a dominant negative interaction, a gain of function interaction, or a partial null phenotype. For example, we see a 50% decrease in the number of ORP1L-positive PVs in cells infected with CBU_0352 mutant *C. burnetii* compared to wild type, and it is possible that a ‘clean’ CBU_0352 knockout would not recruit ORP1L to the PV at all. By deleting the entire *cbu0352* locus, the resulting phenotype will be more easily interpreted.

Can *cbu0352* mutant phenotypes be complemented?

In order to confirm that the reduction in ORP1L-positive PVs is due to the mutation in *cbu0352* as well as the replication deficit reported by Martinez *et al.* [140], I propose to complement the transposon mutant (and the *cbu0352* knockout when it is generated) using FLAG-tagged CBU_0352. While allelic replacement has not yet been

achieved in *C. burnetii*, we can introduce a wild type copy of *cbu0352* that will be inserted into the genome in a random location [161]. If complementation rescues these phenotypes, we will be able to fulfill molecular Koch's postulates and confidently ascribe the growth and ORP1L recruitment phenotypes to the mutation in *cbu0352*.

Identifying ORP1L-interacting proteins

I have shown that CBU_0352 interacts genetically with ORP1L, however, physical interactions with additional bacterial or host proteins may influence ORP1L function or recruitment to the *C. burnetii* PV. To identify ORP1L-interactors, I propose an affinity purification technique to isolate ORP1L-containing protein complexes. Constructs expressing ORP1L fused to a BioEase protein tag could be used for this purpose. The BioEase tag is a 72 amino acid sequence comprising the biotin-targeting domain from *Klebsiella pneumoniae* oxaloacetate decarboxylase (KPBT) and is efficiently biotinylated by eukaryotic cells *in vivo* [162] when the growth media is supplemented with biotin. Biotinylated proteins can be pulled down using a streptavidin conjugated substrate.

Because the ORP1L ankyrin repeats are responsible for PV localization, I could use wild type, Ank, and Δ Ank ORP1L to identify proteins involved in this process. There are several potential results that would indicate a particular protein could play a role in ORP1L recruitment. PV-localized ORP1L-interacting proteins would most likely be revealed as binding to both wild type and Ank ORP1L while not interacting with Δ Ank ORP1L. Proteins that interact with ORP1L, but are not on the PV membrane or interact with ORP1L in an ankyrin-independent manner, would bind to wild type and Δ Ank

ORP1L, but not Ank ORP1L. Such proteins could participate in the PV-ER MCS or in other ORP1L-containing protein complexes. Regardless of the domains involved, any bacterial protein that specifically binds ORP1L would be of interest, as these may be secreted effectors and represent a mechanism for direct bacterial manipulation of ORP1L. In addition to bacterial ORP1L-interacting proteins, we may also identify host proteins that interact with ORP1L only during infection by comparing results from infected and uninfected host cells. These infection-specific host protein interactions could be either bacteria-driven in support of replication or may be host-driven as part of an anti-bacterial response. Regardless of the specific outcome, this line of experimentation has the broad potential to reveal information about the function of ORP1L by elucidating its infection-specific protein-protein interaction network.

Investigating ORP1L function

What is the conformation of ORP1L on the PV?

We have gained some insight into the role ORP1L may be playing in *C. burnetii* PV dynamics, but additional questions remain. The opposing effects of disrupting PV-ER MCS and ORP1L knockdown on PV size indicate that ORP1L is playing two possibly opposing roles. Previous reports have shown that ORP1L exists in two conformations, corresponding to its roles in MCS and LEL trafficking [90]. In order to determine which function of ORP1L is most relevant during *C. burnetii* infection, determining the conformation of ORP1L on the PV could be informative. I propose to use a FRET-based approach based on that used by Rocha *et al.* to determine the conformation of ORP1L

[112]. Towards this end, I have made two intramolecular FRET constructs using the optimized FRET donor-acceptor pair, mTurquoise and mVenus, with wild type and Δ ORD ORP1L. Δ ORD ORP1L is lacking the sterol-binding domain and cannot take on the condensed conformation, so it will serve as a negative control for FRET signal.

These FRET sensors could be used to determine the conformation of ORP1L on the PV throughout the course of *C. burnetii* infection. We know that ORP1L participates in MCS late during infection when the PV is already very large, but we do not know if this is the case during earlier stages of infection. I propose to observe the conformation of ORP1L over a time course of at least 6 days.

What is the effect of ORP1L depletion in macrophages?

The inhalation of contaminated aerosols is the most common route of *C. burnetii* human infection. Paired with phagocytosis as the primary cell entry route, this causes alveolar macrophages to be enriched among the first cells infected [120]. As such, the mouse alveolar macrophage cell line, MH-S, is a good model of *C. burnetii* interactions with host cells. This cell line may also be particularly relevant to this project, as ORP1L is highly expressed in monocytes and macrophages [99].

In order to deplete macrophages of ORP1L, I propose to use lentiviral shRNA targeting ORP1L. To this end, I have optimized transient knockdown in these cells compared to cells treated with a non-targeting “scrambled” (SCR) shRNA and achieved 60-80% knockdown (Figure 24). In subsequent experiments I would use shORP1L 1 and 5, that both exhibited significant knockdown. To explore the effect of ORP1L depletion in MH-S cells, I propose initial characterization of *C. burnetii* growth by FFU assay and PV

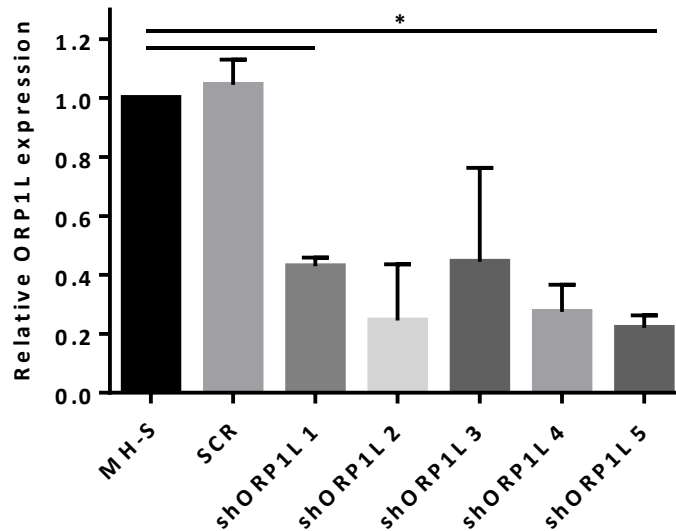


Figure 24. ORP1L knockdown in MH-S cells by lentiviral shRNA

Reduced ORP1L expression is observed in shRNA-treated murine alveolar macrophage cells compared to untreated cells. We observed little difference between untreated cells and cells treated with a non-targeting scrambled shRNA. Mean ORP1L protein expression level observed in two experiments are displayed. Expression levels in each condition were compared to untreated cells (MH-S) by repeated measures one-way ANOVA with Dunnett’s multiple comparison. Error bars represent range. * = $p < 0.05$. SCR = scrambled, non-targeting shRNA.

size by IFA.

What is the effect of ORP1L deletion?

A recent publication reported the CRISPR/Cas9-mediated knockout of ORP1L in epithelial cells (HeLa and 293T) and the subsequent alterations to cholesterol trafficking [111]. These cell lines may be used to determine if complete knockout, as opposed to the partial knockdown achieved by siRNA in this work, has a greater effect on PV

dynamics or *C. burnetii* growth in epithelial cells. Further insights could be gained by using CRISPR/Cas9 to knockout ORP1L in the alveolar macrophage cell line, MH-S. I have designed and made several constructs expressing Cas9 and a single ORP1L-targeting sgRNA from a single plasmid (see Materials and Methods) which could be used to create an ORP1L knockout cell line. I propose to test the effect of ORP1L deletion on PV formation and *C. burnetii* growth in macrophages by microscopy and FFU assays.

A tool for unbiased investigation of *C. burnetii* secreted proteins

C. burnetii relies upon its T4BSS as well as other secretion systems to manipulate the host cell and support its own survival and replication. Identifying the secreted protein effectors and understanding their function is paramount to understanding the intricate interactions between this bacterial pathogen and its host. In recent years, non-canonical amino acids have been used as a tool to selectively label and identify microbial proteins. Mahdavi *et al.* identified several proteins secreted by the human pathogen, *Yersinia enterocolitica*, by specifically labeling the proteins of bacteria expressing a mutant form of the methionyl-tRNA synthetase (MetRS), MetRS^{NLL}, which activates the methionine surrogate, Anl [128] for incorporation into nascently translated proteins. ANL-containing proteins can be labeled with affinity tags for purification or fluorescent tags for visualization using copper-catalyzed “click chemistry” in either fixed cells or in cell lysate samples. This method has also been used for pulse-chase labeling of *Toxoplasma gondii* proteins during growth *in vitro*. In this system, *T. gondii* N-terminally processed proteins, including secreted proteins, were not labeled because the bacterial

MetRS^{NLL} could only charge initiator Met tRNAs with ANL, but could not charge eukaryotic elongator Met tRNAs [163], resulting in ANL incorporation only at the N-terminus of nascent polypeptides. While this should not be a problem within a prokaryotic system, we will need to be wary of such incompatibilities as we attempt to use this system in *C. burnetii*.

In order to implement this protein labeling system in *C. burnetii*, we first needed to express MetRS^{NLL} in the bacteria. I created a plasmid encoding HA-tagged MetRS^{NLL}, with expression controlled by the constitutively active *C. burnetii* promoter, *p1169*. I have transformed this plasmid into wild type bacteria and confirmed expression by Western blot, probing with anti-HA antibody. Next, we will need to verify that *C. burnetii* expressing MetRS^{NLL} will indeed incorporate ANL into proteins when ANL is present in axenic culture and/or during host cell infection. Once this protein labeling system is optimized and verified to be functioning, there are several studies for which it can be used to interrogate ORP1L function as well as general *C. burnetii* biology and pathogenesis.

What bacterial proteins bind ORP1L during C. burnetii infection?

First, this system could be used to identify *C. burnetii* proteins which physically interact with ORP1L in infected cells. I propose pulldown experiments to identify bacterial binding partners of ORP1L. To do this, the BioEASE-ORP1L approach described above could be adapted to investigate whether ANL-labeled bacterial proteins are pulled down with biotinylated ORP1L.

Which C. burnetii proteins are secreted and when?

Labeling bacterial proteins in a non-biased manner allows for the opportunity to isolate and identify secreted proteins. By lysing infected cells with trichloroacetic acid (TCA), one may retain the intact bacteria in the insoluble fraction along with host cellular debris, and identify bacterial proteins in the soluble fraction (which includes secreted proteins) by SDS-PAGE and Western blot, probing for the affinity tag added to ANL labeled proteins by click chemistry. A similar approach was successfully employed to identify FLAG-tagged *C. burnetii* proteins that are translocated into axenic media by Sec-mediated secretion [164]. Affinity tag labeled bacterial proteins could be isolated by immunoprecipitation and identified by mass spectrometry analysis.

Pulse-chase labeling of proteins followed by isolation and identification as described above could begin to clarify the temporal dynamics of protein secretion during host cell infection. For example, such experiments may reveal whether proteins are secreted in sequential cohorts or if all secreted proteins are translocated constitutively throughout infection.

Finally, this system could be used to identify secreted proteins that localize to specific host cellular fractions. For example, bacterial proteins could be isolated from the host nuclear fraction, allowing for identification of effectors that localize to the nucleus, perhaps modulating host gene expression. Two nuclear-localizing *C. burnetii* effector proteins have been previously identified: CBU_1314 associates with host chromatin and regulates the expression levels of at least 16 host genes [78], and AnkG traffics to the host nucleus where it inhibits pathogen-induced apoptosis of the host cell

[165, 166]. Unbiased labeling of bacterial proteins would allow for the relatively rapid identification of additional host-modulating effectors. Recent methods have been published which allow for the isolation of ER membranes, independent of other membrane organelles [167, 168], which was not previously possible with density gradient separation [169]. Identification of ER-localized effector proteins would be particularly relevant to this work.

References

1. Derrick, E., "Q" fever, a new fever entity: clinical features, diagnosis, and laboratory investigation. *Med J Aust*, 1937. **2**: p. 281-299.
2. Dyer, R., Similarity of Australian "Q" fever and a disease caused by an infectious agent isolated from ticks in Montana. *Public Health Rep*, 1939. **54**: p. 1229-1237.
3. McDade, J., Historical aspects of Q fever, in *Q fever*, vol 1, The disease, T. Marrie, Editor. 1990, CRC Press: Boca Raton.
4. Robbins, F.C., R.L. Gauld, and F.B. Warner, Q fever in the Mediterranean area; report of its occurrence in Allied troops; epidemiology. *Am J Hyg*, 1946. **44**: p. 23-50.
5. Cox, H.R., W.C. Tesar, and J.V. Irons, Q fever in the United States; isolation and identification of rickettsias in an outbreak among stock handlers and slaughterhouse workers. *J Am Med Assoc*, 1947. **133**(12): p. 820.
6. Shepard, C.C., An outbreak of Q fever in a Chicago packing house. *Am J Hyg*, 1947. **46**(2): p. 185-92.
7. Topping, N.H., C.C. Shepard, and J.V. Irons, Q fever in the United States; epidemiologic studies of an outbreak among stock handlers and slaughterhouse workers. *J Am Med Assoc*, 1947. **133**(12): p. 813-5.
8. Huebner, R.J., Report of an Outbreak of Q Fever at the National Institute of Health : II. Epidemiological Features. *Am J Public Health Nations Health*, 1947. **37**(4): p. 431-40.

9. Huebner, R.J., Report of an outbreak of Q fever at the National Institute of Health. *Am J Public Health Nations Health*, 1947. **37**(4): p. 431-40.
10. Benenson, A.S. and W.D. Tigertt, Studies on Q fever in man. *Trans Assoc Am Physicians*, 1956. **69**: p. 98-104.
11. Tigertt, W.D., A.S. Benenson, and W.S. Gochenour, Airborne Q fever. *Bacteriol Rev*, 1961. **25**: p. 285-93.
12. Anno, G., and Deverill, A., Consequence Analytic Tools for NBC Operations Volume 1 – Biological Agent Effects and Degraded Personnel Performance for Tularemia, Staphylococcal Enterotoxin B (SEB) and Q-Fever. 1998, Defense Special Weapons Agency.
13. Heppell, C.W., J.R. Egan, and I. Hall, A human time dose response model for Q fever. *Epidemics*, 2017.
14. Brooke, R.J., et al., Human dose response relation for airborne exposure to *Coxiella burnetii*. *BMC Infect Dis*, 2013. **13**: p. 488.
15. Tamrakar, S.B., et al., Dose-response model of *Coxiella burnetii* (Q fever). *Risk Anal*, 2011. **31**(1): p. 120-8.
16. Madariaga, M.G., et al., Q fever: a biological weapon in your backyard. *Lancet Infect Dis*, 2003. **3**(11): p. 709-21.
17. McQuiston, J.H. and J.E. Childs, Q fever in humans and animals in the United States. *Vector Borne Zoonotic Dis*, 2002. **2**(3): p. 179-91.
18. Agerholm, J.S., *Coxiella burnetii* associated reproductive disorders in domestic animals--a critical review. *Acta Vet Scand*, 2013. **55**: p. 13.

19. Babudieri, B. and C. Moscovici, Experimental and natural infection of birds by *Coxiella burnetii*. *Nature*, 1952. **169**(4292): p. 195-6.
20. Stephen, S. and K.N. Rao, Coxiellosis in reptiles of South Kanara district, Karnataka. *Indian J Med Res*, 1979. **70**: p. 937-41.
21. Duron, O., et al., The Importance of Ticks in Q Fever Transmission: What Has (and Has Not) Been Demonstrated? *Trends Parasitol*, 2015. **31**(11): p. 536-52.
22. Fishbein, D.B. and D. Raoult, A cluster of *Coxiella burnetii* infections associated with exposure to vaccinated goats and their unpasteurized dairy products. *Am J Trop Med Hyg*, 1992. **47**(1): p. 35-40.
23. Pearson, T., et al., High prevalence and two dominant host-specific genotypes of *Coxiella burnetii* in U.S. milk. *BMC Microbiol*, 2014. **14**: p. 41.
24. Kim, S.G., et al., *Coxiella burnetii* in bulk tank milk samples, United States. *Emerg Infect Dis*, 2005. **11**(4): p. 619-21.
25. Biggs, H.M., et al., *Coxiella burnetii* Infection in a Community Operating a Large-Scale Cow and Goat Dairy, Missouri, 2013. *Am J Trop Med Hyg*, 2016. **94**(3): p. 525-31.
26. Ganter, M., Zoonotic risks from small ruminants. *Vet Microbiol*, 2015. **181**(1-2): p. 53-65.
27. Honarmand, H., Q Fever: an old but still a poorly understood disease. *Interdiscip Perspect Infect Dis*, 2012. **2012**: p. 131932.
28. Hellenbrand, W., T. Breuer, and L. Petersen, Changing epidemiology of Q fever in Germany, 1947-1999. *Emerg Infect Dis*, 2001. **7**(5): p. 789-96.

29. Carrieri, M.P., et al., Investigation of a slaughterhouse-related outbreak of Q fever in the French Alps. *Eur J Clin Microbiol Infect Dis*, 2002. **21**(1): p. 17-21.
30. Roest, H.I., et al., The Q fever epidemic in The Netherlands: history, onset, response and reflection. *Epidemiol Infect*, 2011. **139**(1): p. 1-12.
31. Roest, H.I., et al., Molecular epidemiology of *Coxiella burnetii* from ruminants in Q fever outbreak, the Netherlands. *Emerg Infect Dis*, 2011. **17**(4): p. 668-75.
32. Raoult, D., Host factors in the severity of Q fever. *Ann N Y Acad Sci*, 1990. **590**: p. 33-8.
33. Rolain, J.M., M.N. Mallet, and D. Raoult, Correlation between serum doxycycline concentrations and serologic evolution in patients with *Coxiella burnetii* endocarditis. *J Infect Dis*, 2003. **188**(9): p. 1322-5.
34. Bernit, E., et al., Neurological involvement in acute Q fever: a report of 29 cases and review of the literature. *Arch Intern Med*, 2002. **162**(6): p. 693-700.
35. Ayres, J.G., et al., Post-infection fatigue syndrome following Q fever. *QJM*, 1998. **91**(2): p. 105-23.
36. Wildman, M.J., et al., Chronic fatigue following infection by *Coxiella burnetii* (Q fever): ten-year follow-up of the 1989 UK outbreak cohort. *QJM*, 2002. **95**(8): p. 527-38.
37. Harris, R.J., et al., Long-term persistence of *Coxiella burnetii* in the host after primary Q fever. *Epidemiol Infect*, 2000. **124**(3): p. 543-9.
38. Brouqui, P., et al., Chronic Q fever. Ninety-two cases from France, including 27 cases without endocarditis. *Arch Intern Med*, 1993. **153**(5): p. 642-8.

39. Houpikian, P. and D. Raoult, Blood culture-negative endocarditis in a reference center: etiologic diagnosis of 348 cases. *Medicine (Baltimore)*, 2005. **84**(3): p. 162-73.
40. Kampschreur, L.M., et al., Delayed diagnosis of chronic Q fever and cardiac valve surgery. *Emerg Infect Dis*, 2013. **19**(5): p. 768-70.
41. Raoult, D., et al., Treatment of Q fever endocarditis: comparison of 2 regimens containing doxycycline and ofloxacin or hydroxychloroquine. *Arch Intern Med*, 1999. **159**(2): p. 167-73.
42. Houpikian, P., et al., Changing clinical presentation of Q fever endocarditis. *Clin Infect Dis*, 2002. **34**(5): p. E28-31.
43. Raoult, D., F. Fenollar, and A. Stein, Q fever during pregnancy: diagnosis, treatment, and follow-up. *Arch Intern Med*, 2002. **162**(6): p. 701-4.
44. Raoult, D. and A. Stein, Q fever during pregnancy--a risk for women, fetuses, and obstetricians. *N Engl J Med*, 1994. **330**(5): p. 371.
45. Carcopino, X., et al., Q Fever during pregnancy: a cause of poor fetal and maternal outcome. *Ann N Y Acad Sci*, 2009. **1166**: p. 79-89.
46. Lim, W.S., J.T. Macfarlane, and C.L. Colthorpe, Treatment of community-acquired lower respiratory tract infections during pregnancy. *Am J Respir Med*, 2003. **2**(3): p. 221-33.
47. Baca, O.G., D.A. Klassen, and A.S. Aragon, Entry of *Coxiella burnetii* into host cells. *Acta Virol*, 1993. **37**(2-3): p. 143-55.

48. Gilk, S.D., et al., Bacterial colonization of host cells in the absence of cholesterol. *PLoS Pathog*, 2013. **9**(1): p. e1003107.
49. Kazar, J., E. Skultetyova, and R. Brezina, Phagocytosis of *Coxiella burnetii* by macrophages. *Acta Virol*, 1975. **19**(5): p. 426-31.
50. Coleman, S.A., et al., Temporal analysis of *Coxiella burnetii* morphological differentiation. *J Bacteriol*, 2004. **186**(21): p. 7344-52.
51. Newton, H.J., J.A. McDonough, and C.R. Roy, Effector protein translocation by the *Coxiella burnetii* Dot/Icm type IV secretion system requires endocytic maturation of the pathogen-occupied vacuole. *PLoS One*, 2013. **8**(1): p. e54566.
52. Romano, P.S., et al., The autophagic pathway is actively modulated by phase II *Coxiella burnetii* to efficiently replicate in the host cell. *Cell Microbiol*, 2007. **9**(4): p. 891-909.
53. Campoy, E.M., M.E. Mansilla, and M.I. Colombo, Endocytic SNAREs are involved in optimal *Coxiella burnetii* vacuole development. *Cell Microbiol*, 2013. **15**(6): p. 922-41.
54. Ariel, B.M., T.N. Khavkin, and N.I. Amosenkova, Interaction between *Coxiellae burnetii* and the cells in experimental Q-rickettsiosis. *Histologic and electron microscope studies. Pathol Microbiol (Basel)*, 1973. **39**(6): p. 412-23.
55. Heinzen, R.A., et al., Differential interaction with endocytic and exocytic pathways distinguish parasitophorous vacuoles of *Coxiella burnetii* and *Chlamydia trachomatis*. *Infect Immun*, 1996. **64**(3): p. 796-809.

56. Beron, W., et al., *Coxiella burnetii* localizes in a Rab7-labeled compartment with autophagic characteristics. *Infect Immun*, 2002. **70**(10): p. 5816-21.
57. Larson, C.L. and R.A. Heinzen, High-Content Imaging Reveals Expansion of the Endosomal Compartment during *Coxiella burnetii* Parasitophorous Vacuole Maturation. *Front Cell Infect Microbiol*, 2017. **7**: p. 48.
58. Gutierrez, M.G., et al., Autophagy induction favours the generation and maturation of the *Coxiella*-replicative vacuoles. *Cell Microbiol*, 2005. **7**(7): p. 981-93.
59. Campoy, E.M., F.C. Zoppino, and M.I. Colombo, The early secretory pathway contributes to the growth of the *Coxiella*-replicative niche. *Infect Immun*, 2011. **79**(1): p. 402-13.
60. Howe, D. and R.A. Heinzen, Fractionation of the *Coxiella burnetii* parasitophorous vacuole. *Methods Mol Biol*, 2008. **445**: p. 389-406.
61. Burton, P.R., et al., Some ultrastructural effects of persistent infections by the rickettsia *Coxiella burnetii* in mouse L cells and green monkey kidney (Vero) cells. *Infect Immun*, 1978. **21**(2): p. 556-66.
62. Howe, D., et al., Maturation of the *Coxiella burnetii* parasitophorous vacuole requires bacterial protein synthesis but not replication. *Cell Microbiol*, 2003. **5**(7): p. 469-80.
63. Babudieri, B., Q fever: a zoonosis. *Adv Vet Sci*, 1959. **5**: p. 81-182.

64. TF McCaul, T.H., JC Williams, Ultrastructural and biological aspects of *Coxiella burnetii* under physical disruptions., in *Rickettsiae and rickettsial diseases*, R.A. E Burgdorfer, Editor. 1981, Academic Press: New York. p. 267-280.
65. Hatchette, T.F., et al., Goat-associated Q fever: a new disease in Newfoundland. *Emerg Infect Dis*, 2001. **7**(3): p. 413-9.
66. Arricau Bouvery, N., et al., Experimental *Coxiella burnetii* infection in pregnant goats: excretion routes. *Vet Res*, 2003. **34**(4): p. 423-33.
67. Hackstadt, T. and J.C. Williams, Biochemical stratagem for obligate parasitism of eukaryotic cells by *Coxiella burnetii*. *Proc Natl Acad Sci U S A*, 1981. **78**(5): p. 3240-4.
68. Wiebe, M.E., P.R. Burton, and D.M. Shankel, Isolation and characterization of two cell types of *Coxiella burnetii* phase I. *J Bacteriol*, 1972. **110**(1): p. 368-77.
69. Zamboni, D.S., et al., *Coxiella burnetii* express type IV secretion system proteins that function similarly to components of the *Legionella pneumophila* Dot/Icm system. *Mol Microbiol*, 2003. **49**(4): p. 965-76.
70. Zusman, T., G. Yerushalmi, and G. Segal, Functional similarities between the icm/dot pathogenesis systems of *Coxiella burnetii* and *Legionella pneumophila*. *Infect Immun*, 2003. **71**(7): p. 3714-23.
71. Guzman-Herrador, D.L., et al., DNA Delivery and Genomic Integration into Mammalian Target Cells through Type IV A and B Secretion Systems of Human Pathogens. *Front Microbiol*, 2017. **8**: p. 1503.

72. Berger, K.H., J.J. Merriam, and R.R. Isberg, Altered intracellular targeting properties associated with mutations in the *Legionella pneumophila* dotA gene. *Mol Microbiol*, 1994. **14**(4): p. 809-22.
73. Beare, P.A., et al., Dot/Icm type IVB secretion system requirements for *Coxiella burnetii* growth in human macrophages. *MBio*, 2011. **2**(4): p. e00175-11.
74. Carey, K.L., et al., The *Coxiella burnetii* Dot/Icm system delivers a unique repertoire of type IV effectors into host cells and is required for intracellular replication. *PLoS Pathog*, 2011. **7**(5): p. e1002056.
75. Segal, G., M. Purcell, and H.A. Shuman, Host cell killing and bacterial conjugation require overlapping sets of genes within a 22-kb region of the *Legionella pneumophila* genome. *Proc Natl Acad Sci U S A*, 1998. **95**(4): p. 1669-74.
76. Seshadri, R., et al., Complete genome sequence of the Q-fever pathogen *Coxiella burnetii*. *Proc Natl Acad Sci U S A*, 2003. **100**(9): p. 5455-60.
77. MacDonald, L.J., R.C. Kurten, and D.E. Voth, *Coxiella burnetii* alters cyclic AMP-dependent protein kinase signaling during growth in macrophages. *Infect Immun*, 2012. **80**(6): p. 1980-6.
78. Weber, M.M., et al., Modulation of the host transcriptome by *Coxiella burnetii* nuclear effector Cbu1314. *Microbes Infect*, 2016. **18**(5): p. 336-45.
79. Pan, X., et al., Ankyrin repeat proteins comprise a diverse family of bacterial type IV effectors. *Science*, 2008. **320**(5883): p. 1651-4.

80. Weber, M.M., et al., Identification of *Coxiella burnetii* type IV secretion substrates required for intracellular replication and *Coxiella*-containing vacuole formation. *J Bacteriol*, 2013. **195**(17): p. 3914-24.
81. Angot, A., et al., Exploitation of eukaryotic ubiquitin signaling pathways by effectors translocated by bacterial type III and type IV secretion systems. *PLoS Pathog*, 2007. **3**(1): p. e3.
82. Voth, D.E., et al., The *Coxiella burnetii* cryptic plasmid is enriched in genes encoding type IV secretion system substrates. *J Bacteriol*, 2011. **193**(7): p. 1493-503.
83. Bork, P., Hundreds of ankyrin-like repeats in functionally diverse proteins: mobile modules that cross phyla horizontally? *Proteins*, 1993. **17**(4): p. 363-74.
84. de Felipe, K.S., et al., Evidence for acquisition of *Legionella* type IV secretion substrates via interdomain horizontal gene transfer. *J Bacteriol*, 2005. **187**(22): p. 7716-26.
85. Nagai, H., et al., A C-terminal translocation signal required for Dot/Icm-dependent delivery of the *Legionella* RalF protein to host cells. *Proc Natl Acad Sci U S A*, 2005. **102**(3): p. 826-31.
86. Chen, C., et al., Large-scale identification and translocation of type IV secretion substrates by *Coxiella burnetii*. *Proc Natl Acad Sci U S A*, 2010. **107**(50): p. 21755-60.
87. Simons, K. and W.L. Vaz, Model systems, lipid rafts, and cell membranes. *Annu Rev Biophys Biomol Struct*, 2004. **33**: p. 269-95.

88. Simons, K. and D. Toomre, Lipid rafts and signal transduction. *Nat Rev Mol Cell Biol*, 2000. **1**(1): p. 31-9.
89. Stuken, E., et al., Intra-Golgi protein transport depends on a cholesterol balance in the lipid membrane. *J Biol Chem*, 2003. **278**(52): p. 53112-22.
90. van der Kant, R., et al., Late endosomal transport and tethering are coupled processes controlled by RILP and the cholesterol sensor ORP1L. *J Cell Sci*, 2013. **126**(Pt 15): p. 3462-74.
91. Eden, E.R., et al., Annexin A1 Tethers Membrane Contact Sites that Mediate ER to Endosome Cholesterol Transport. *Dev Cell*, 2016. **37**(5): p. 473-83.
92. van Meer, G., D.R. Voelker, and G.W. Feigenson, Membrane lipids: where they are and how they behave. *Nat Rev Mol Cell Biol*, 2008. **9**(2): p. 112-24.
93. Lange, Y., Disposition of intracellular cholesterol in human fibroblasts. *J Lipid Res*, 1991. **32**(2): p. 329-39.
94. Thiele, C. and J. Spandl, Cell biology of lipid droplets. *Curr Opin Cell Biol*, 2008. **20**(4): p. 378-85.
95. Goldstein, J.L. and M.S. Brown, Atherosclerosis and its complications: contributions from the Association of American Physicians, 1886-1986. *Trans Assoc Am Physicians*, 1986. **99**: p. ccxxxi-ccxlvii.
96. Laitinen, S., et al., Family of human oxysterol binding protein (OSBP) homologues. A novel member implicated in brain sterol metabolism. *J Lipid Res*, 1999. **40**(12): p. 2204-11.

97. Lehto, M., et al., The OSBP-related protein family in humans. *J Lipid Res*, 2001. **42**(8): p. 1203-13.
98. Haslam, R.J., H.B. Koide, and B.A. Hemmings, Pleckstrin domain homology. *Nature*, 1993. **363**(6427): p. 309-10.
99. Johansson, M., et al., The two variants of oxysterol binding protein-related protein-1 display different tissue expression patterns, have different intracellular localization, and are functionally distinct. *Mol Biol Cell*, 2003. **14**(3): p. 903-15.
100. Johansson, M., et al., The oxysterol-binding protein homologue ORP1L interacts with Rab7 and alters functional properties of late endocytic compartments. *Mol Biol Cell*, 2005. **16**(12): p. 5480-92.
101. Raiborg, C., E.M. Wenzel, and H. Stenmark, ER-endosome contact sites: molecular compositions and functions. *EMBO J*, 2015. **34**(14): p. 1848-58.
102. Rocha, N., et al., Cholesterol sensor ORP1L contacts the ER protein VAP to control Rab7-RILP-p150 Glued and late endosome positioning. *J. Cell. Biol.*, 2009. **185**(7): p. 1209-1225.
103. Johansson, M., et al., Activation of endosomal dynein motors by stepwise assembly of Rab7-RILP-p150Glued, ORP1L, and the receptor betaIII spectrin. *J Cell Biol*, 2007. **176**(4): p. 459-71.
104. Jordens, I., et al., The Rab7 effector protein RILP controls lysosomal transport by inducing the recruitment of dynein-dynactin motors. *Curr Biol*, 2001. **11**(21): p. 1680-5.

105. Culver-Hanlon, T.L., et al., A microtubule-binding domain in dynactin increases dynein processivity by skating along microtubules. *Nat Cell Biol*, 2006. **8**(3): p. 264-70.
106. Wubbolts, R., et al., Opposing motor activities of dynein and kinesin determine retention and transport of MHC class II-containing compartments. *J Cell Sci*, 1999. **112 (Pt 6)**: p. 785-95.
107. Wyles, J.P., C.R. McMaster, and N.D. Ridgway, Vesicle-associated membrane protein-associated protein-A (VAP-A) interacts with the oxysterol-binding protein to modify export from the endoplasmic reticulum. *J Biol Chem*, 2002. **277**(33): p. 29908-18.
108. Cianciola, N.L., et al., Adenovirus RIDalpha uncovers a novel pathway requiring ORP1L for lipid droplet formation independent of NPC1. *Mol. Biol. Cell.*, 2013. **24**(21): p. 3309-25.
109. Kobuna, H., et al., Multivesicular body formation requires OSBP-related proteins and cholesterol. *PLoS Genetics*, 2010. **6**(8).
110. Johansson, M., et al., The two variants of oxysterol binding protein-related protein-1 display different tissue expression patterns, have different intracellular localization, and are functionally distinct. *Mol. Biol. Cell*, 2003. **14**(3): p. 903-15.
111. Zhao, K. and N.D. Ridgway, Oxysterol-Binding Protein-Related Protein 1L Regulates Cholesterol Egress from the Endo-Lysosomal System. *Cell Rep*, 2017. **19**(9): p. 1807-1818.

112. Rocha, N., et al., Cholesterol sensor ORP1L contacts the ER protein VAP to control Rab7-RILP-p150 Glued and late endosome positioning. *J Cell Biol*, 2009. **185**(7): p. 1209-25.
113. Howe, D. and R.A. Heinzen, *Coxiella burnetii* inhabits a cholesterol-rich vacuole and influences cellular cholesterol metabolism. *Cell Microbiol*, 2006. **8**(3): p. 496-507.
114. Howe, D. and R.A. Heinzen, Replication of *Coxiella burnetii* is inhibited in CHO K-1 cells treated with inhibitors of cholesterol metabolism. *Ann N Y Acad Sci*, 2005. **1063**: p. 123-9.
115. Czyz, D.M., et al., Host-directed antimicrobial drugs with broad-spectrum efficacy against intracellular bacterial pathogens. *MBio*, 2014. **5**(4): p. e01534-14.
116. Infante, R.E., et al., NPC2 facilitates bidirectional transfer of cholesterol between NPC1 and lipid bilayers, a step in cholesterol egress from lysosomes. *Proc Natl Acad Sci U S A*, 2008. **105**(40): p. 15287-92.
117. Mulye, M., et al., Elevated Cholesterol in the *Coxiella burnetii* Intracellular Niche Is Bacteriolytic. *MBio*, 2017. **8**(1).
118. Ren, Q., et al., Comparative DNA microarray analysis of host cell transcriptional responses to infection by *Coxiella burnetii* or *Chlamydia trachomatis*. *Ann N Y Acad Sci*, 2003. **990**: p. 701-13.
119. Mahapatra, S., P. Ayoubi, and E.I. Shaw, *Coxiella burnetii* Nine Mile II proteins modulate gene expression of monocytic host cells during infection. *BMC Microbiol*, 2010. **10**: p. 244.

120. Graham, J.G., et al., Virulent *Coxiella burnetii* pathotypes productively infect primary human alveolar macrophages. *Cell Microbiol*, 2013. **15**(6): p. 1012-25.
121. Mulye, M., Zapata, B., Gilk, S.D., Alternating lipid droplet homeostasis affects *Coxiella burnetii* intracellular growth. *PLoS One*, 2018.
122. Justis, A.V., et al., Interactions between the *Coxiella burnetii* parasitophorous vacuole and the endoplasmic reticulum involve the host protein ORP1L. *Cell Microbiol*, 2017. **19**(1).
123. Beare, P.A., et al., Characterization of a *Coxiella burnetii* ftsZ mutant generated by Himar1 transposon mutagenesis. *J. Bacteriol.*, 2009. **191**(5): p. 1369-1381.
124. Cockrell, D.C., et al., A method for purifying obligate intracellular *Coxiella burnetii* that employs digitonin lysis of host cells. *J. Microbiol. Methods*, 2008. **72**(3): p. 321-325.
125. Omsland, A., et al., Host cell-free growth of the Q fever bacterium *Coxiella burnetii*. *Proc. Natl. Acad. Sci. USA*, 2009. **106**(11): p. 4430-4434.
126. Beare, P.A. and R.A. Heinzen, Gene inactivation in *Coxiella burnetii*. *Methods Mol Biol*, 2014. **1197**: p. 329-45.
127. Sanjana, N.E., O. Shalem, and F. Zhang, Improved vectors and genome-wide libraries for CRISPR screening. *Nat Methods*, 2014. **11**(8): p. 783-784.
128. Mahdavi, A., et al., Identification of secreted bacterial proteins by noncanonical amino acid tagging. *Proc Natl Acad Sci U S A*, 2014. **111**(1): p. 433-8.
129. Ngo, J.T., et al., Cell-selective metabolic labeling of proteins. *Nat Chem Biol*, 2009. **5**(10): p. 715-7.

130. Coleman, S.A., et al., Proteome and antigen profiling of *Coxiella burnetii* developmental forms. *Infect. Immun.*, 2007. **75**(1): p. 290-8.
131. Sun, Q., et al., Rubicon controls endosome maturation as a Rab7 effector. *Proc Natl Acad Sci U S A*, 2010. **107**(45): p. 19338-43.
132. Ghigo, E., et al., *Coxiella burnetii* survival in THP-1 monocytes involves the impairment of phagosome maturation: IFN-gamma mediates its restoration and bacterial killing. *J Immunol*, 2002. **169**(8): p. 4488-95.
133. Johansson, M. and V.M. Olkkonen, Assays for interaction between Rab7 and oxysterol binding protein related protein 1L (ORP1L). *Methods Enzymol.*, 2005. **403**: p. 743-58.
134. Yan, D., et al., Expression of human OSBP-related protein 1L in macrophages enhances atherosclerotic lesion development in LDL receptor-deficient mice. *Arterioscler. Thromb. Vasc. Biol.*, 2007. **27**(7): p. 1618-24.
135. Vihervaara, T., et al., Sterol binding by OSBP-related protein 1L regulates late endosome motility and function. *Cell Mol. Life Sci.*, 2011. **68**(3): p. 537-51.
136. Moffatt, J.H., P. Newton, and H.J. Newton, *Coxiella burnetii*: turning hostility into a home. *Cell. Microbiol.*, 2015. **17**(5): p. 621-31.
137. Larson, C.L., et al., *Coxiella burnetii* effector protein subverts clathrin-mediated vesicular trafficking for pathogen vacuole biogenesis. *Proc. Natl. Acad. Sci. USA*, 2013. **110**(49): p. E4770-9.
138. Winchell, C.G., et al., *Coxiella burnetii* type IV secretion-dependent recruitment of macrophage autophagosomes. *Infect. Immun.*, 2014. **82**(6): p. 2229-38.

139. McDonough, J.A., et al., Host pathways important for *Coxiella burnetii* infection revealed by genome-wide RNA interference screening. *MBio*, 2013. **4**(1): p. e00606-12.
140. Martinez, E., et al., Identification of OmpA, a *Coxiella burnetii* protein involved in host cell invasion, by multi-phenotypic high-content screening. *PLoS Pathog*, 2014. **10**(3): p. e1004013.
141. Lifshitz, Z., et al., Computational modeling and experimental validation of the *Legionella* and *Coxiella* virulence-related type-IVB secretion signal. *Proc Natl Acad Sci U S A*, 2013. **110**(8): p. E707-15.
142. Cianciola, N.L., et al., Adenovirus Modulates Toll-Like Receptor 4 Signaling by Reprogramming ORP1L-VAP Protein Contacts for Cholesterol Transport from Endosomes to the Endoplasmic Reticulum. *J Virol*, 2017. **91**(6).
143. Derre, I., R. Swiss, and H. Agaisse, The lipid transfer protein CERT interacts with the *Chlamydia* inclusion protein IncD and participates to ER-*Chlamydia* inclusion membrane contact sites. *PLoS Pathogens*, 2011. **7**(6): p. e1002092.
144. Elwell, C.A., et al., *Chlamydia trachomatis* co-opts GBF1 and CERT to acquire host sphingomyelin for distinct roles during intracellular development. *PLoS Pathogens*, 2011. **7**(9): p. e1002198.
145. Graham, J.G., et al., Identification of ElpA, a *Coxiella burnetii* pathotype-specific Dot/Icm type IV secretion system substrate. *Infect Immun*, 2015. **83**(3): p. 1190-8.

146. Liu, P., et al., The Role of CzcRS Two-Component Systems in the Heavy Metal Resistance of *Pseudomonas putida* X4. *Int J Mol Sci*, 2015. **16**(8): p. 17005-17.
147. Anton, A., et al., CzcD is a heavy metal ion transporter involved in regulation of heavy metal resistance in *Ralstonia* sp. strain CH34. *J Bacteriol*, 1999. **181**(22): p. 6876-81.
148. Kamna Singh, D.B.S., Dennis G. Cvitkovitch, An intimate link: two-component signal transduction systems and metal transport systems in bacteria. *Future Microbiol*, 2015. **9**(11): p. 1283-1293.
149. Beare, P.A., et al., Essential role for the response regulator PmrA in *Coxiella burnetii* type 4B secretion and colonization of mammalian host cells. *J Bacteriol*, 2014. **196**(11): p. 1925-40.
150. Schulze-Luehrmann, J., et al., LAMP proteins account for the maturation delay during the establishment of the *Coxiella burnetii*-containing vacuole. *Cell Microbiol*, 2016. **18**(2): p. 181-94.
151. Newton, H.J., et al., A screen of *Coxiella burnetii* mutants reveals important roles for Dot/Icm effectors and host autophagy in vacuole biogenesis. *PLoS Pathogens*, 2014. **10**(7): p. e1004286.
152. Martinez, E., et al., *Coxiella burnetii* effector CvpB modulates phosphoinositide metabolism for optimal vacuole development. *Proc Natl Acad Sci U S A*, 2016.
153. Cianciola, N.L., et al., Adenovirus RIDalpha uncovers a novel pathway requiring ORP1L for lipid droplet formation independent of NPC1. *Mol Biol Cell*, 2013. **24**(21): p. 3309-25.

154. van der Kant, R., et al., Cholesterol-binding molecules MLN64 and ORP1L mark distinct late endosomes with transporters ABCA3 and NPC1. *J Lipid Res*, 2013. **54**(8): p. 2153-65.
155. Phillips, M.J. and G.K. Voeltz, Structure and function of ER membrane contact sites with other organelles. *Nat Rev Mol Cell Biol*, 2016. **17**(2): p. 69-82.
156. Weber-Boyvat, M., et al., Ligand-dependent localization and function of ORP-VAP complexes at membrane contact sites. *Cell Mol Life Sci*, 2015. **72**(10): p. 1967-87.
157. Graham, J.G., et al., Identification of ElpA, a *Coxiella burnetii* pathotype-specific Dot/Icm type IV secretion system substrate. *Infect. Immun.*, 2015. **83**(3): p. 1190-8.
158. Kentala, H., M. Weber-Boyvat, and V.M. Olkkonen, OSBP-Related Protein Family: Mediators of Lipid Transport and Signaling at Membrane Contact Sites. *Int Rev Cell Mol Biol*, 2016. **321**: p. 299-340.
159. Glaser, P., et al., Secretion of cyclolysin, the calmodulin-sensitive adenylate cyclase-haemolysin bifunctional protein of *Bordetella pertussis*. *EMBO J*, 1988. **7**(12): p. 3997-4004.
160. Larson, C.L., et al., *Coxiella burnetii* effector proteins that localize to the parasitophorous vacuole membrane promote intracellular replication. *Infect Immun*, 2015. **83**(2): p. 661-70.
161. Beare, P.A., et al., Two systems for targeted gene deletion in *Coxiella burnetii*. *Appl Environ Microbiol*, 2012. **78**(13): p. 4580-9.

162. Zen, K.H., T.G. Consler, and H.R. Kaback, Insertion of the polytopic membrane protein lactose permease occurs by multiple mechanisms. *Biochemistry*, 1995. **34**(10): p. 3430-7.
163. Wier, G.M., et al., New method for the orthogonal labeling and purification of *Toxoplasma gondii* proteins while inside the host cell. *MBio*, 2015. **6**(2): p. e01628.
164. Stead, C.M., et al., Sec-mediated secretion by *Coxiella burnetii*. *BMC Microbiol*, 2013. **13**: p. 222.
165. Eckart, R.A., et al., Antiapoptotic activity of *Coxiella burnetii* effector protein AnkG is controlled by p32-dependent trafficking. *Infect Immun*, 2014. **82**(7): p. 2763-71.
166. Schafer, W., et al., Nuclear trafficking of the anti-apoptotic *Coxiella burnetii* effector protein AnkG requires binding to p32 and Importin-alpha1. *Cell Microbiol*, 2017. **19**(1).
167. Parsons, H.T., Preparation of Highly Enriched ER Membranes Using Free-Flow Electrophoresis. *Methods Mol Biol*, 2018. **1691**: p. 103-115.
168. Imai, J., et al., Purification of the Membrane Compartment for Endoplasmic Reticulum-associated Degradation of Exogenous Antigens in Cross-presentation. *J Vis Exp*, 2017(126).
169. Baghirova, S., et al., Sequential fractionation and isolation of subcellular proteins from tissue or cultured cells. *MethodsX*, 2015. **2**: p. 440-5.

Curriculum Vitae

Anna Victoria Justis

Education

Bachelor of Science, Molecular Biology
Minors in Chemistry and Honors Program
University of Wyoming, 2012

Doctor of Philosophy
“*Recruitment and function of ORP1L on the Coxiella burnetii parasitophorous vacuole*”
Minor in Life Sciences
Department of Microbiology and Immunology, Indiana University, 2018

Honors and Awards

University Fellowship from Indiana University, 2013-2014

Abstract Award, Honorable mention. 22nd Annual Midwest Microbial Pathogenesis Conference. Aug 2015.

Immunology and Infectious Diseases T32 Pre-doctoral Fellow. Dec 2015-Dec 2017.

IUPUI Graduate Professional Student Government GPEG travel award to attend AAAS Annual Meeting. Feb 2017.

Publications

Justis, A.V., Hansen, B., Beare, P.A., King, K.B., Heinzen, R.A., and Gilk, S.D. (2017) Interactions between the *Coxiella burnetii* parasitophorous vacuole and the endoplasmic reticulum involve the host protein ORP1L. *Cellular Microbiology*, 19 (1), e12637. doi:10.1111/cmi.12637.

Samanta, D., Mulye, M., Clemente, T.M., **Justis, A.V.**, & Gilk, S.D. (2017). Manipulation of Host Cholesterol by Obligate Intracellular Bacteria. *Frontiers in Cellular and Infection Microbiology*, 7, 165. doi:10.3389/fcimb.2017.00165.

Presentations

Justis, A.V., King, K.B., Gilk, S.D., “The host cell protein ORP1L mediates interactions between the *Coxiella burnetii* vacuole and the endoplasmic reticulum”. Poster presentation, *Midwest Microbial Pathogenesis Conference*, Chicago, IL, September 12-14, 2014.

Justis, A.V., Beare, P.A., Hansen, B., Heinzen, R.A., Gilk, S.D. "The host cell protein ORP1L mediates interactions between the *Coxiella burnetii* vacuole and the host endoplasmic reticulum". Poster presentation, *Meeting of the American Society for Rickettsiology*, Lake Tahoe, CA, June 20-23, 2015.

Justis, A.V., Beare, P.A., Hansen, B., Heinzen, R.A., Gilk, S.D. "The host protein ORP1L mediates interactions between the *Coxiella burnetii* vacuole and host endoplasmic reticulum" Poster presentation, *Midwest Microbial Pathogenesis Conference*, Indianapolis, IN, August 28-30, 2015.

Justis, A.V., Winfree, S., Hansen, B., Beare, P.A., Heinzen, R.A., Gilk, S.D. "Host cholesterol-binding protein ORP1L is involved in *Coxiella burnetii* vacuole development and endoplasmic reticulum membrane contact sites". Poster presentation, *Midwest Microbial Pathogenesis Conference*, Champaign-Urbana, IL, September 23-25, 2016.

Justis, A.V., Winfree, S., Hansen, B., Beare, P.A., Heinzen, R.A., Gilk, S.D. "Host cholesterol-binding protein ORP1L is involved in *Coxiella burnetii* vacuole development and endoplasmic reticulum membrane contact sites". Poster presentation, *Indiana Biology of Intracellular Pathogens Retreat*, Indianapolis, IN, June 23, 2017.

Justis, A.V., Winfree, S., Bryan Hansen, Paul A. Beare, Robert A. Heinzen, Stacey D. Gilk. "Oxysterol-binding protein-related protein 1L is involved in *Coxiella burnetii* vacuole development and endoplasmic reticulum membrane contact sites." Poster presentation, *Midwest Microbial Pathogenesis Conference*, Notre Dame, IN, August 25-27, 2017.

Clemente, T.M., Mulye, M., **Justis, A.V.**, Gilk, S.D. "IL-17 pathway is downregulated by type IV effector proteins during *Coxiella burnetii* infection." Poster, *Midwest Microbial Pathogenesis Conference*, Notre Dame, IN, August 25-27, 2017.

Professional Service

Microbiology and Immunology Department, Student Representative, 2016-2017

IU School of Medicine Curriculum Committee, Graduate Student Representative, 2016-2017 academic year

IBMG Travel Grant Review Committee, Microbiology and Immunology Representative, Fall 2016 and Spring 2017

Fong-Clontech Seminar Series, Committee Co-Chair, Fall 2017